2007

Mac Layer And Routing Protocols For Wireless Ad Hoc Networks With Asymmetric Links And Performance Evaluation Studies

Guoqiang Wang
University of Central Florida

MAC LAYER AND ROUTING PROTOCOLS FOR WIRELESS AD HOC NETWORKS WITH ASYMMETRIC LINKS AND PERFORMANCE EVALUATION STUDIES

by

GUOQIANG WANG
B.S. Southeast University, 2001
M.S. University of Central Florida, 2007

A dissertation submitted in partial fulfillment of the requirements
for the degree of Doctor of Philosophy
in the School of Electrical Engineering and Computer Science
in the College of Engineering and Computer Science
at the University of Central Florida
Orlando, Florida

Summer Term
2007

Major Professors:
Dan C. Marinescu
Damla Turgut

ABSTRACT

In a heterogeneous *mobile ad hoc network (MANET)*, assorted devices with different computation and communication capabilities co-exist. In this thesis, we consider the case when the nodes of a MANET have various degrees of mobility and range, and the communication links are asymmetric. Many routing protocols for ad hoc networks routinely assume that all communication links are symmetric, if node A can hear node B and node B can also hear node A. Most current MAC layer protocols are unable to exploit the asymmetric links present in a network, thus leading to an inefficient overall bandwidth utilization, or, in the worst case, to lack of connectivity. To exploit the asymmetric links, the protocols must deal with the asymmetry of the path from a source node to a destination node which affects either the delivery of the original packets, or the paths taken by acknowledgments, or both. Furthermore, the problem of hidden nodes requires a more careful analysis in the case of asymmetric links.

MAC layer and routing protocols for ad hoc networks with asymmetric links require a rigorous performance analysis. Analytical models are usually unable to provide even approximate solutions to questions such as end-to-end delay, packet loss ratio, throughput, etc. Traditional simulation techniques for large-scale wireless networks require vast amounts of storage and computing cycles rarely available on single computing systems. In our search for an effective solution to study the performance of wireless networks we investigate the time-parallel simulation.

Time-parallel simulation has received significant attention in the past. The advantages, as well as, the theoretical and practical limitations of time-parallel simulation have been extensively researched for many applications when the complexity of the models involved severely limits the applicability of analytical studies and is unfeasible with traditional simulation techniques. Our goal is to study the behavior of large systems consisting of possibly thousands of nodes over extended periods of time and obtain results efficiently, and time-parallel simulation enables us to achieve this objective.

We conclude that MAC layer and routing protocols capable of using asymmetric links are more complex than traditional ones, but can improve the connectivity, and provide better performance. We are confident that approximate results for various performance metrics of wireless networks obtained using time-parallel simulation are sufficiently accurate and able to provide the necessary insight into the inner workings of the protocols.

To my parents.

ACKNOWLEDGMENTS

I would like to thank my advisors Dr. Marinescu and Dr. Turgut, as well as the committee members Dr. Bölöni and Dr. Bassiouni. In particular, I would like to thank my advisor, Dr. Dan C. Marinescu who gave me the freedom to explore, exceptional thoughts, and sound advices when most needed, through every step of my Ph.D study. I also greatly appreciate my co-advisor, Dr. Damla Turgut for the constant encouragement, invaluable directions, and comments throughout. I would like to single out Dr. Ladislau Bölöni who always gave me timely help and novel advices. I am also indebted to Dr. Bassiouni for his critical feedback and comments. Last but not least, thanks to all my lab mates and friends in University of Central Florida, who accompanied me along this path. Finally, I am forever grateful to my Mom and Dad who provide constant support in a faraway country.

TABLE OF CONTENTS

LIST OF FIGURES

LIST OF TABLES

LIST OF ACRONYMS/NOTATIONS

ACK	ACKnowledgment
A^{4}LP	Location-Aware Power-Aware routing protocol for MANETs with Asymmetric links
AODV	Ad hoc On-Demand Distance Vector routing protocol
AsyMAC	a MAC layer protocol for MANETs with Asymmetric links
CBR	Constant Bit Rate
CSMA/CA	Carrier Sense Multiple Access with Collision Avoidance
CSMA/CD	Carrier Sense Multiple Access with Collision Detection
CTS	Clear To Send
CW	Contention Window
DIFS	Distributed Inter-Frame Spacing
DSDV	Destination-Sequenced Distance Vector routing protocol
GPS	Global Positioning Systems
ISA	Initial State Approximation
LAR	Location-Aided Routing protocol
m-AODV	AODV with m-limited forwarding
m-A^{4}LP	A^{4}LP with m-limited forwarding

MAC	Medium Access Control
MANET	Mobile Ad hoc NETwork
NAV	Network Allocation Vector
NS-2	Network Simulation version 2
OLSR	Optimized Link State Routing protocol
PDES	Parallel Discrete Event Simulation
RTS	Ready To Send
SIFS	Short Inter-Frame Spacing
TACK	Tunneled ACKnowledgment
TCTS	Tunneled Clear To Send
TCP	Transport Control Protocol
TPS	Time-Parallel Simulation
TPS-C	Time-Parallel Simulation with Compressed history
TPS-I	Time-Parallel Simulation with an Iterative approach
TPS-CU	Time-Parallel Simulation with Compressed history and Uncompressed interval
TPS-U	Time-Parallel Simulation with Uncompressed interval
UDP	User Datagram Protocol
XCTS	eXtended Clear To Send
XRTS	eXtended Ready To Send

$\Gamma_{i,j}$	the complementary range of node j to reach node i
δ_M	the absolute error of measurement M
ε_{max}	the error threshold
$\varepsilon_{\mathbf{M}}$	the relative error for a metric M
$\varepsilon_{\mathbf{PLR}}$	the relative error for the packet loss ratio
$\varepsilon_{\mathbf{PDR}}$	the relative error for the packet delivery ratio
$\varepsilon_{\mathbf{TPT}}$	the relative error for the throughput
$\eta(\hat{S}, S)$	the compression ratio of the compressed history $\hat{S}$
κ	the speedup of an algorithm
$\kappa(i, j)$	a forwarding cutoff attached to a transmitted packet sending from node j to node i
λ_c	the regular routing table update frequency
λ_i	the routing table update frequency of the compressed history $\underline{\hat{S_i}}$
$\Lambda_k(i, j)$	the area of the intersection of $\Gamma_{i,j}$ and Π_k
$\pi_{i,j}$	the j-th (starts from 0) time interval of π_i
Π_k	the circle centered at the current location of node k
τ	the time interval of a simulation
$\|\tau\|$	the duration of the time interval of a simulation
$\mathcal{A}$	the geographic area of a simulation
C_i	one of the hierarchical levels of systems in a heterogeneous MANET

$C(M)$	the complementary measure of M
d_{ij}	the distance between node i and node j
$\mathcal{E}$	the set of events of a simulation
$\hat{\mathcal{E}}$	the set of events that produce significant perturbations
F	a MAC protocol that silences nodes during a transmission
$\mathcal{F}$	the final state of a simulation
$\mathcal{F}^a$	area-based forwarding fitness function
$\mathcal{F}^d$	distance-based forwarding fitness function
H_{sr}	the set of hidden nodes of a transmission T_{sr}
$H3_{sr}$	the hidden nodes of a transmission T_{sr} in $P3_r$
H-$node$	the high-range node of an asymmetric link
I	an ideal algorithm that correctly silences all nodes during a transmission
$\mathcal{I}$	the initial state of a simulation
Id_i	the unique id of node i
$In_i(t)$	the set of In-bound neighbors of i at time t
$InOut_i(t)$	the set of In/Out-bound neighbors of i at time t
k_{95}	the number of iterations to reach 95% accuracy, in the TPS-I algorithm
$L^{(k)}$	the time-parallel simulation set after k-th iteration, in the TPS-I algorithm
L-$node$	the low-range node of an asymmetric link

$L_i(t)$	the geographical position of node i at time t
$\overline{Misc_(F)}$	the average misclassification of an algorithm F
$Misc_{sr}(F)$	the misclassification ratio of an algorithm F for a transmission T_{sr}
$\overline{Miss_(F)}$	the average miss ratio of an algorithm F
$Miss_{sr}(F)$	the miss ratio of an algorithm F for a transmission T_{sr}
$mXHR3_{sr}$	the minimal extended hidden nodes relay set of a transmission T_{sr} in $P3_r$
$MXHR3_{sr}$	the minimum extended hidden nodes relay set of a transmission T_{sr} in $P3_r$
$\mathcal{N}$	the set of nodes in a heterogeneous MANET
$P_i^{res}(t)$	the residual power of node i at time t
$R_i(t)$	the transmission range of node i at time t
$\mathcal{R}_{ij}(t)$	the reachability function that describes the connection between node i and j
$Out_i(t)$	the set of Out-bound neighbors of i at time t
P_i	the i-th simulation segment of a time-parallel simulation set
$P_{i,j}$	the j-th sub-interval of the simulation segment P_i
$P3_i$	the three-party proxy set coverage of node i
RT_i	the routing table of node i
S	the six-tuple that describes the simulation of a MANET, $S = (\mathcal{A}, \tau, \mathcal{E}, \mathcal{I}, \mathcal{F}, \mathcal{T})$
$\hat{S}$	the compressed history of a simulation S
$\underline{S_i}$	the complete sequential simulation prior to S_i

$\underline{\hat{S}_i}$	the compressed history of the prior simulation of S_i
$\mathcal{S}_{sr}(F)$	the set of nodes that silenced by algorithm F during a transmission T_{sr}
$\mathcal{S}_{sr}(I)$	the ideal set of nodes that should be silenced during a transmission T_{sr}
S_{Ui}	the uncompressed interval before the simulation S_i
S_{Wi}	the warmup interval before the simulation S_i
$\hat{S}_{Ui}$	the compressed history of the prior simulation simulation of S_{Ui}
t_e	the extinction time
T_c	the normalized compressed history duration
T_i	the segment duration
T_u	the uncompressed interval duration
$t(e)$	the firing time of an event e
$T(S)$	a function that calculates the execution time of a simulation S
$\mathcal{T}$	the trace of a simulation
V_i	the vicinity of node i
$XH3_{sr}$	the extended hidden nodes of a transmission T_{sr} in $P3_r$
$XHR3_{sr}$	the extended hidden nodes relay set of a transmission T_{sr} in $P3_r$

CHAPTER 1
INTRODUCTION

Routing protocols for ad hoc networks routinely assume that all communication links are bidirectional, however, in a *heterogeneous mobile ad hoc network (MANET)*, most communication links are asymmetric. In this dissertation, we mainly concern ourselves with developing a *MAC layer and routing protocol* suite for heterogeneous MANETs with *asymmetric links*.

Performance studies for new communication protocols are necessary to justify various design decisions and to tune the parameters of the protocols. To simulate the behavior of large wireless networks over extended periods of time is not feasible with existing techniques. Parallel simulation offers a glimpse of hope.

1.1 Routing in Heterogeneous MANETs

Mobile ad hoc networks allow nodes with different hardware capabilities and power limitations to communicate with one another. Most communication channels in such networks are unidirectional due to heterogeneity of the nodes and to power constraints. Yet, routing protocols for MANETs routinely assume that all communication links are bidirectional. In this dissertation, we consider the case when the nodes of a MANET have various degrees of mobility and range and the communication links are asymmetric; node i may be able to reach node j, but j may not be able to reach i. Power consumption is a major concern for a MANET as nodes become inoperative once they have depleted their power. *Power-aware* routing algorithms minimize the power consumption and, whenever possible, avoid the nodes with a low level of residual power. The task of minimizing power consumption can be facilitated when the location of individual nodes are known. Global Positioning Systems (GPS) [DJ96] are routinely embedded into mobile systems and *location-aware* routing algorithms have the potential to extend the life of individual nodes of a MANET.

In a wireless environment, at any given time, an asymmetric link supports unidirectional communication between a pair of mobile stations and requires a set of relay stations for the transmission of packets in the other direction. Throughout this dissertation the term “asymmetric” is related to the transmission range of a node at time t and a communication channel linking two nodes. Two nodes linked by an asymmetric link at time t may find themselves in close proximity, or may be able to increase their transmission range and to reach each other at time $t+\tau$ and thus be connected by a bi-directional link. Thus, we feel compelled to make a distinction between unidirectional and asymmetric links in wireless networks. We shall drop this distinction whenever the context allows us to.

Asymmetric links are present in wireless networks for a variety of physical, logical, operational, and legal reasons:

(a) The transmission range is limited by the node hardware. The hardware properties of the node (for instance, the antenna or the RF circuits) determine the maximum transmission range. The

different transmission ranges of the nodes lead to asymmetric links, which cannot be avoided except by physically changing the nodes' hardware components, for instance by installing a different antenna.

(b) Power limitation. Different nodes may have different power constraints. For instance, node A may have sufficient power reserves and a transmission range enabling it to reach node B; however, node B has limited power, and either (i) cannot reach node A, or (ii) may choose not to reach node A to save power. The two scenarios influence the design of the protocols in different ways. In the second scenario, node B is capable to reach node A and we could exploit this capability for short transmissions when necessary, e.g., during a network setup phase.

(c) Interference. Node A can reach node B and node B can reach node A, but if node B would transmit at a power level sufficient to reach node A, it would interfere with node C who might be a licensed user of the spectrum. This scenario is critical for transmitters which attempt to opportunistically exploit unused parts of the licensed spectrum (such as unused television channels). Even if operating in the unlicensed bands, dynamic spectrum management arrangements might have given the priority to node C, thus node B needs to refrain from sending at a power level above a given threshold.

(d) Stealth considerations. Node A and node B attempt to communicate and they wish to hide the existence or the exact location of node B from node O. One way to achieve this is to restrict the transmission power of node B to the minimum and/or transmit on frequencies which make location

detection more difficult. This is especially important in military/battlefield applications where low probability of detection (LPD) is an important consideration [FCS, JTR].

(e) Dynamic spectrum management. In the emerging field of software defined radios, the nodes can transmit virtually in any band across the spectrum, but they need to share the spectrum with devices belonging to licensed operators as well as devices with limited flexibility. Once any of the reasons discussed previously force a link to be unidirectional additional constraints, e.g., the need for a reverse path between some pairs of nodes may cause other links to change their status and operate in a unidirectional mode, even when there is no other reason for the unidirectionality.

Inability of some MAC layer protocols to exploit the asymmetry of some of the communication channels could lead to an inefficient bandwidth utilization, or, in the worst case, to inability to connect some of the nodes. To exploit the asymmetric links, the protocols must be able to deliver the acknowledgements back to the sender in a direction opposite to the direction of the asymmetric link. Furthermore, the problem of hidden nodes appears more often and in more complex forms than in the case of symmetric links. Depending whether the routing protocol of a MANET is able to handle asymmetric links, the MAC layer protocol might need to hide the existence of asymmetric links with a symmetric overlay. The challenge for a MAC layer protocol able to exploit asymmetric links is to solve the hard problems mentioned above, while keeping the cost incurred lower than the benefits obtained from the utilization of the asymmetric links. MAC layer protocols for asymmetric links were previously proposed by Poojary et al. [PKD01], Fujii et al. [FTB02] and others.

We discuss briefly two potential applications of the network and MAC layer protocols for location- and power-aware networks with asymmetric links: software radios and ad hoc grids. Recent advances in the performance of major components of wireless systems (microprocessors, A/D converters, RF components, batteries) allow the development of a family wireless networking technologies which replace the traditional digital circuits by software modules and limit analog processing to a bare minimum. A software radio has *distinctive* advantages over a traditional one: (a) it covers a wide operational frequency spanning multiple bands of the spectrum, (b) can support multiple networking protocols, (c) a single hardware unit can be programmed to work with multiple waveforms and (d) a software radio can be updated to work with new protocols, designed after the radio hardware. Through their flexibility, software radios can enable many innovative applications, and, at the same time, provide a significant boost to networking research.

An *ad hoc grid* is a heterogeneous system without a fixed infrastructure, all its components are mobile [MMJ03]; it consists of a hierarchy of systems with different hardware, software, and communication capabilities. Informally, we identify four classes of systems: *C1, C2, C3*, and *C4*. Powerful laptops or regular desktop computers with significant amounts of secondary storage, a variety of I/O devices, high speed network access, and long life batteries, mounted on all-terrain vehicles, airplanes, ships are called *C1* systems. Robots (terrestrial or airborne) and laptops with infrared, wireless, and/or satellite communication, are examples of *C2* systems. Wearable computers, PDAs with little or no secondary storage and crossover devices (e.g., portable phones with PDA) are included in the *C3* systems category. A *C4* system is a low-cost smart sensor, e.g., a video camera, an infrared detector, a source of light, a generator of acoustic signals, or another type of sensor or actuator. Most systems are expected to have GPS capabilities, or, as in the case of sensors, to record their approximate position at the time when they were installed. The hierarchy presented here serves only an illustrative purpose as the number of programmable mobile devices increases every day (see for example http://www.fawcette.com/wireless/sherman/).

There are many potential applications of ad hoc grids for wild fire prevention and control, disaster management, peace keeping operations in a remote part of the world, sporting events, discovery expeditions, natural resource exploration, and battlefield management. Olympic Games, Tour de France, the Trans-Africa car rally, the dog sled race in Alaska, archeological excavations, an expedition to K9, and underwater oil exploration, are just a few practical cases when a grid-like environment is necessary to reliably support the coordinated effort of a group of individuals working under extreme conditions. Communication and computing facets of an ad hoc grid are deeply intertwined. One node may request computations distributed over a set of nodes (e.g., running models to determine the humidity and combustion in an area affected by a wild fire, population evacuation models, and so on).

In this dissertation, we are concerned with the communication aspect of ad hoc grids and we introduce a routing protocol A^{4}LP (a Location-Aware and Power-Aware routing protocol designed primarily for heterogeneous MANETs with Asymmetric links), and a MAC layer protocol Asy-MAC (A MAC layer protocol for wireless networks with Asymmetric links). Most of the existing routing protocols focus on a single aspect such as either location- or power-awareness and do not generally consider the existence of asymmetric links even though a heterogeneous MANET is mostly composed of asymmetric links. Therefore, the novelty of our routing protocol comes from the combined effects of not only location and power-awareness but also the usage of asymmetric links throughout. The MAC layer protocol uses a geometric analysis of the hidden node problem in the presence of asymmetric links for a more precise determination of the nodes which need to be silenced during a transmission. We introduced a set of metrics characterizing the ability of a MAC layer protocol to silence nodes which can cause collisions.

1.2 The Time-Parallel Simulation

New communication protocols require rigorous performance studies; analytical modeling, and simulation, prior to the implementation and measurements once a system becomes available allow us to assess the benefits and the shortcomings of new protocols. Many analytical results obtained throughout the years for Random Multiple Access (RMA) methods cannot be readily extended to the MAC layer of wireless networks. Analytical model of the physical layer of ad hoc networks must consider factors such as: (1) the nodes are mobile and the network topology may change rapidly; (2) the transmission range of a node may change over time due to the power consumption; (3) the transmissions from different nodes interfere with each other when the network density is high and/or when the network load is relatively high; (4) a link may be unidirectional due to power constraints or interference; (5) the geographical locations of the nodes affects the patterns of collisions; (6) the hidden node problem complicates the decision when a node transmits a packet.

The network layer models are also very intricate; they require a large number of parameters, and the state is very complex. All these considerations make one wonder whether it is possible to draw significant practical conclusions about the behavior of MANETs solely based on analytical performance modeling. Thus, simulation seems to be the only alternative to evaluate the performance of routing protocols for MANETs.

For traditional simulation approaches, the state space needed to save various simulation parameters as well as the execution time increase rapidly as the number of nodes in the network increases. With traditional simulation approaches, the simulation of large-scale wireless networks suffers greatly from insufficiency of data storage and computational resources. As we resort to techniques that might be helpful to enhance the scalability of the simulation approach, we recognize parallel simulation as a good candidate.

Time-parallel simulation, the simulation of large systems by partitioning the time domain, rather than the space domain, has received significant attention in the past. The advantages, as well as, the theoretical and practical limitations of time-parallel simulation have been extensively researched for many applications. As a general rule time-parallel simulation requires the simulated process to be regenerative, a situation rarely encountered in practice. Yet, oftentimes we are satisfied with approximate results which could give us some qualitative rather than quantitative results important for the design of a system.

In this dissertation, we discuss time-parallel simulation of large wireless networks over extended periods of time. Such systems are rarely amenable to analytical modeling or subject to traditional simulation techniques due to the complexity of the models involved, the large number of nodes, and the very large number of events.

Systems consisting of a few thousand nodes are rather common. Indeed, let us consider a simple scenario. In a university classroom, 120 students attend a class; each student has a cell phone (GSM source), a PDA and laptop (two 802.11b WiFi sources). There are five Bluetooth sources: PDA, laptop, cell phone, headset, and mouse. Some of the students might have WiFi enabled cameras, Bluetooth enabled audio players, and matching head phones. All in all, it does not seem out of the ordinary to have 3 WiFi and 7 Bluetooth sources per person. Thus, even without considering that many of the WiFi nodes have a transmission range long enough to cover neighboring classrooms as well, in order to study the networking environment of one classroom we have to simulate a system with 1200 wireless sources operating in the same frequency band.

A wireless network with 1200 nodes pushes the limits of serial simulators such as NS-2. Even when feasible, such simulation requires a significant computation power and can take a very long time. An alternative is a parallel implementation of the simulation. Spatial-parallel simulation based upon a partitioning of the geographic area into either overlapping or non-overlapping domains is rather impractical.

The question we pose is if an approximate time-parallel simulation of wireless ad hoc networks is feasible and if the quality of the results produced by such a simulation is acceptable. To analyze and predict the performance of time-parallel simulation of wireless ad hoc networks, we introduce the notion of perturbation of measurements and present a layer-by-layer analysis of the impact of perturbations on the functioning of a wireless network. This model allows us to predict the accuracy of the simulation relative to various measurements through an analysis of the protocols involved at each layer.

1.3 Contributions

We decided to study wireless networks with asymmetric links because the asymmetry is an inherent consequence of power limitations of mobile devices. It turns out that there are other practical and technical reasons why asymmetry, the fact that node A can reach node B in one hop while node B needs more than one hop to reach node A, is ubiquitous in wireless ad hoc networks.

Routing and medium access control under these circumstances are challenging and have been addressed by relatively few research groups. Power constraints make broadcasting of topological information, routes, or data packets, impractical. Like other groups, in our work we attempt to restrict the set of nodes retransmitting a packet and we define a *fitness function* that can be computed independently by every node and allow it to decide whether it should retransmit a packet. This fitness function could reflect geographic information, security constraints, power limitations, and possibly other considerations. The hidden node problem is a major issue and complicates even further the logic of MAC layer and network protocols. The solution we propose in this dissertation aims to silence a set of nodes that match as closely as possible the ones that would interfere with the transmission of a node.

Once we have developed the logic of MAC layer and routing protocols that exploit asymmetric links we had to provide convincing arguments that these new protocols are functional, and, even though more complex than the ones that ignore the asymmetry, can lead to an acceptable level of performance. We turned to analytical modeling and realized shortly that it would be rather difficult, if possible at all, to develop analytical models. We also realized the limitations of existing simulation tools such as NS-2. Thus, we turned our attention to time-parallel simulation that could allow us to use existing tools, but study networks with a larger number of nodes and for extended periods of time. The critical issue for time-parallel simulation is the estimation of the initial state for each group of events processed concurrently and the realization that there are inherent accuracy-speedup trade-offs. We developed several techniques to partition the set of successive events and to estimate the initial state for each partition. Critical to our thinking is the concept of *perturbation* caused by an event. Our latest approach, is to create a *compressed history* that identifies *significant* events. The compressed history methodology is based upon the conjectured principle of temporal locality of perturbations. One could consider a more general approach to define significant events, or an application-specific approach as in the case of wireless ad hoc networks discussed in this dissertation. In the former case we define several classes of events and choose to include in the compressed history only events from one or several classes deemed to perturb the initial state of the measurement phase the most. In the later case we carry out a careful analysis of the process and select events from several classes and include them in the compressed history.

1.4 Organization

The reminder of this dissertation is organized as follows.

Chapter 2 gives an introduction and provides a survey of the literature on routing protocols, MAC layer protocols, and the time-parallel simulation. Through Chapter 3-6 we first proposed an algorithm, followed by a performance study of the algorithm.

Chapter 3 introduces m-limited forwarding along with two forwarding fitness functions. We also present a variant of the Ad-hoc On-demand Distance Vector (AODV) routing algorithm [PR99] that supports m-limited forwarding, which we call m-AODV. Then, we present the results of the simulation study with a discussion of the effect of network load, node mobility and node density. The optimal values of m are discussed, followed by a comparison of AODV, Location-Aided Routing (LAR) [KV98], and m-AODV with two forwarding fitness functions.

Chapter 4 describes the routing protocol (A^{4}LP) and the MAC layer protocol (AsyMAC) for heterogeneous MANETs. We introduce the system model for heterogeneous mobile ad hoc networks and discuss some topology-related concepts. Then, we present the A^{4}LP protocol and the AsyMAC protocol in every aspects. In the end, we illustrate the A^{4}LP/AsyMAC protocol combination in a simulation and case study section.

Chapter 5 describes a time-parallel algorithm for simulation of wireless ad hoc networks. First, we present our model of the propagation of perturbations in wireless networks, the impact of the protocols at the various layers of the networking stack and the application for time-parallel simulation. Several warmup strategies are also introduced. Then, we describe the details of a time-parallel simulation algorithm with iteratively extended warmup interval, for simulation of wireless ad hoc networks. Finally, we present a series of simulation studies investigating the speedup and precision of the proposed methods for typical wireless networking scenarios.

Chapter 6 present a time-parallel algorithm for simulation of wireless ad hoc networks, with the initial state approximated by the compressed history strategy. We propose the application of compressed history and uncompressed interval in the time-parallel simulation of wireless ad hoc networks. Then, we discussed several strategies to generate the compressed history and methods to balance the execution time of different segments. We also discussed the compromise of speedup and accuracy of the time-parallel simulation with compressed history strategy. In the end, a series of simulation studies that investigate the speedup and precision of the proposed methods for typical wireless networking scenarios are presented.

Chapter 7 concludes the work in this dissertation.

CHAPTER 2
RELATED WORK

This chapter surveys published research covering MAC layer and routing protocols, as well as the time-parallel simulation as a method to assess the performance of such protocols. We discuss routing protocols and MAC layer protocols in Sections 2.1 and 2.2 respectively. Analytical models of wireless networks are surveyed in Section 2.3 and time-parallel simulation in Section 2.4.

2.1 Routing Protocols

In a heterogeneous MANET, assorted devices with different computation and communication capabilities co-exist. As opposed to static networks, where symmetric links are the standard, routing in a heterogeneous MANET is dominated by asymmetric links. There are several reasons. (i) Due to the varying transmission ranges of the devices, only the devices with stronger communication capability may reach the devices with weaker communication capability. (ii) In order to achieve power-awareness, it is assumed that devices adjust their transmitting power according to their residual power such that their lifetime are extended. In the process, some of the symmetric links may become asymmetric when the communication capability of a node degrades due to decrease in the residual power. (iii) The transmission ranges of devices with same communication capabilities may vary due to fading and random transient phenomena.

Ad hoc routing protocols are generally classified into two categories:

- *table-driven*, or *proactive*, such as DSDV [PB94], CGSR [CWL97], DREAM [BCS98], OLSR [CJL01], and WRP [MG96];
- *on-demand*, *reactive*, or *source-initiated*, such as DSR [JM96], AODV [PR99], LAR [KV98], TORA [PC97], ORB [TCC06], and ABR [Toh97].

In case of *proactive routing protocols*, nodes periodically propagate routing update advertisements to their neighbors in order to maintain up-to-date routing information. Routes are immediately available upon the request of a node. No periodical route information propagation is required. Proactive protocols are energy inefficient for several reasons: (i) the control message overhead grows quadratically with the number of nodes. The routing advertisement is introduced into the network by frequent system-wide broadcasting; (ii) nodes maintain routes for each destination in the network, which is nearly impossible for most of the nodes in a heterogeneous system [MMJ03]; (iii) a considerable fraction of the routes are never used and maintaining them causes unnecessary power consumption.

In *reactive routing protocols*, a route is discovered on demand when the source needs to send a packet to a destination. Routes are valid only for a limited period, after which are considered to be obsolete. Reactive protocols require less bandwidth and power than proactive ones, but discovering routes on demand leads to higher latency.

Hybrid protocols, such as Zone Routing Protocol (ZRP) [HP98] and Landmark Routing Protocol (LANMAR) [PGH00], combine the features of both proactive and reactive protocols. In a hybrid protocol, routes for a subset of nodes are maintained in a routing table proactively while routes for the remaining nodes are discovered when needed.

Location-aware protocols, such as Location-Aided Routing (LAR) [KV98] and Distance Routing Effect Algorithm for Mobility (DREAM) [BCS98] use information provided by an attached GPS unit. LAR is a reactive protocol that makes use of location information during the discovery process to reduce the overhead caused by flooding. LAR allows nodes to forward a packet only if they are located on the path towards the destination. As the location information might be approximate or outdated, instead of point locations LAR defines two zones: the *expected zone* of destination and the *request zone* of the sender. A route request is rebroadcasted only by nodes in the request zone. LAR can be applied in conjunction with existing reactive protocols such as DSR and AODV. Distance Routing Effect Algorithm for Mobility (DREAM) [BCS98] uses two techniques to reduce the amount of exchanged routing information. The first technique relies on the *distance effect*: the observation that the greater the distance between two nodes, the slower they appear to be moving with respect to each other. Accordingly, the location information in the routing tables can be updated less often for the nodes farther apart from each other, while preserving the routing accuracy. The second technique requires the nodes to determine their own mobility rate and send location updates more or less often depending on their mobility. Instead of maintaining a routing table of unique next hops for each destination, DREAM forwards packets to a set of recipients it believes to be located in the general direction that guarantees that the destination can be found with a given probability p. The data delivery in DREAM requires a considerable amount of duplicate copies, which consumes a lot of bandwidth and is energy inefficient for networks with high load and/or high node density.

Congestion control schemes [BDF01a, Pre05, HZ01] aim to avoid or resolve congestions at a node and divert the traffic to other routes. Boukerche *et. al.* [BDF01a] proposed a probabilistic congestion control scheme based on local tuning of protocol parameters for a randomized version of DSDV (R-DSDV). Different nodes can independently determine the routing table advertisement frequency according to probabilities. By reducing the routing table advertisement frequency, the congestion at a node can be resolved as the node reduces the traffic load routed through the node itself probabilistically. In [Pre05], the congestion control problem is addressed as a convex optimization problem with routing and link access constraints, which are described in a network traffic model and a link contention model. The solution is provided via a dual decomposition and sub-gradient algorithm. The scheme proposed in [HZ01] aims to route data packets circumventing congested path so that the traffic load over the network is balanced and the end-to-end delay is lowered. During the route setup stage, the destination selects the path with the minimum nodal activity; congested paths can be avoided as packets are transmitted along the least-active path. In our proposed approach, m-limited forwarding, we aim to reduce the contention and congestion at the locality of a node by limiting the number of nodes to rebroadcast a packet. With the advanced broadcast technique, supported by the m-limited forwarding, the packet delivery fraction and overall power consumption of all nodes are improved.

Low power consumption is critical for wireless communication protocols [JSA01, MDP02]. Mobile devices are generally operated by battery power, and in some situations the power source may not be rechargeable due to inaccessible terrains. Most of the current protocols calculate paths by minimizing either the hop count or the transmission delay. Nodes along the critical paths are chosen more often causing the depletion of their energy sooner than the other nodes. *Power-aware protocols* [SWR98, XHE01, SHM02] take into account power consumption when determining a route. In [ALF03], the authors propose to add a device-type aware into the routing protocol to force the externally-powered nodes to forward more traffic and perform additional routing functions than a battery-powered nodes, so that the system lifetime is prolonged.

Our proposed protocol, A^{4}LP, is both *location-* and *power-aware* routing protocol supporting asymmetric links that may be suitable for heterogeneous MANETs. We classify A^{4}LP as a hybrid protocol due to the following aspects. The routes to In-, Out-, and In/Out-bound are maintained by periodical neighbor updates and immediately available upon request, while the routes to other nodes in the network are obtained by a path discovery protocol. A^{4}LP introduces an advanced flooding technique - *m-limited forwarding*. Receivers can re-broadcast a packet only if it qualifies a certain *fitness* value specified by the sender. The flooding cost is reduced and shortest high quality path is likely to be selected as a result of m-limited forwarding. Moreover, the metrics used to choose from multiple paths are based on the *power consumed per packet* and *transmission latency*.

2.2 MAC Layer Protocols

MAC layer protocols allow a group of users to share a communication medium in a fair, stable, and efficient way. A MAC layer protocol for MANETs must address several specific problems:

1. Mobility - the connection between nodes can become unstable because of the independent movement of the nodes;
2. Higher error rates - a wireless channel has a higher *Bit Error Rate* (BER) than a wired network;
3. Inability to detect collisions during some periods of time - wireless transceivers work in a half-duplex mode; nodes do not "listen" when "talk" and do not "talk" when "listen". The sender is unable to detect the collision and the receiver is unable to notify the sender of the collision during the transmission of a packet. *Collision avoidance* is almost mandatory.

Carrier Sensing Multiple Access (CSMA) [KT75], requires every node to sense the channel before transmitting, and if the channel is busy, refrain from transmitting a packet. CSMA reduces the possibility of collisions in the vicinity of the sender. Multiple Access Collision Avoidance (MACA) [Kar90] and its variant MACAW [BDS94] are alternative medium access control schemes for wireless ad hoc networks that aim to solve the hidden node problem by reducing the possibility of collisions in the vicinity of the receiver.

The Floor Acquisition Multiple Access (FAMA) [FG95] protocol consists of both carrier sensing and a collision avoidance handshake between the sender and receiver of a packet. Once the control of the channel is assigned to one node, all other nodes in the network should become silent. Carrier Sensing Multiple Access based on Collision Avoidance (CSMA/CA), the combination of CSMA and MACA, is considered a variant of FAMA protocols. The IEEE 802.11 standard [MAC99] is the best-known instance of CSMA/CA.

The IEEE 802.11 standard specifies distributed coordinated function (DCF) and point coordination function (PCF) as two modes to access the medium. The DCF mode is mandatory and based on CSMA/CA protocol while the PCF mode is optional. Nodes working with DCF contend for the medium access and attempt to send frames when no other nodes are transmitting. If a node senses the medium is busy, it starts a random back off timer that generates a random period of time in its contention window, and wait for the next attempt until the timer expires. The random back off timer increases the chance of different nodes to re-attempt to transmit their data at a different time so that collisions are significantly reduced. Acknowledgements are required to be sent at the receiver since the sender cannot detect whether a collision has occurred. IEEE 802.11 employs a RTS/CTS handshake before the transmission of a long frame to notify hidden nodes to reserve the medium for that transmission. All nodes other than the sender and the receiver that receive the RTS/CTS packets will set their network allocation vector (NAV) periods according to the reservation time specified in the RTS/CTS packets. A node cannot attempt to send a frame when its NAV is not zero. The PCF is defined in the IEEE 802.11 standard to achieve quality of service (QoS) delivery and priority access for real-time traffic for infrastructure based ad hoc networks. The access point polls nodes according to a polling list during a contention-free period, only the polled station is allowed to transmitting data during a specific duration of time. PCF allows synchronous data frames since it is a contention-free protocol. However, there are few access point in the market that actually implement PCF. Other optional functions of the IEEE 802.11 standard include Wired Equivalent Privacy (WEP) protocol, Power Save Mode (PSM), Fragmentation, and so on.

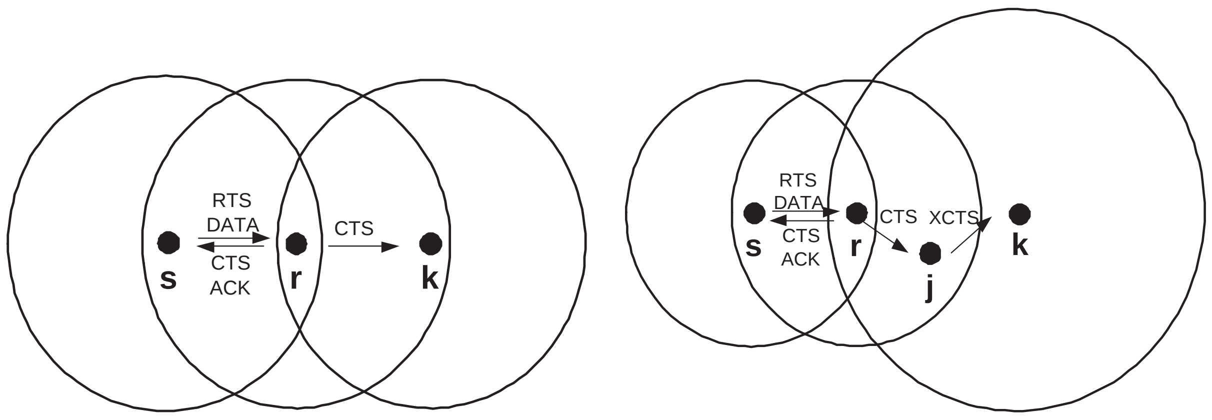

(a) (b)

Figure 2.1: (a) Hidden node problem in a "classical" wireless network with mobile nodes. All links are assumed to be bidirectional. A hidden node is a node out of the range of the sender and in the range of the receiver. Node k is a hidden node for a transmission from node s to node r. (b) Hidden node problem in a heterogeneous wireless network with mobile nodes. A hidden node is a node out of the range of the sender and whose range covers the receiver. Node k is a hidden node as for a transmission from node s to node r.

Several potential problems and issues of wireless ad hoc networks with unidirectional links have been addressed in [Pra99] and [Aga00]. One of the important issues is the hidden node problem, which becomes more complicated with the existence of unidirectional links. In a wireless network with symmetric links only, a *hidden node* is generally defined as *a node out of the range of the sender and in the range of the receiver* [Bha97]. According to this definition such a node is hidden from the sender but exposed from the receiver (See Figure 2.1(a)). The hidden node problem can be solved by a RTS/CTS handshake mechanism proposed by MACA [Kar90] (RTS stands for *Request to Send* and CTS for *Clear to Send*). [XHG03] analyzes the effectiveness of RTS/CTS handshake mechanism, and indicates that some of the hidden nodes may not be covered by the receiver due to the fact that it requires much lower power to interrupt a packet reception than to successfully deliver a packet.

We can define a hidden node in wireless ad hoc networks with asymmetric links as *a node out of the range of the sender and whose range covers the receiver* (See Figure 2.1(b)). Thus, a hidden node is hidden from the sender and possibly from the receiver as well. The RTS/CTS handshake mechanism is not a solution for such networks since a CTS packet may not be able to reach the hidden nodes.

Several solutions to the hidden node problem in wireless ad hoc networks with asymmetric links are discussed in the literature. Poojary et al. [PKD01] propose that a node rebroadcasts a CTS packet if it is received from a low-power node. To decrease the probability of collisions, each node waits a random number (1 . . . 6) of SIFS (Short Inter-Frame Spacing) periods before transmitting a CTS packet. Fujii et al. [FTB02] made several improvements relative to [PKD01]: (i) not only CTS but also RTS packets are rebroadcasted; (ii) nodes with a CTS packet to rebroadcast, first sense the channel and transmit only if the channel is not busy; and (iii) only high-power nodes rebroadcast RTS or CTS packets. The solutions proposed by [PKD01] and [FTB02] can lead to inefficient use of the channel if nodes are *misclassified* as hidden nodes. In such situations, nodes that could have been active are silenced due to misclassification, severely degrading the channel utilization. [PKD01] and [FTB02] routinely assume routing over symmetric links so that the sender is able to receive both CTS and ACK packets. In the presence of asymmetric links, however, the sender might not receive the CTS or ACK packets, thus the sender cannot trigger the transmission of DATA packets, and does not know whether a transmission was successful or not. The MAC layer protocol to be presented in Section 4.3 is designed to handle these situations as well.

Bao et al. [BG01] propose a collision-free dynamic channel access scheduling algorithm – PANAMA. Two scheduling algorithms are proposed for wireless networks with unidirectional links, NAMA-UN that is node activation oriented and supports broadcast traffic efficiently, and PAMA-UN that is link activation oriented and is more suitable for relaying unicast traffic. The channel access is allocated for NAMA-UN and PAMA-UN alternatively, with each scheduling algorithm lasting for a fixed amount of time. In PANAMA, the sender node is able to detect the hidden node that also attempts to relay traffic to the receiver. The winner of a contention is the node with higher priority. When the link from the hidden node to the receiver is unidirectional, the hidden node may not be aware of the sender. In these cases, the hidden node is automatically considered as having a higher priority.

The protocols considered previously are based on the modification of the MAC layer protocol. In contrast, the Sub Routing Layer (SRL) project [RM02, RCM02] handles asymmetric links by adding an intermediary layer between the MAC and network layers. This layer partially isolates the routing protocol from the MAC layer, although it still allows the routing protocol to directly contact the MAC layer. For unidirectional links, reverse paths are computed using the Reverse Distributed Bellman-Ford algorithm. The SRL implementation also signals the detection of new neighbors and the loss of (unidirectional) links.

In this dissertation, we are going to introduce a new MAC layer protocol for MANETs with Asymmetric links (AsyMAC). AsyMAC currently works with A^{4}LP, since they share the process of neighbor discovery and neighbor maintenance.

2.3 Analytical Models of Wireless Networks

As protocols for the communication networks are designed and developed, it is important to have their performance evaluated and justified before applying them into the industry. There are two general approaches to obtain such performance statistics, analytical modeling and simulation.

The research for analytical modeling of communication networks was started almost one century ago, with the works of A. K. Erlang [Erl09, Erl17]. Erlang's initiative is to develop a mathematical model for telephone traffic to predict the load on telephone stations and estimate the necessary equipment and personnel according to the number of subscribers. It might be out of Erlang's expectation that his work eventually becomes the foundation of the whole domain of applied probability, and is now called queueing theory. The queueing theory is extensively applied in the design and analysis of new networking protocols. Later, C. Shannon presented the mathematical theory of communications, which demonstrated the theoretical limits on the speed of information transmission over a noisy channel [Sha48, Sha49]. Shannon's work is considered as another cornerstone work since his mathematical theory gave a formal definition of communication systems for the first time, and it also introduced message coding as well as the entropy for information. Shannon's theory is particularly useful for wireless medium with lots of contenders, where a noisy channel can be abstracted and introduced to model the interfering signals from other devices nearby.

Analytical modeling of wireless networks is proposed in recent years as a way to analyze the performance of protocols and networking behaviors of wireless networks. However, the analytical modeling is not a universal technique to analyze the networking behaviors of wireless networks due to its limitations. For the physical layer, the connectivity between two nodes, or say link availability, is modeled. The *unit disk model* [SKM95] is a simple model in which two nodes are connected as long as they are within a distance r, and the distribution of the nodes is described by a uniform distribution in a compact region. The transmission regions of a node is represented by a disk of random radius or a random convex figure, which corresponds to the different transmitting powers of the nodes. Based on the unit disk model, the connectivity of the multi-hop networks is studied in [CR89, Pen97, GK98, XK04], and the throughput capacity is discussed in [GK00, Jac03]. The unit disk model ignores the interference effect at the receiving node imposed by the noise signals from its neighboring nodes, thus it is not applicable when the load of the network is relatively high. A more realistic signal reception model done by P. Jacquet [Jac98] and F. Baccelli, B. Blaszczyszyn and P. Mühlethaler [BBM03] is based on the Signal-to-Interference-Ratio (SIR) inequality that takes the noise signal into account. In the SIR based model, the connectivity of two nodes with distance R is defined as a *coverage* probability (p_R) that a node is located inside the coverage of the other node. The distribution of the nodes is generated by the Poisson point process $\chi = \{X_i\}$ with certain intensity λ, and the emitting power of the nodes P_i is another random variable. The coverage function of two nodes at distance R depends on the distribution of $\{P_i\}$. The solutions are given for the cases that $\{P_i\}$ has an exponential distribution and P_i is a constant [Jac98]. With the SIR based model, the connectivity of multi-hop networks is studied in [DBT03, DBT05], and the throughput capacity is discussed in [GT02]. The SIR based model is limited by the fact that p_R is difficult to be found for general distribution of $\{P_i\}$ [BBM03], which is the case for heterogeneous MANETs where all nodes have quite different communication capabilities. The geometric-free model is a solution for *a special case* of wireless networks in which the connectivity of two nodes is not dependent on their geographical locations due to random obstacles that partially block signals. Some characteristics of such model is studied in [CL03, GHH06]. As we can see, there are limitations on all the listed models for the physical layer: the unit disk model is not applicable when the network traffic becomes high; the SIR based model is limited for homogeneous MANETs or when the distribution of the emitting powers is known; the geometric-free model is only for a special case of wireless networks.

Analytical models for the MAC layer are studied in [Bia00, SKM03]. The backoff mechanism of IEEE 802.11 is studied under heavy traffic assumption with a Markov chain model that approximates the evolution of the delay timer. Two important behaviors for MAC protocols are discussed: (1) the probability that a transmission occurring at a channel is successful; and (2) the maximal achievable throughput. One of the main assumptions of most models of MAC layer is that the probability of a collision p_c for a node that is trying to transmit is constant. Although the underlying physical model is not explicitly mentioned, according to the above assumption, we can conclude that the analytical model is limited to wireless networks that (1) the nodes in the networks are uniformly distributed; (2) all the nodes should transmit with a constant emitting power; (3) the network traffic is fully loaded at each node. The MAC layer model is limited if any of the above conditions is not met, since any of the violation may lead to a non-constant collision probability p_c. The models proposed in [Bia00, SKM03] only models a simplified version of IEEE 802.11, in which the RTS/CTS handshake is not taken into account and hidden node problem is not analyzed as well.

For the network layer, several analytical models are proposed to solve the problem on which the model is concerned. In the work [CJV02], T. Clausen, P. Jacquet and L. Viennot analyzed the average path length for the routing protocols that use flooding during their path discovery phase, such as AODV [PR99] and DSR [JM96]. The network performance of OLSR [CJL01] is investigated in [JV00, CJV04, ABJ03]. A study of AODV and the performance compared to OLSR is introduced in [Leb05, Leb06], in which the analytical model relies on the SIR based physical model [Jac98, BBM03] and the MAC layer model proposed in [Bia00, SKM03]. Since there are too many state variables in the network layer, the analytical model for the network layer fails or becomes inaccurate as long as some of the state variables are unavailable, guessed, approximated, or impractical to be modeled.

As discussed above, the current analytic models of wireless networks for the physical, MAC and network layers have many unsolved issues and problems, which could keep researchers from conducting performance measurements for wireless networks solely based on such models. Thus, after a review of the literature on the analytical modeling of wireless networks, we are more confident to claim that simulation is the only practical alternative to investigate the performance of protocols for wireless networks.

2.4 The Time-Parallel Simulation

Simulation of wireless networks is important for protocol design and wireless system research. As the research progresses from relatively simple systems composed of several nodes connected to a wireless access point to large systems which might be composed of thousands of nodes (such as wireless sensor networks), the size of the simulation problem becomes so large that it clearly exceeds the capabilities of a single machine. Therefore, it is important to look into parallel simulation approaches. Parallel discrete event simulation (PDES) reduces the overall execution time by parallel execution of the simulation on multiple processors. There are two main avenues for parallel simulation: space-parallel simulation (distributed simulation), and time-parallel simulation. In the space-parallel simulation approach [Fuj90, MWM91], the simulation model is decomposed into a number of components on a spatial basis. Each component is modeled by a *logical processor*. Logical processors establish a communication mechanism among each other to avoid or fix possible causality errors. There are two general mechanisms to avoid/correct causality errors: optimistic mechanisms and conservative mechanisms. With optimistic mechanisms [Jef85], a processor can execute an event e without the knowledge of its prior events, and state recovery methods [SE98, Qua01, QS03b, QS03a] are required to restore the state of the simulation once causality errors are detected. Instances of optimistic space-parallel simulations include [CFE94, CFL95, Fuj89, Bri91, Wie01, QS03b, QS03a]. In conservative simulations, a processor does not execute an event e until all events that may affect event e are executed. Instances of conservative space-parallel simulations include [LL90, Nic92, HN93, PDN].

Load balancing in PDES refers to distributing the workload over different processors evenly. An efficient load balancing scheme can greatly improve the speedup of PDES, due to the fact that the overall progress of the simulation is decided by the progress of the slowest processor. Various load balancing approaches for space-parallel simulations can be found in [DHB00, RJ90, GT93, BT94, AT96, WN96, BD97, DS98, CT99, SS00].

The Parallel/Distributed Network Simulator (PDNS) [PDN] project uses a space-parallel simulation approach based on the NS-2 network simulator [VIN]. However, the applicability of PDNS is limited to *wired* networks, and the traffic simulated at different spatial partitions cannot affect each other. The SWiMNet parallel simulator [BDF99, BF00, BDF01b], is used for the simulation of personal communication services (PCS) networks with fixed channel assignment by specifying fine grained mobility, variable call process, and arbitrary coverage area. It is based on a combination of optimistic and conservative paradigms and makes use of the event pre-computation by the model independence within the PCS model. WiPPET [PKL98], an optimistic parallel simulator for evaluating the performance of wireless protocols, exploits the parallelism of multi-channel radio networks either by geographic locations of the resources or by different radio channels. Table 2.1 presents a comparison of PDNS, SWiMNet, WiPPET and the time-parallel simulation approach proposed in this work.

Table 2.1: A comparison of PDNS, SWiMNet, WiPPET and the time-parallel simulation approach (TPS) proposed in this work

	PDNS	**SWiMNet**	**WiPPET**	**TPS**
Application domain	wired networks	PCS networks	multi-channel radio networks	wireless ad hoc networks
Parallelism	space-parallel	space-parallel	space-parallel	time-parallel
Error Control Scheme	conservative	conservative / optimistic	optimistic	state matching
Main Issues	The interference between different logic processors must be limited. The optimistic approach requires a large amount of memory.			Efficient estimation of the initial state of the simulation segments.

In the time-parallel simulation approach [AO95, HA96, HA98, LL91, WA92, WA93], the long period of simulation time is partitioned into smaller adjacent simulation intervals, and each simulation interval is assigned to a processor with a *guessed* initial state. The simulation terminates when the final state of each interval matches the initial state of its successive interval. Thus, state matching is one of the key problems of time-parallel simulation. In [LL91], the authors propose a time-parallel simulation algorithm based on state matching. A simulation is defined as *partial regenerative* if there exists a subset of the system state variables such that the subsystem represented by the subset can repeat its state infinitely. The system is then partitioned at the *regeneration points* which starts a *regenerative substate*. [NFC93, NFC94] indicate that in some cases the *regeneration points* of a regenerative simulation can be found without performing a detailed simulation; the state matching problem can be solved by performing a pre-computation. Wang and Abrams propose a *pre-simulation* to identify regenerative points by using Markovian modeling [WA93].

Kiesling [Kie05] mentioned that the widespread use of time-parallel simulation is restricted by the state-match problem, due to the difficulty in identifying regeneration points, especially for models with complex states. Unfortunately, time-parallel simulation of wireless networks belongs to this category. Kiesling pointed out that the use of approximate solutions can facilitate the temporal decomposition of simulation models. Since errors are introduced, an error control method must be provided for approximate time-parallel simulation. The simulation starts with guessed incorrect initial states, and fix-up computations are re-executed to reduce the error. Although time-parallel simulation rarely allows us to obtain accurate results, approximate results [HA98, WA92, Kie04, Kie05] can be produced efficiently.

The major difficulty in the parallel simulation approaches is to solve the dependencies among the partitions. A careful study of the temporal dependencies for wireless networks with various traffic patterns shows that there are few strong dependencies which span a large temporal interval. By ignoring the weak dependencies we can achieve fast simulation results which are a good approximation of the exact results. Furthermore, we can assemble a system where coarse approximations are obtained very quickly, while the continuation of the simulation process yields results with increasingly higher precision. In the knowledge of the approximate results, the researcher might decide whether the expensive continuation of the simulation is justified or not.

CHAPTER 3
IMPROVING ROUTING PERFORMANCE THROUGH M-LIMITED FORWARDING IN POWER-CONSTRAINED WIRELESS AD HOC NETWORKS

Ad hoc routing protocols use nodes with limited power reserves for forwarding packets in wireless ad hoc networks. Most routing protocols disseminate routing information by flooding, a technique which requires a significant consumption of energy and bandwidth.

m-limited forwarding [WJM04, WTB07a] is a technique to reduce the cost of disseminating information in a power-constrained environment by limiting the cardinality of the subset of nodes which retransmit a packet. In case of flooding, the number of messages increases geometrically with the distance from the source while for m-limited forwarding the increase is only linear. In this chapter, we analyze m-limited forwarding and perform a simulation study in networks with symmetric and asymmetric links. Our performance studies report on power savings and packet loss for a location-aware mobile ad hoc network.

The chapter is organized as follows. Section 3.1 introduces m-limited forwarding along with two forwarding fitness functions: distance-based and area-based fitness functions. We also present a variant of the Ad-hoc On-demand Distance Vector (AODV) routing protocol [PR99], m-AODV, which is modified from the AODV source code in NS-2 to support m-limited forwarding. Section 3.2 describes the simulation environment and presents the results of the simulation study with a discussion of the effect of network load, node mobility, and node density. The optimal values of m are discussed followed by a comparison of AODV, Location-Aided Routing (LAR), and m-AODV with two forwarding fitness functions. We also compare m-A^{4}LP using the two forwarding fitness functions with AODV in heterogeneous network scenarios. We summarize our findings in Section 3.3.

3.1 m-limited Forwarding

Maintaining the routing tables of the nodes of an ad hoc network up-to-date can consume a large fraction of the network bandwidth and requires a significant power consumption, especially when high node mobility demands frequent updates and when routing information is disseminated by flooding. Thus, techniques which improve on the dissemination of routing information can significantly improve the performance of the routing protocols.

m-limited forwarding [WJM04, WTB07a] is a technique to reduce the cost of disseminating information in a power-constrained environment by limiting the cardinality of the subset of nodes which will retransmit a packet. In case of flooding, when node j transmits a route update packet, all neighbors within the transmission range of the node retransmit the packet. We wish to limit the size of the subset of nodes which forward the packet to at most m. The nodes in this subset, called *m-forwarding subset* should be the ones optimally positioned vis-a-vis the packet destination node and with the most favorable balance of power. The parameter m must satisfy a subset of sometimes contradictory requirements, e.g., minimize the power consumption, ensure some stability of the routes when the nodes move within a certain area, minimize error rates, and minimize the number of retransmissions.

Whenever a packet is sent from node j to node i the sender of a packet provides a "hint" in the form of a *forwarding cutoff*, $\kappa(i,j)$ which is attached to the transmitted packet. Each node k determines if it belongs to the selected subset by evaluating its own *forwarding fitness function* $\mathcal{F}_k(i,j)$ related to the current transmission and compares the value of this function with the forwarding cutoff. The node k forwards the packet if and only if its fitness is higher than the forwarding cutoff. If the location of the destination is not known, the sender sets $\kappa(i,j) = -1$ and all nodes will retransmit the packet.

The forwarding cutoff is set such that in average m nodes forward the packet at every hop. Note that information regarding the position and the residual power of each node in the set may not be very accurate, due to node mobility and to node activity which affects the residual power. As a result, the forwarding cutoff may allow fewer than m nodes to forward, if some have moved away from their location known to node j, or have further depleted their power reserves. The actual number of nodes forwarding the packet may be larger than m if new nodes have moved into the optimal forwarding area, or recharged their batteries.

We assume that none of the nodes attempts to save power by refusing to replay packets. Non-cooperative nodes may affect the proper functionality of the protocol in many ways, as discussed in Section 3.3.

3.1.1 Alternative Forwarding Fitness Functions

The forwarding fitness function $\mathcal{F}_k(i,j)$ measures the fitness of a node k as the next hop, where j is the sender and i is the destination. Depending on the definition of "fitness" we can define several alternative fitness functions.

The *distance-based forwarding fitness function* $\mathcal{F}^d$ is defined by the following expression:

$$\mathcal{F}^d_k(i,j) = \frac{1}{d_{ik}+1} \tag{3.1}$$

where j is the sender, i is the destination, k is the next hop candidate, d_{ik} is the distance between node i and node k. Note that the function has a value of 1 when the distance to the destination is 0, and is gradually decreasing to 0 as the distance of destination increases.

This function favors the nodes closest to the destination node i and still reachable from node j. This is the optimal choice in a network where all nodes have the same transmission range.

However, in networks which include nodes with different transmission ranges, this greedy approach can be suboptimal. To illustrate this, let us consider the scenario in Figure 3.1. The scenario contains the sender j, the destination i, and two candidate nodes k_1 and k_2 as the next hop on the path from j to i. The transmission range of a node is a circle centered at the current location of the node: Π_j, Π_{k_1}, and Π_{k_2}. Intuitively, node k_2 is a better choice than node k_1 when routing from j to i, although it is actually in the opposite direction from j. However, the larger transmission range of k_2 compensates for its less advantageous geographic location.

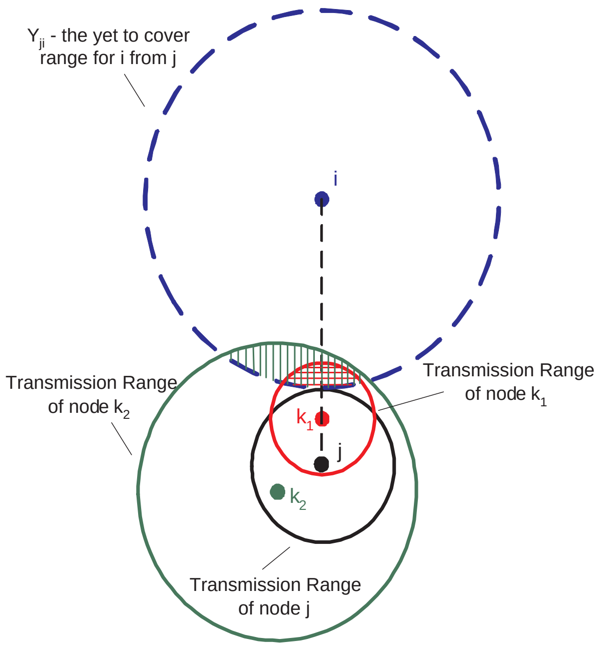
Y_{ji} - the yet to cover range for i from j
i
Transmission Range of node k_2
Transmission Range of node k_1
k_1
j
k_2
Transmission Range of node j

Figure 3.1: A configuration including the sender j, the destination i, and two candidate nodes k_1 and k_2 as the next hop on the path from j to i. The circles centered at the current location with the radius equal to the range of these nodes, Π_j, Π_{k_1}, and Π_{k_2} are also shown. The circle centered at the current position of node i and with a radius equal to $d_{ij} - R_j$ is called the "complementary range of j to reach i" and denoted by $\Gamma_{i,j}$. Call $\Lambda_k(i,j)$ the area of the intersection of $\Gamma_{i,j}$ and Π_k. We see that $\Lambda_{k_1}(i,j) < \Lambda_{k_2}(i,j)$.

Based on this observation, we develop a somewhat more complex *area-based forwarding fitness function* in an attempt to optimize the number of "favorable" nodes towards the destination reachable from the new node, but not from the current one. We define "favorable" as the nodes closer to the destination than the maximum range of the current node. We assume that the nodes of the network are uniformly distributed, i.e. that the number of nodes in a given area is proportional with the size of the area. This simplified assumption will be relaxed in the future as discussed in Section 3.3.

The circle centered at the destination i and with a radius r_{ij} equal to $d_{ij} - R_j$ is called the "complementary range of j to reach i" and denoted by $\Gamma_{i,j}$. Call $\Lambda_k(i,j)$ the area of the intersection of $\Gamma_{i,j}$ and Π_k. In our example in Figure 3.1, $\Lambda_{k_1}(i,j) < \Lambda_{k_2}(i,j)$. We will use the $\Lambda_k(i,j)$ as the new forwarding fitness function:

$$\mathcal{F}_k^a(i,j) = \Lambda_k(i,j) \tag{3.2}$$

In the following, we derive an analytic expression for $\Lambda_k(i,j)$. The relationship between $\Lambda_k(i,j)$ and Π_k can be *exterior*, *exterior tangent*, *secant*, *interior tangent* or *interior*. We notice that interior tangent and interior cannot happen when $\Gamma_{i,j}$ covers Π_k since the center of Π_k is outside of $\Gamma_{i,j}$. In case $d_{ik} \geq R_k + r_{ij}$, the two circles $\Gamma_{i,j}$ and Π_k are exterior or exterior tangent, thus $\Lambda_k(i,j) = 0$. In the case when $d_{ik} \leq R_k - r_{ij}$, the two circles $\Gamma_{i,j}$ and Π_k are either interior or interior tangent, thus $\Lambda_k(i,j) = area(\Gamma(i,j)) = \pi r_{ij}^2$.

In case $R_k - r_{ij} < d_{ik} < R_k + r_{ij}$, two circles $\Gamma_{i,j}$ and Π_k are secant. In Figure 3.2, the area of the overlapping region is the sum of two areas: (1) the area enclosed by arc $\widehat{ANB}$ and line segment $\overline{AOB}$, called $area(ANBO)$; (2) the area enclosed by arc $\widehat{AMB}$ and line segment $\overline{AOB}$, called $area(AMBO)$. $area(ANBO)$ is the difference between area of the sector enclosed by line segment $\overline{KA}$, arc $\widehat{ANB}$ and line segment $\overline{BK}$ and the area of the triangle KAB. Denote the $\theta = \angle AKB$, $\varphi = \angle AIB$. By the "law of cosines", $\theta = 2\arccos(\frac{R_k^2+d_{ik}^2-r_{ij}^2}{2 \cdot R_k \cdot d_{ik}})$, and

$$\begin{aligned} area(ANBO) &= area(KANB) - area(KAB) \\ &= \frac{1}{2}\theta|\overline{KA}|^2 - 2 \cdot \frac{1}{2}(|\overline{KA}|sin\frac{\theta}{2})(|\overline{KA}|cos\frac{\theta}{2}) \\ &= \frac{1}{2}R_k^2(\theta - sin\theta). \end{aligned} \tag{3.3}$$

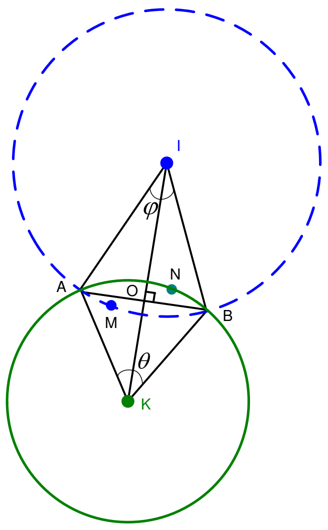

Figure 3.2: The area of the overlapping region is the sum of area(ANBO) and area(AMBO). The area(ANBO) is the difference of sector(KANB) and triangle(KAB). The area(AMBO) is the difference of sector(IANB) and triangle(IAB).

Similarly, $\varphi = 2\arccos(\frac{r_{ij}^2+d_{ik}^2-R_k^2}{2\cdot r_{ij}\cdot d_{ik}})$, and $area(AMBO) = \frac{1}{2}r_{ij}^2(\varphi - sin\varphi)$. Thus,

$$\Lambda_k(i,j) = \frac{1}{2}(R_k^2(\theta - sin\theta) + r_{ij}^2(\varphi - sin\varphi)) \tag{3.4}$$

To summarize the above discussed cases in a single expression:

$$\mathcal{F}_k^a(i,j) = \begin{cases} 0 & \text{if } R_k \le d_{ik} - r_{ij}; \\ \dfrac{R_k^2(\theta - sin\theta) + r_{ij}^2(\varphi - sin\varphi)}{2} & \text{if } \; d_{ki} - r_{ij} < R_k < d_{ki} + r_{ij} \\ \pi \cdot r_{ij}^2 & \text{if } R_k \ge d_{ki} + r_{ij}. \end{cases} \tag{3.5}$$

where R_k is the range of node k, $r_{ij} = d_{ij} - R_j$, $\theta = 2\arccos\frac{R_k^2+d_{ik}^2-r_{ij}^2}{2\cdot R_k\cdot d_{ki}}$, and $\varphi = 2\arccos\frac{r_{ij}^2+d_{ik}^2-R_k^2}{2\cdot r_{ij}\cdot d_{ik}}$.

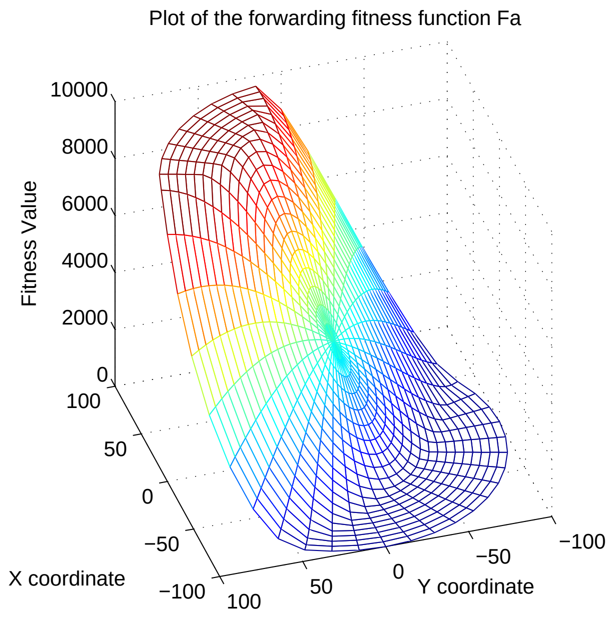

Figure 3.3: The plot of the area-based forwarding fitness function $\mathcal{F}_k^a(i,j)$ in function of the location of the candidate node. The current node is at (0,0) while the destination node is at (110,110). The function is plotted for a candidate node k with transmission range of 150 meters and locations spanning the transmission range of the current node.

Figure 3.3 shows the forwarding fitness function candidate node k with a transmission range of 150 meters and varying location. The sender is at location (0, 0), the destination is at location (110, 110), and the current node as well as the destination node has a transmission range of 100 meters. Note that the value of the fitness is zero in the area where the candidate node can provide no benefit compared to the current node. Similarly, the fitness has a maximum value of 10000 in the zones where the transmission range of the candidate node is completely covering the transmission range of the destination. Note that the fitness has positive values even in some of the zones which are opposite to the destination, due to the fact that the candidate node has a larger transmission range than the current node, which compensates for its unfavorable location.

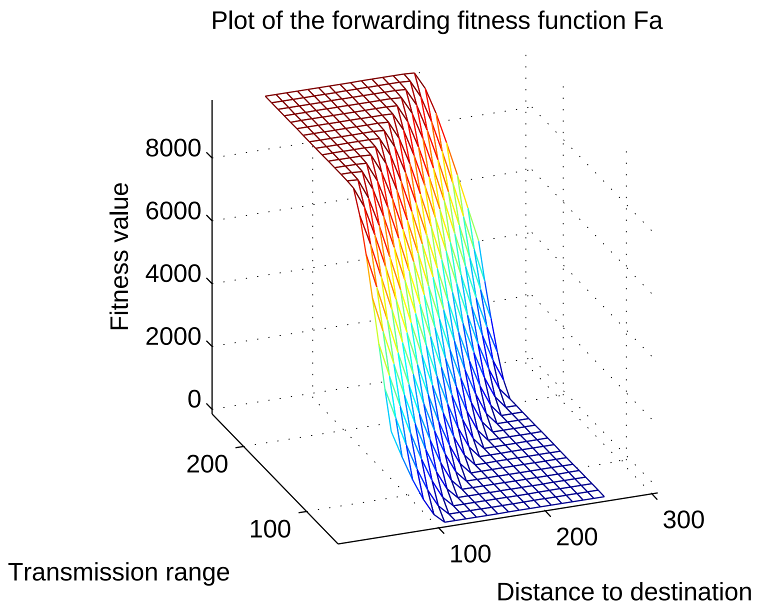

Figure 3.4: The plot of the area-based forwarding fitness function $\mathcal{F}_k^a(i,j)$, for candidate node k with different location and different transmission range. The scenario is the same as above except the transmission range is variable in the range of [50, 250].

Figure 3.4 plots the forwarding fitness function $\mathcal{F}^a$ for the case circle $\Gamma_{i,j}$ and Π_k are secant, for candidate node k with different location and different transmission range. The scenario is the same as above except the transmission range is variable in the range of [50, 250]. We combine the location of candidate node k to a single parameter - distance to the destination. The distance between node k and the destination is in the range $[110\sqrt{2} - 100, 110\sqrt{2} + 100]$. The figure indicates the fitness value increases as the transmission range of candidate node increases, or the distance to the destination decreases, or both. The fitness value achieves maximum when candidate node is nearest to the destination and with largest transmission range.

3.1.2 Ad hoc On-Demand Distance Vector Routing with m-Limited Forwarding (m-AODV)

Ad hoc On-Demand Distance Vector Routing (AODV) [PR99] is a reactive algorithm where routes are discovered and established only on demand and are maintained only if they are used by some sources. Nodes that do not lie on active paths do not maintain routing information or exchange routing tables. Only symmetric links participate in routing which is ensured by periodical *hello* packets. The freshness of routes are ensured by sequence numbers as well as route maintenance.

We introduce a modified algorithm m-AODV which replaces flooding with m-limited forwarding in the route discovery process, and it is based upon the following modifications to AODV:

1. We added the transmission range of the node to the *hello* packet of AODV. When a node receives a *hello* packet from its neighbor, the node adds the neighbor as well as its transmission range into the *neighbor table*.

2. We introduced the *location-update* packet, which is an infrequent system-wide broadcast packet. A *location-update* packet contains the id of a node and its location. When a node receives a *location-update* packet from any other node in the system, it adds the sender as well as its location information into a *location table*.

3. Route discovery is done through the m-limited forwarding algorithm. The forwarding fitness function is evaluated based on the information in the neighbor and location tables. We support the distance-based $\mathcal{F}^d$ as well as the area-based $\mathcal{F}^a$ fitness functions.

3.2 Simulation Study

In this section, we report the results of a simulation study. The objectives of our simulation study are twofold. First, we aim to determine the optimal values of m for m-limited forwarding. Although theoretical considerations allow us to determine that the optimal range is in the low single digits, the problem is too complex for an analytical solution. Therefore, we will determine the optimal value by studying the performance in a simulation environment. The second objective is to study the impact of m-limited forwarding on the performance of the routing algorithm. For this study, we have implemented the m-AODV routing protocol as presented in Section 3.1.2 in the NS-2 simulator [BEF00, VIN]. We implemented m-AODV using both proposed fitness functions, $\mathcal{F}^d$ and $\mathcal{F}^a$. We compared our implementation of the m-AODV algorithm with the default AODV implementation from the CMU wireless extension package [CMU]. We compared the routing algorithms in terms of average power consumption and packet loss ratio.

To perform a meaningful comparison of the algorithms, we created a scenario of a wireless system with mobile nodes and realistic traffic patterns. To describe the movement of nodes in the system we used the "random waypoint" model [BMJ98, JM96]. Each node randomly picks a destination on the map, moves to the destination at a *constant speed*, and then pauses for the *pause time*. After the pause time, it continues the movement following the same pattern.

In our simulations, we use traffic patterns generated by *Constant Bit Rate* (CBR) sources sending UDP packets to another node. A node cannot be simultaneously source and destination. Each CBR source is active for a time interval called *CBR duration*. Our simulation allows a *setup duration* before generating any traffic, during which the sender may transmit *hello* and *location-update* packets. We also set an *end duration*, during which CBR sources are not allowed to send data packets, so that data packets will not be lost due to the lack of simulation time. The remaining simulation time, the time after the *setup duration* and before the *end duration*, is divided into equal time slices. During each time slice, we regenerate CBR sources for different pairs of senders and destinations. The start time of the CBR source is randomly picked in the first half of the time slice, and the *CBR duration* is set to half of the *time slice* so that it will not cross two *time slices*. Figure 3.5 illustrates the relationship among *simulation time*, *setup duration*, *end duration*, *time slice* and *CBR duration*. The CBR sources generate 128-byte packets (in general small data packets favor AODV [DPR01]).

In our simulation, we choose a 500×500 m^2 square area and the default number of nodes is 80. Every node has a transmission range of 100 meters. We run several simulation experiments and vary the number of nodes, the speed in the "random waypoint" model, and the number of CBR sources. The number of nodes ranges from 50 to 140, the node speed ranges from 1 to 10 m/s, and

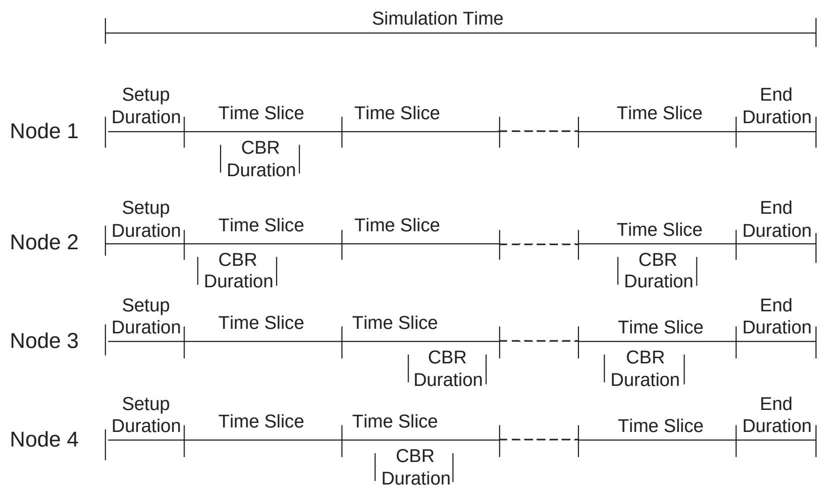

Figure 3.5: The illustration of relationship among *simulation time*, *setup duration*, *end duration*, *time slice* and *CBR duration*. Four nodes and two CBR sources are included in this example.

the number of CBR sources ranges from 4 to half of number of the nodes. Table 3.1 illustrates the default settings and the range of the parameters for our simulation experiments.

Table 3.1: The default values and the range of the parameters for our simulation studies

Field	**Value**	**Range**
simulation area	500×500 (m^2)	
number of nodes	80	50 - 140
transmission range	100 (m)	
speed	1 (m/s)	1 - 10 (m/s)
pause time	15 (s)	
total simulation time	900 (s)	
setup duration	50 (s)	
end duration	50 (s)	
duration of time slices	10 (s)	
number of CBR sources	25	4 - 40
offered network load	25 (Kbps)	4 - 40 (Kbps)
CBR packet size	128 (bytes)	
CBR sending rate	1 (Kbps)	
CBR duration	5 (s)	

3.2.1 Performance Metrics

We consider two performance metrics:

- *Packet Loss Ratio* – The ratio of all data packets received to the number of data packets sent during the simulation.

- *Average Power Consumption Per Node* – The ratio of total power dissipated by all nodes to the number of nodes in the network, during the simulation. Nodes dissipate power in the following actions: transmitting packets, receiving (overhearing) packets, and idle listening.

For each setting (fixed number of CBR sources, fixed speed, fixed number of nodes), we repeat the simulation 20 times with different randomization seeds. These two performance metrics are studied for varying network load, node mobility, and node density.

3.2.2 Determining the Optimal Value of m

Intuitively, the optimal value of m is a small, single digit number. A large value would not provide any benefit compared to flooding, while a too small value would adversely affect the routing performance through the lack of redundancy. The problem is too complex for an analytical solution, but we can determine the optimal value through simulation (as well as experimentally in a real setting).

In a series of experiments, we have investigated 1-, 2-, 3-, and 4-limited forwarding using both fitness functions $\mathcal{F}^d$ and $\mathcal{F}^a$. A rough estimation of the average number of neighbors of a node in our scenario follows: the simulation area is 250000 m^2 (500m $\times$ 500m). The average node density is $\frac{80}{250000} = \frac{1}{3125}$. The transmission range of a node is a disk of 100m radius, thus the transmission area covers $10000\pi \approx 31400$ m^2. In average we will have about 10 nodes in that area, one being the node considered and the other 9 being its neighbors (in fact, considering the nodes close to the edge of the simulated area, the average number of neighbors is somewhat lower). Thus, values of m larger than 4 are very close to the flooding technique.

The metrics considered in the determination of the optimal m are the packet loss ratio and average power consumption. We are not considering the average latency, due to its dependency on the packet loss ratio.

Routing performance function of network load. The packet loss for AODV or m-AODV protocols can be due to the following reasons: (i) the forwarding set calculated by the fitness function excludes nodes on the critical path from the source node to the destination node; (ii) nodes move out a region and cause route failure; (iii) due to frequent changes of the network topology the cached routing tables become outdated; and (iv) packets are lost at the MAC layer. There are several reasons for a packet to be dropped at the MAC layer. In a static network, a packet is dropped after its transmission was retried 16 times with a limited binary exponential backoff algorithm. In a mobile ad hoc network, however, a failure at the MAC layer occurs when the nodes move out from transmission range while waiting for a right to transmit or waiting for their retransmission time. A packet may be lost after the first collision, because by the time it retransmits, the node is no longer in the transmission range. Similarly, a packet can be lost even before the first transmission if the destination node moves out of the transmission range while the source node is waiting for an available transmission slot.

Figures 3.6(a) and 3.6(b) illustrate the packet loss ratio versus network load, with fitness functions $\mathcal{F}^d$ and $\mathcal{F}^a$ respectively. The major reasons for 1-limited forwarding to drop packets are (i) and (ii); while the major reason for 4-limited forwarding and flooding to drop packets is (iv) in this scenario. When the traffic load is light, (i) and (ii) are the major reasons, 1-limited forwarding performs the worst, while the performance of 2-, 3-, 4-limited forwarding are comparable and their curves almost merge. When the traffic load is high, (iv) becomes the major reason of packet loss, thus the performance of 4-limited is degraded compared to 2-, 3-limited forwarding and tends to increase with the increase of network load. For the flooding based scheme, (iv) is always the major issue, thus it performs much worse than m-limited forwarding based scheme in most cases. For flooding based protocols the (i) reason is not relevant, as there is no fitness function based decision whether to forward a packet or not.

With AODV, the power consumption is caused by (i) transmission, reception, or overhearing of data packets and route discovery packets; (ii) idle listening; and (iii) MAC layer overhead including RTS/CTS, retransmission, and so on. With m-AODV, additional power is consumed by (iv) transmission and reception of *hello* packets and *location-update* packets.

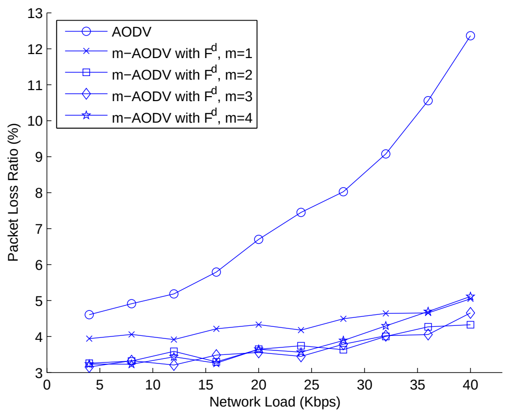

(a)

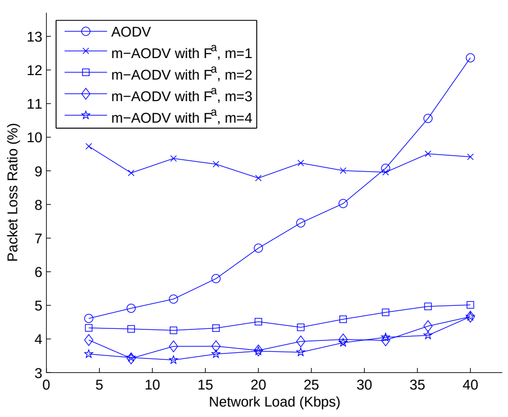

(b)

Figure 3.6: Packet loss ratio versus network load. Number of nodes = 80, Speed = 1 m/s, m = 1,2,3,4. (a) m-AODV with distance-based fitness function $\mathcal{F}^d$; (b) m-AODV with area-based fitness function $\mathcal{F}^a$. m-AODV with both fitness functions outperforms AODV, for all $m >= 2$. $m = 2$ and $m = 3$ are better options for both fitness functions.

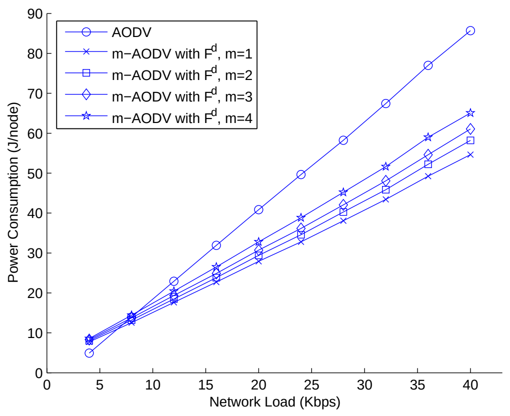

(a)

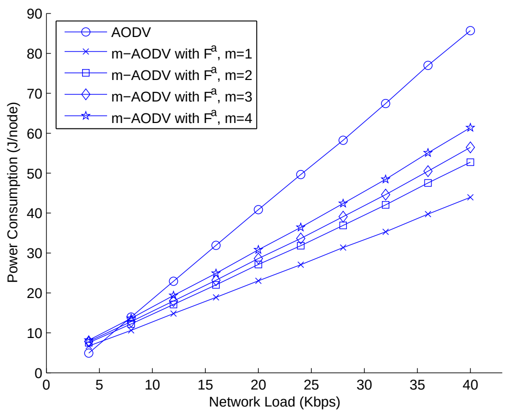

(b)

Figure 3.7: Average power consumption versus network load. Number of nodes = 80, Speed = 1 m/s, m=1,2,3,4. (a) m-AODV with distance-based fitness function $\mathcal{F}^d$; (b) m-AODV with area-based fitness function $\mathcal{F}^a$. The average power consumption increases linearly as the network load increases. m-AODV with area-based fitness function $\mathcal{F}^a$ consumes less power than m-AODV with distance-based fitness function $\mathcal{F}^d$ for the same network load.

Figures 3.7(a) and 3.7(b) illustrate the average power consumption function of the network load, for both fitness functions $\mathcal{F}^d$ and $\mathcal{F}^a$. The average power consumption increases linearly as the network load increases. When the network load is light, AODV consumes the least power since it does not need to send *hello* packets or *location-update* packets. As the network load increases, as expected, AODV needs more power than m-AODV. m_1-AODV consumes less power than m_2-AODV for $1 \leq m_1 < m_2 \leq 4$, for both fitness functions. m-AODV with fitness function $\mathcal{F}^a$ consumes less power than m-AODV with fitness function $\mathcal{F}^d$ for the same network load.

Routing performance function of node mobility. Figures 3.8(a) and 3.8(b) illustrate the packet loss ratio versus node mobility, for both fitness functions $\mathcal{F}^d$ and $\mathcal{F}^a$. Node mobility is measured by the speed of the node movement. The packet loss ratio of 1-limited forwarding is noticeably greater than all other schemes as the node mobility increases. When the node mobility is relatively high, 4-limited forwarding performs the best, followed by 3-limited forwarding and flooding. As the node mobility increases, the performance of 2-limited forwarding becomes a little worse than AODV. Thus, m = 1 is an unacceptable value as it is not suitable for networks with a relatively high node mobility. $m = 3$ and $m = 4$ are better options when node mobility is relatively high.

Figures 3.9(a) and 3.9(b) illustrate the average power consumption versus node mobility, for both fitness functions $\mathcal{F}^d$ and $\mathcal{F}^a$. We find that AODV consumes the most power, while among the m-limited schemes, 1-limited forwarding consumes the least power, followed by 2-, 3-, 4-limited forwarding. When node mobility increases, the routing table becomes outdated quickly

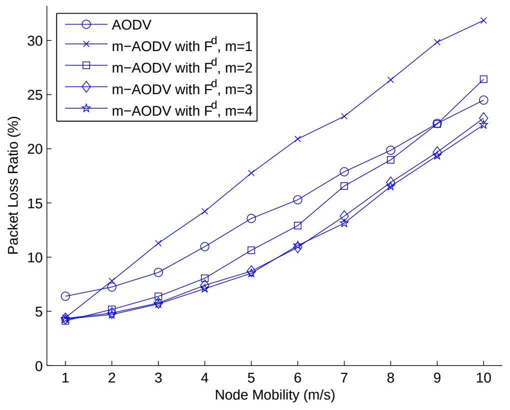

(a)

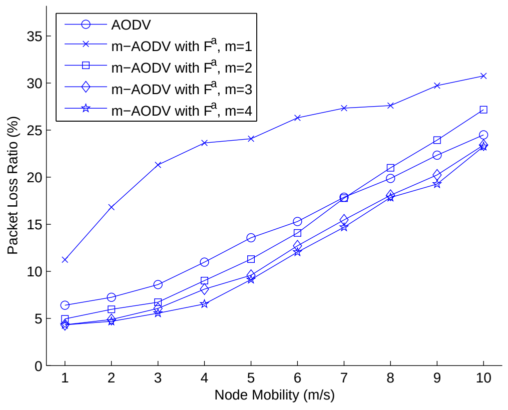

(b)

Figure 3.8: Packet loss ratio versus node mobility. Number of nodes = 80, Offered load = 25 Kbps, m=1,2,3,4. (a) m-AODV with distance-based fitness function $\mathcal{F}^d$; (b) m-AODV with area-based fitness function $\mathcal{F}^a$. The packet loss ratio of 1-limited forwarding is noticeably the greatest. $m = 3$ and $m = 4$ are better options when the node mobility is relatively high.

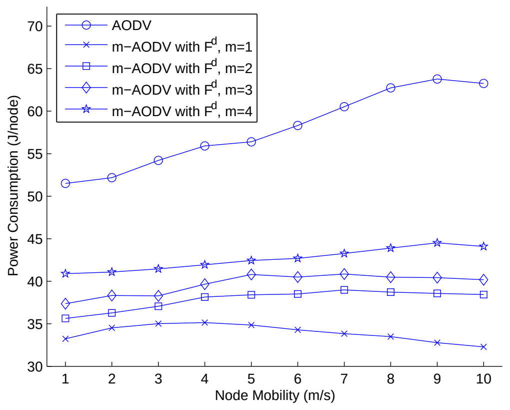

(a)

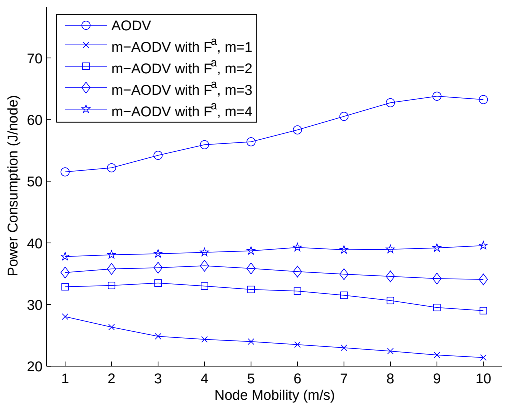

(b)

Figure 3.9: Average power consumption versus node mobility. Number of nodes = 80, Offered load = 25 Kbps, m=1,2,3,4. (a) m-AODV with distance-based fitness function $\mathcal{F}^d$; (b) m-AODV with area-based fitness function $\mathcal{F}^a$. AODV consumes the most power. Among the m-limited schemes, 1-limited forwarding consumes the least power, followed by 2-, 3-, 4-limited forwarding.

and additional power is dissipated to find new routes, thus the average power consumption of all routing schemes increases. However, as node mobility is further increased, the packet loss ratio increases thus the power consumed for transmitting and receiving data packets is reduced as more data packets are dropped. For all schemes based on m-limited forwarding, the portion of power consumption reduced by dropping data packets exceeds the additional power used to find new routes, thus the overall power consumption is reduced. The power used to find new routes by the AODV protocol is still the dominating factor of power consumption, thus the average power consumption still increases. Overall, the average power consumption increases steadily with the mobility for the AODV protocol. The average power consumption increases to a maximum value, then decreases with the further increase of the node mobility for the m-AODV protocol.

Routing performance function of network density. Figures 3.10(a) and 3.10(b) show the packet loss ratio function of the network density, for both fitness functions $\mathcal{F}^d$ and $\mathcal{F}^a$. We notice that for low network density, the packet loss ratio of all schemes is high - a consequence of the low connectivity. The 1-limited forwarding performs the worst at these values. For higher network densities, the m-limited forwarding based schemes have a lower packet loss ratio than *plain* AODV. We note that 2- and 3-limited forwarding have a lower packet loss ratio than 1- and 4-limited forwarding. For 1-limited forwarding, only one hop is chosen to forward a route discovery packet, thus the whole path will fail if one of the hops fails. For m-limited forwarding with ($m \geq 4$), the packets are lost due to the higher number of collisions in the forwarding of the route discovery packet.

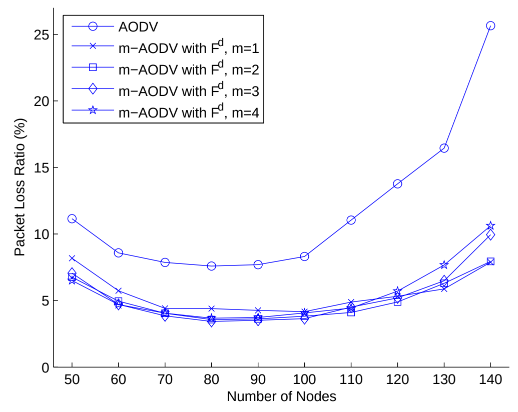

(a)

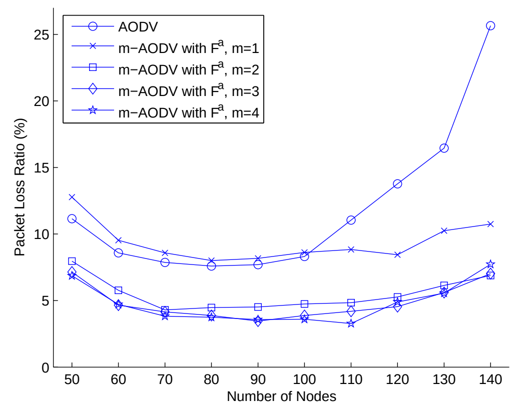

(b)

Figure 3.10: Average power consumption versus node density. Offered load = 25 Kbps, Speed = 1 m/s, m=1,2,3,4. (a) m-AODV with distance-based fitness function $\mathcal{F}^d$; (b) m-AODV with area-based fitness function $\mathcal{F}^a$. For low network density, 1-limited forwarding performs the worst. For higher network densities, all m-limited forwarding based schemes have a lower packet loss ratio than *plain* AODV. $m = 2$ and 3 are better options when network density is relatively high.

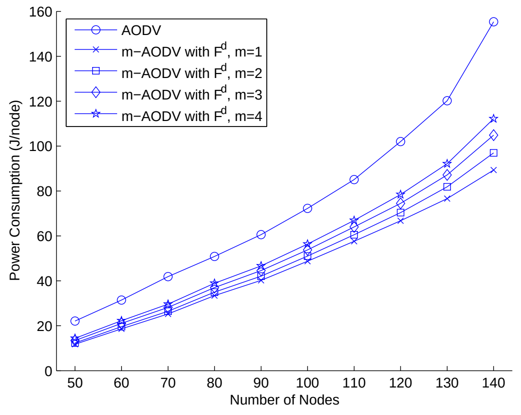

(a)

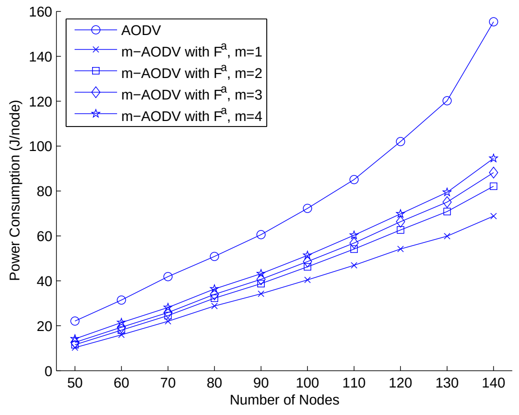

(b)

Figure 3.11: Average power consumption versus node density. Offered load = 25 Kbps, Speed = 1 m/s, m=1,2,3,4. (a) m-AODV with distance-based fitness function $\mathcal{F}^d$; (b) m-AODV with area-based fitness function $\mathcal{F}^a$. The power consumption for all schemes increases as network density increases. AODV consumes the most power, followed by 4-, 3-, 2-, and 1-limited forwarding.

From Figures 3.11(a) and 3.11(b), we observe that the average power consumption per node for all schemes increases as network density increases. This is explained by the fact that at a higher network density, more nodes overhear every transmission and the route discovery packet is also retransmitted by more nodes. AODV consumes the most power, followed by 4-, 3-, 2-, and 1-limited forwarding.

Summary. The experiments performed show that there is no single choice of m which performs the best in every situation. 1-limited forwarding performs poorly for low network load and/or high mobility. 2-limited forwarding performs poorly for high node mobility. On the other hand, 4-limited forwarding does not perform well for high network load. We find that 3-limited forwarding shows the most consistent performance across a wide range of parameters. Therefore, unless we have the possibility to hand optimize the algorithm for a specific network and transmission scenario, $m = 3$ is the safest choice. We will use this value in the remainder of our simulations.

3.2.3 Performance Improvement of m-limited Forwarding in MANETs with Bidirectional Links

In the following, we study the performance improvement of m-limited forwarding for ad hoc networks with symmetric links. We note that this is the most frequently encountered situation in practice, because most of the current MAC protocols cannot handle unidirectional links. The unidirectional links are therefore ignored at the level of the MAC protocol, and the routing protocol sees a network composed entirely of symmetric links.

In the following simulation experiments, we are comparing *plain* AODV with m-AODV with 3-limited forwarding for the two proposed fitness functions $\mathcal{F}^d$ and $\mathcal{F}^a$, as well as the Location-Aided Routing (LAR) protocol. We use the same scenario and traffic patterns as in the previous simulations.

Routing performance function of network load. The packet loss ratio versus network load is presented in Figure 3.12. The packet loss ratio increases with the network load increasing for all schemes, while for *plain* AODV it is increasing at a higher rate than LAR and both of the 3-limited forwarding based schemes. $\mathcal{F}^d$ strictly requires nodes to forward the traffic on the positive direction to the destination, as a reason, some of the nodes on the critical path but on a negative direction may be excluded. Thus, m-AODV with $\mathcal{F}^d$ performs a little better than m-AODV with $\mathcal{F}^a$. LAR and both of the 3-limited forwarding based schemes have a comparable packet loss ratio when the traffic load is light. When the traffic load is heavy, as the number of next hops restricted by LAR is larger than that restricted by 3-limited forwarding based schemes, more packets are dropped by LAR due to collisions or excessive retransmission failures at the MAC layer.

Figure 3.13 illustrates the average power consumption versus network load. For lightly loaded networks, 3-limited forwarding consumes more power due to the dissemination of *hello* packets and *location-update* packets. When the network load increases, the power dissipation of *plain* AODV increases much faster than that of m-limited forwarding schemes. The next hops to forward traffic established by $\mathcal{F}^a$ is more restricted, compared to $\mathcal{F}^d$. Oftentimes, less than 3 nodes are included in the forwarding set calculated by $\mathcal{F}^a$, as a result, m-AODV with $\mathcal{F}^a$ consumes less

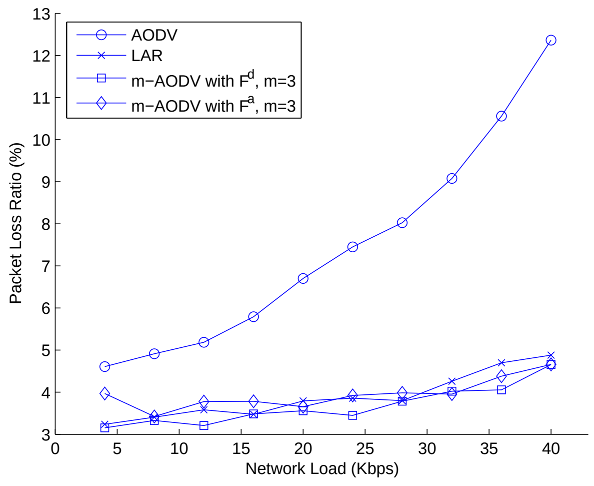

Figure 3.12: Packet loss ratio versus network load. Number of nodes = 80, Speed = 1 m/s. We compare AODV, LAR, and m-AODV with fitness functions $\mathcal{F}^d$ and $\mathcal{F}^a$. AODV performs the worst. m-AODV outperforms LAR when the network load is relatively high.

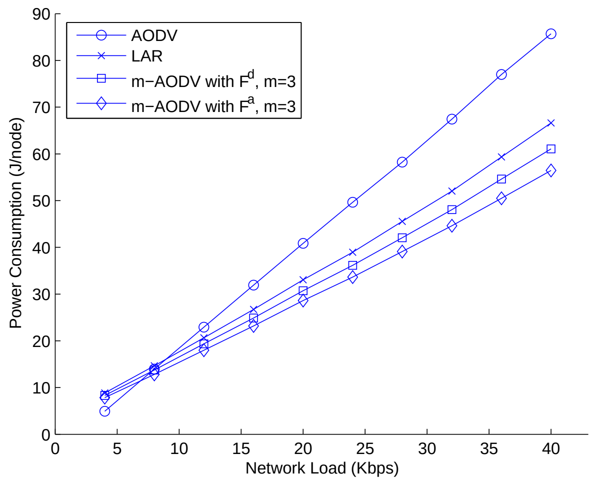

Figure 3.13: Average power consumption versus network load. Number of nodes = 80, Speed = 1 m/s. We compare AODV, LAR, and m-AODV with fitness functions $\mathcal{F}^d$ and $\mathcal{F}^a$. AODV consumes the most power, and m-AODV consumes less power than LAR, for the same network load.

power than m-AODV with $\mathcal{F}^d$. Compared to m-limited forwarding schemes, LAR allows more nodes to serve as the next hop as long as they are inside the request zone, thus, LAR routing scheme consumes more power than 3-limited forwarding with both $\mathcal{F}^d$ and $\mathcal{F}^a$ based schemes.

Routing performance function of node mobility. Figure 3.14 illustrates the packet loss ratio versus node mobility. All routing schemes are very sensitive to node mobility and the packet loss ratio increases when mobility increases. For example, for *plain* AODV the packet loss ratio increases from 6.40% at 1 m/s to 24.50% at 10 m/s, in average. *Plain* AODV has a higher packet loss ratio than LAR and m-AODV for relatively high values of mobility. Among the other protocols, m-AODV with $\mathcal{F}^a$ is slightly worse than LAR and m-AODV with $\mathcal{F}^d$.

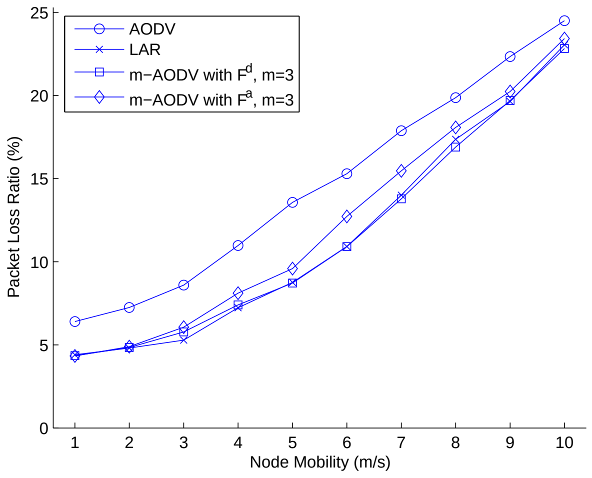

Figure 3.14: Packet loss ratio versus node mobility. Number of nodes = 80, Offered network load = 25 Kbps. We compare AODV, LAR, and m-AODV with fitness functions $\mathcal{F}^d$ and $\mathcal{F}^a$. AODV performs the worst. m-AODV with distance-based fitness function $\mathcal{F}^d$ achieves a similar performance with LAR, which performs slightly better than m-AODV with area-based fitness function $\mathcal{F}^a$.

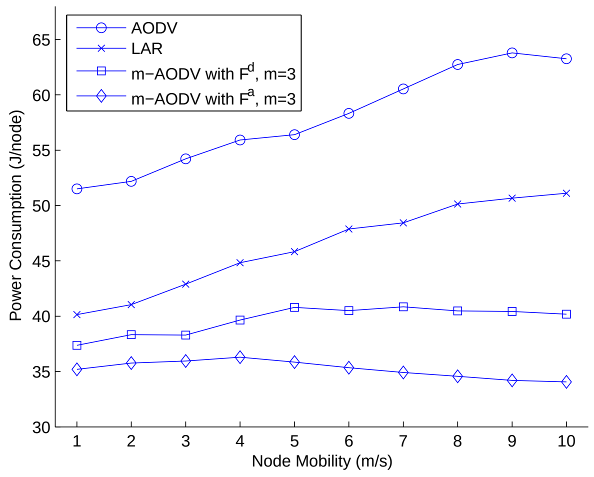

Figure 3.15: Average power consumption versus node mobility. Number of nodes = 80, Offered network load = 25 Kbps. We compare AODV, LAR, and m-AODV with fitness functions $\mathcal{F}^d$ and $\mathcal{F}^a$. AODV consumes the most power, and m-AODV consumes less power than LAR, for the same node mobility.

Figure 3.15 illustrates the average power consumption versus node mobility. We find the *plain* AODV and LAR are more sensitive to node mobility than m-AODV. With the mobility increasing, the power dissipated by AODV and LAR increases accordingly, while the power consumption of both 3-limited forwarding based schemes remain at a certain level. For the two 3-limited forwarding based schemes, the $\mathcal{F}^d$ based scheme consumes less power than the $\mathcal{F}^a$ based scheme.

Routing performance function of network density. Figure 3.16 illustrates the packet loss ratio versus node density. The packet loss ratio decreases when the number of nodes increases from 50 to 80, and then starts to increase when the number of nodes further increases. When the network density is relatively low, a percentage of packets are dropped due to unavailable routes; when the network density is relatively high, excessive collisions become the major reason that

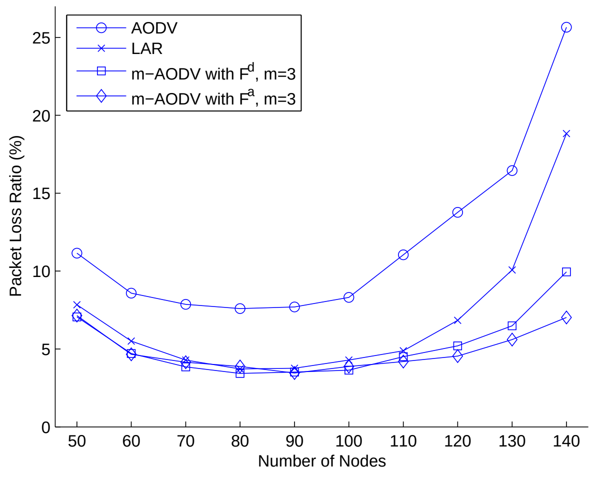

Figure 3.16: Packet loss ratio versus network density. Speed = 1 m/s, Offered network load = 25 Kbps. We compare AODV, LAR, and m-AODV with fitness functions $\mathcal{F}^d$ and $\mathcal{F}^a$. AODV performs the worst. m-AODV outperforms LAR when the network density is relatively high.

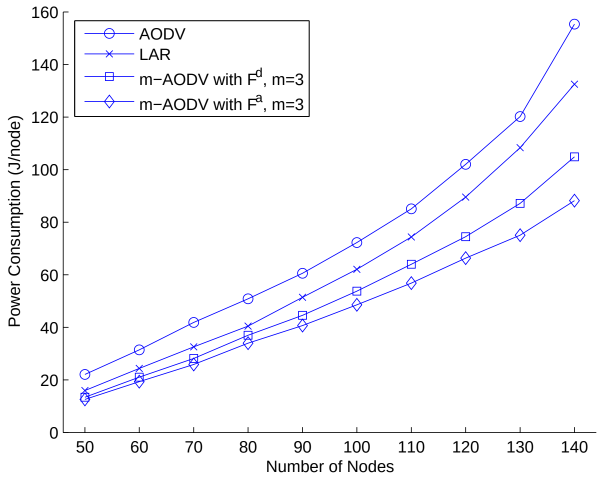

Figure 3.17: Average power consumption versus network density. Speed = 1 m/s, Offered network load = 25 Kbps. We compare AODV, LAR, and m-AODV with fitness functions $\mathcal{F}^d$ and $\mathcal{F}^a$. AODV consumes the most power, and m-AODV consumes less power than LAR, for the same network density.

packets are lost during the transmission. The packet loss ratio for AODV and LAR at high node density increases faster than m-AODV due to excessive number of collisions. m-AODV with $\mathcal{F}^a$ outperforms m-AODV with $\mathcal{F}^d$ at higher node density.

Figure 3.17 illustrates the average power consumption versus network density. With the increase in the network density, the power dissipated by every routing scheme increases accordingly. The increase in the power dissipation by *plain* AODV is slightly larger than LAR, followed by m-AODV with $\mathcal{F}^d$, and m-AODV with $\mathcal{F}^a$. The $\mathcal{F}^a$ based scheme consumes less power than the $\mathcal{F}^d$ based scheme.

Summary. We find that m-AODV exhibits a consistently lower power consumption for almost all operating scenarios, except when the network load is light. In that case, the overhead of m-limited forwarding due to the dissemination of *hello* and *location-update* packets exceeds the benefits gained by reducing the retransmissions.

In general, the more "difficult" a scenario (high network load and/or high node mobility), the greater the benefits of m-limited forwarding in terms of power consumption. The distance-based fitness function $\mathcal{F}^d$ leads to lower power consumption with an approximately constant difference versus the area-based fitness function $\mathcal{F}^a$.

We also find that the m-limited forwarding lowers the packet loss ratio in all scenarios. Although the packet loss ratio is naturally increasing for all algorithms when the scenario becomes more "difficult" (high network load and/or high node mobility), the benefits of m-limited forwarding become greater with the increase in the difficulty of the scenario. The two fitness functions $\mathcal{F}^d$

and $\mathcal{F}^a$ have a similar evolution, with the distance-based function $\mathcal{F}^d$ having a lower packet loss ratio with an approximately constant difference.

The general conclusion is m-AODV outperforms *plain* AODV and LAR for everything but the easiest scenarios (with light network load and low node mobility). The distance based fitness function $\mathcal{F}^d$ is a better choice in these cases, as the benefits of the area-based function $\mathcal{F}^a$ cannot be observed in a network formed exclusively of symmetric links.

3.2.4 m-limited Forwarding in MANETs with Asymmetric Links

We find that for homogeneous MANETs the simpler, distance-based $\mathcal{F}^d$ forwarding fitness function actually performs slightly better than the more complex, area-based $\mathcal{F}^a$ function, in terms of packet loss ratio. The reason for this is that, as shown in Section 3.1, the benefits of the area-based function appear only in the case of asymmetric links. Most wireless networks are composed of heterogeneous nodes due to the differences in the physical possibilities of the nodes, such as power, size and shape of antennas and so on. However, most MAC layer and routing protocols require the existence of bidirectional links. These protocols ignore the large number of asymmetric links present in heterogeneous networks. For instance the IEEE 802.11 MAC protocol works only on bidirectional links, and most ad hoc routing protocols (including AODV) require bidirectional links. This property is also inherited by the m-AODV variant.

In order to study the improvement provided by the area-based fitness function $\mathcal{F}^a$, we need to test it with a pair of MAC and routing protocols which both support asymmetric links. One such pair is the AsyMAC (Asymmetric MAC) protocols [WTB06a, WTB07b] and the m-A^{4}LP routing protocol [WJM04, WJM06].

To show the benefits of the approach, we created a scenario with a set of heterogeneous nodes. In our simulation, we have four categories of nodes – *C1, C2, C3*, and *C4*. The transmission ranges of nodes in category *C1, C2, C3*, and *C4* are 200, 150, 100, and 50 meters, respectively. The ratio of the number of nodes of each category is |C1|:|C2|:|C3|:|C4| =1:2:3:4. Thus, for default 80 nodes, the number of nodes in category *C1, C2, C3*, and *C4* are 8, 16, 24, 32, respectively. We run a simulation comparing three protocol stacks: m-A^{4}LP with the underlying AsyMAC protocol in the variants with the distance-based $\mathcal{F}^d$ and the area-based $\mathcal{F}^a$ fitness function and a more traditional ad hoc networking stack with *plain* AODV on top of the 802.11 MAC protocol.

Note that this is a relatively "difficult" scenario for the AODV/802.11 protocol set, due to the large number of nodes with small transmission range and the relatively low density of nodes. Therefore, we expect a high packet loss ratio for the AODV/802.11 stack.

The results of the experiments are presented in Figure 3.18. We find that the m-A^{4}LP/AsyMAC based protocol stacks have a much lower packet loss ratio than AODV/802.11. This is due to their ability to exploit the asymmetric links which exist in the environment. Furthermore, in this scenario we find that the area-based fitness function $\mathcal{F}^a$ yields a lower packet loss ratio than the distance based function $\mathcal{F}^d$. This is due to the fact that $\mathcal{F}^a$ can make a better choice of the set of forwarding nodes in the presence of asymmetric links.

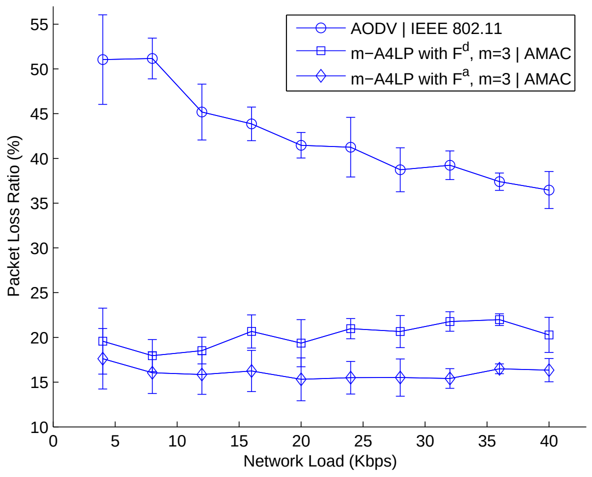

Figure 3.18: Packet loss ratio versus network load. Speed = 1 m/s, Number of nodes = 80. Nodes fall into four categories with transmission range of 200 (*C1*), 150 (*C2*), 100 (*C3*), and 50 (*C4*) meters. |C1|:|C2|:|C3|:|C4| =1:2:3:4. AODV/802.11, A^4LP/AsyMAC based on 3-limited forwarding with $\mathcal{F}^d$, and A^4LP/AsyMAC based on 3-limited forwarding with $\mathcal{F}^a$ are compared.

3.3 Summary

In this chapter we introduced m-limited forwarding, a technique to optimize the performance of ad hoc routing algorithms by reducing the power consumption as well as the fraction of the network bandwidth used to disseminate routing information. m-limited forwarding limits the cardinality of the subset of nodes which retransmit a packet to m nodes. A forwarding fitness function is used to select the m-nodes; we introduced two alternative functions: a distance-based function $\mathcal{F}^d$ and an area-based function $\mathcal{F}^a$.

We evaluate the performance of m-limited forwarding through a series of simulation studies. Our first objective is to determine the optimal value of m, the cardinality of the set of nodes which retransmit a packet containing routing information. We have found that m = 3 yields reasonable output.

A second set of experiments study MANETs with bidirectional links and investigate two routing algorithms, AODV and LAR enhanced with m-limited forwarding. For most simulation scenarios, m-AODV has a lower power consumption and a lower packet loss ratio than either *plain* AODV or LAR. Our simulation studies indicate that the distance-based fitness function $\mathcal{F}^d$ performs better than the area-based function $\mathcal{F}^a$.

Finally, we compared the performance of the two fitness functions in a network with asymmetric links. Since AODV and the most commonly used MAC protocols cannot take advantage of asymmetric links, we used the m-A^{4}LP routing protocol and the AsyMAC (asymmetric MAC) protocol on the MAC and network layer. Our simulation studies indicate that the m-A^{4}LP/AsyMAC protocol stack yields a lower packet loss ratio than the AODV/802.11 stack, and the area-based fitness function $\mathcal{F}^a$ outperforms the distance-based function $\mathcal{F}^d$ for this scenario.

A natural extension of the current research is the ability to improve the performance of the routing algorithms by improving the accuracy of the forwarding fitness function. For instance, the area-based fitness function assumes that the number of nodes in the area is proportional with the size of the area, which is true only if the density of the nodes is uniform and static. If we have information about a non-uniform node density we can introduce a *density weighted area-based* fitness function where the fitness is expressed as the size of the area times the node density in the given part of the network. If, in addition, we have information about asymmetric and/or dynamically changing transmission ranges, this information can also be integrated in the fitness function. Naturally, there is a delicate balance between the cost of obtaining the necessary information, and the performance improvement which can be obtained through a fitness function with improved accuracy. We conjecture that the cost of obtaining additional information is justified only in “difficult scenarios”, such as nodes with highly heterogeneous transmission ranges or scenarios with abrupt changes in node density. The in-depth evaluation of this conjecture and the design of low-overhead information gathering and distribution algorithms is a subject of future work.

Another topic for future research is the study of the security and fairness aspects of the protocol. In the current protocol, a node can become a parasite on the system if either (a) refuses to participate in the forwarding by quietly dropping packets or (b) misreports its own position such that the node is avoided by the routes established in the network. While these misbehaviors can be in principle detected externally, the network needs a service which monitors the participants and takes appropriate actions against misbehaving nodes. Note that our protocol is not dependent on the power resources of the nodes. It is very difficult to detect nodes which misrepresent their power resources, because external observers do not normally have access to the internal power monitors of a node.

CHAPTER 4
MAC LAYER AND ROUTING PROTOCOLS FOR WIRELESS NETWORKS WITH ASYMMETRIC LINKS

Mobile ad hoc networks allow nodes with different hardware capabilities and power limitations to communicate with one another. Most communication channels in such networks are unidirectional due to heterogeneity of the nodes and to power constraints. Yet, routing protocols for MANETs routinely assume that all communication links are bidirectional. In this dissertation, we consider the case when the nodes of a MANET have various degrees of mobility and range and the communication links are asymmetric. Power consumption is a major concern for a MANET as nodes become inoperative once they have depleted their power. *Power-aware* routing algorithms minimize the power consumption and, whenever possible, avoid the nodes with a low level of residual power. *Location-aware* routing algorithms have the potential to extend the life of individual nodes of a MANET, when the location of the nodes are known by the embedded GPS systems.

In a wireless environment, at any given time, an asymmetric link supports unidirectional communication between a pair of mobile stations and requires a set of relay stations for the transmission of packets in the other direction. Asymmetric links are common in wireless networks for a variety of physical, logical, operational, and legal considerations. The transmission range of a node might be limited by the capabilities of the hardware or by power limitations. A node might need to limit its transmission power to avoid interference with a licensed user of the spectrum, or because of dynamic spectrum management considerations. In military applications, considerations of stealth might require some nodes to reduce their transmission power. In addition to these, [KRD06] mentions some schemes have been proposed recently to maintain optimum network topology by tuning the transmission range of individual nodes [RH00, WLB01, GTS04], which leads to possible unidirectional links.

Inability of some MAC layer protocols to exploit the asymmetry of some of the communication channels could lead to an inefficient bandwidth utilization, or, in the worst case, to inability to connect some of the nodes. To exploit the asymmetric links, the protocols must be able to deliver the acknowledgements back to the sender in a direction opposite to the direction of the asymmetric link. Furthermore, the problem of hidden nodes appears more often and in more complex forms than in the case of symmetric links. Depending whether the routing protocol of a MANET is able to handle asymmetric links, the MAC layer protocol might need to hide the existence of asymmetric links with a symmetric overlay. The challenge for a MAC layer protocol able to exploit asymmetric links is to solve the hard problems mentioned above, while keeping the cost incurred lower than the benefits obtained from the utilization of the asymmetric links.

In this chapter, we introduce a MAC layer and routing protocol for heterogeneous MANETs with asymmetric links. The routing protocol A^{4}LP, which is both *location-aware* and *power-aware*, is designed to support routing over asymmetric links. A^{4}LP introduces an advanced flooding technique - *m-limited forwarding*, which significantly reduces average power consumption as well as packet loss ratio. The MAC layer protocol (AsyMAC) supports reliable transmission over asymmetric links. AsyMAC requires fewer nodes to maintain silence during a transmission than the protocols proposed in [PKD01,FTB02], as a result, the bandwidth utilization of the network is extended.

This chapter is organized as follows. We begin with an introduction of the system model for heterogeneous MANETs and discuss several topology-related concepts in Section 4.1. We present a detailed description of our proposed A^{4}LP routing protocol for MANETs with asymmetric links in Section 4.2. Section 4.3 describes the AsyMAC protocol in details which serves as the underlying MAC layer protocol for A^{4}LP routing protocol. The simulation and case study for the A^{4}LP/AsyMAC protocol combination is illustrated in Section 4.4. Finally, we summarize the findings of the A^{4}LP/AsyMAC protocol combination in Section 4.5.

4.1 The Model of the System

4.1.1 The System Model for Heterogeneous MANETs

Let $\mathcal{N}$ be the set of nodes in a heterogeneous MANET. We make several assumptions:

a. The number of nodes is relatively small, say $\mid \mathcal{N} \mid \leq 10^4$.

b. All nodes use the same frequency to communicate with one another. Once a node sends a message all the nodes in its transmission range hear the broadcast.

c. The mobility of individual nodes is limited and differs from one node to the other.

d. Nodes are able to adjust their transmitting power according to their residual power so that their lifetime are extended.

Every node $i \in \mathcal{N}$ is characterized by a minimal set of attributes, two time-invariants and two time-dependents:

1. Id, Id_i; a unique string used for node identification.

2. Class, C_i; the nodes of a heterogeneous MANET are classified into several classes based on the hardware and software resources. Throughout this thesis we assume a four level hierarchy.

3. Location at time t, $L_i(t)$; the geographical coordinates of the position of the node at time t.

4. Residual power at time t, $P_i^{res}(t)$; the amount of power available at time t. Let P_i^{max} be the maximum level of power that can be stored at node i. There are two water marks (e.g., high water mark $HWM_i = 0.7P_i^{max}$ and low water mark $LWM_i = 0.2P_i^{max}$), and say that at time t the node operates at

   - *full-power level* if $P_i^{res}(t) \geq HWM_i$,

   - *normal-power level* if $P_i^{res}(t) > LWM_i$ and $P_i^{res}(t) < HWM_i$, or

   - *low-power level* if $P_i^{res}(t) \leq LWM_i$.

Other attributes can be derived from the ones in the minimal set.

The *transmission range* of node i at time t, $R_i(t)$, is a function of the residual power and possibly other factors including the configuration of the terrain, atmospheric conditions, and so on. For simplicity we assume that

$$R_i(t) = constant \times P_i^{res}(t) \tag{4.1}$$

The *distance* between two nodes, $i, j \in \mathcal{N}$, $d_{ij}(t)$ is a function of the position of the two nodes

$$d_{ij}(t) = d_{ji}(t) = f(L_i(t), L_j(t)) \tag{4.2}$$

The *average velocity* of a node i over a time interval $\Delta t = t_2 - t_1,\ \ t_2 > t_1$ is

$$v_i^{\Delta t} = f(L_i(t_2), L_i(t_1))/\Delta t \tag{4.3}$$

The *mobility region* of node i over a time interval $\Delta t = t_2 - t_1,\ \ t_2 > t_1$ is a circle of radius

$$M_i^{\Delta t} = v_i^{\Delta t} \times \Delta t \tag{4.4}$$

centered at $L_i(t_1)$.

The connection between two nodes is described by the Boolean *reachability function* $\mathcal{R}_{ij}(t)$ which can be interpreted as follows: a node i can send a packet to node j at time t if and only if $\mathcal{R}_{ij}(t) = \textsf{true}$. A link between two nodes is symmetric if $\mathcal{R}_{ij}(t) = \mathcal{R}_{ji}(t) = \textsf{true}$. Note, that the reachability is a time varying function; the connection can be affected by various channel conditions, fading, the mobility of the node or the mobility of the obstacles in the field.

We assume that every node is aware of the current values of the reachability function between itself and the neighboring nodes (in both direction). In the A^{4}LP/AsyMAC protocol stack, it is the role of the *neighbor discovery protocol* of A^{4}LP to find these values and keep them up-to-date. Although neighbor discovery is a common feature of ad hoc routing protocols, most protocols will not detect outbound neighbors, because the confirmation message will not reach back to the originating node. Asymmetric routing protocols, such as A^{4}LP have a provision to route back the confirmation messages even in the absence of a direct link, thus allowing the discovery of the full asymmetric reachability matrix. In the following definitions we omit the time parameter even though all the sets are variable in time, a fact which needs to be considered by the protocols relying on them.

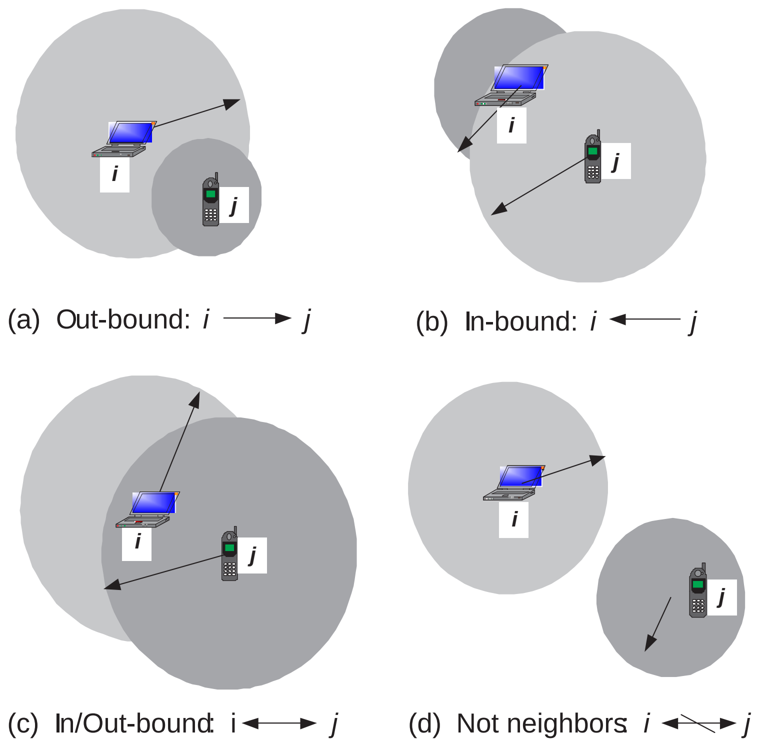

(a) Out-bound: $i \longrightarrow j$ (b) In-bound: $i \longleftarrow j$

(c) In/Out-bound: $i \longleftrightarrow j$ (d) Not neighbors: $i \cancel{\longleftrightarrow} j$

Figure 4.1: The neighbor relationship between two nodes. (a) j is an Out-bound neighbor of i. (b) j is an In-bound neighbor of of i. (c) j is an In/Out-bound neighbor of i. (d) i and j are not neighbors.

Definition 1: Two nodes $i, j \in \mathcal{N}$ are in *neighbor* relationship at time t if there is a direct communication link between them. We recognize several types of neighbors:

(i) *Out-bound neighbor:* j is the out-bound neighbor of i, if i can reach j but j cannot reach i, as seen in Figure 4.1(a). In this case the link L_{ij} between the two nodes is unidirectional

$$\mathcal{R}_{ij}(t) = \textsf{true} \quad \text{and} \quad \mathcal{R}_{ji}(t) = \textsf{false}$$

Call $Out_i(t) \subset \mathcal{N}$ the set of Out-bound neighbors of i at time t.

(ii) *In-bound neighbor:* j is the In-bound neighbor of i, if j can reach i but i cannot reach j, as seen in Figure 4.1(b). In this case the link L_{ji} between the two nodes is unidirectional

$$\mathcal{R}_{ij}(t) = \textsf{false} \quad \text{and} \quad \mathcal{R}_{ji}(t) = \textsf{true}$$

Call $In_i(t) \subset \mathcal{N}$ the set of In-bound neighbors of i at time t.

(iii) *In/Out-bound neighbor:* j is the In/Out-bound neighbor of i, if i and j can reach each other, as seen in Figure 4.1(c). In this case the link L_{ij} between the two nodes is bidirectional

$$\mathcal{R}_{ij}(t) = \textsf{true} \quad \text{and} \quad \mathcal{R}_{ji}(t) = \textsf{true}$$

Call $InOut_i(t) \subset \mathcal{N}$ the set of In/Out-bound neighbors of i at time t.

The scenario that two nodes are not neighbors is illustrated in Figure 4.1(d).

Definition 2: If node i is an Out-bound neighbor of node j, we call i the *high-range node* (H-node) and j the *low-range node* (L-node) of the asymmetric link L_{ij}.

Definition 3: A set of m nodes $i_1, i_2, \dots i_m \in \mathcal{N}$ are in an *m-party proxy set* if each node can reach the other $m-1$ nodes either directly or through a subset of the other $m-2$ members of the set.

Proposition 1: At least one of the links of an m-party proxy set must be bidirectional.

Proof: Suppose Proposition 1 is false, that is, there exists an m-party proxy set with no bidirectional links. Let the m nodes in the m-party proxy relationship be $i_1, i_2, \cdots, i_m \in \mathcal{N}$ and arbitrarily pick up an asymmetric link (i_u, i_v) where $1 \le u, v \le m, u \ne v$. Thus, node i_u can reach node i_v directly, but the reciprocal is not true, $\mathcal{R}_{i_u i_v}(t) = \textsf{true}$ and $\mathcal{R}_{i_v i_u}(t) = \textsf{false}$:

$$R_{i_u}(t) \ge d_{i_u i_v}(t) > R_{i_v}(t) \tag{4.5}$$

By the definition of m-party proxy set, there exists at least a path for node i_v to reach node i_u. Let us choose the shortest path from node i_v to node i_u. There are no duplicate nodes on this path, otherwise a shorter path can be obtained by removing the sub-path consisting of all the nodes connecting the two duplicate nodes. Call the set of nodes on the shortest path $(i_v, i_{N_1}, i_{N_2}, \cdots, i_{N_p} \cdots, i_{N_k}, i_u)$, where $N_p \ne N_q, N_p \ne u, N_p \ne v, 1 \le p, q \le k \le m-2, p \ne q$. Similar to (4.5), we have

$$\begin{aligned} R_{i_v}(t) &\ge d_{i_v i_{N_1}}(t) > R_{i_{N_1}}(t) \\ &\ge d_{i_{N_1} i_{N_2}}(t) > R_{i_{N_2}}(t) \\ &\ge \cdots > R_{i_{N_p}}(t) \ge d_{i_{N_p} i_{N_{p+1}}}(t) > R_{i_{N_{p+1}}}(t) \\ &\ge \cdots > R_{i_{N_k}}(t) \ge d_{i_{N_k} i_u}(t) > R_{i_u}(t) \end{aligned} \tag{4.6}$$

Equations (4.5) and (4.6) are contradictory, thus, Proposition 1 must be true. ■

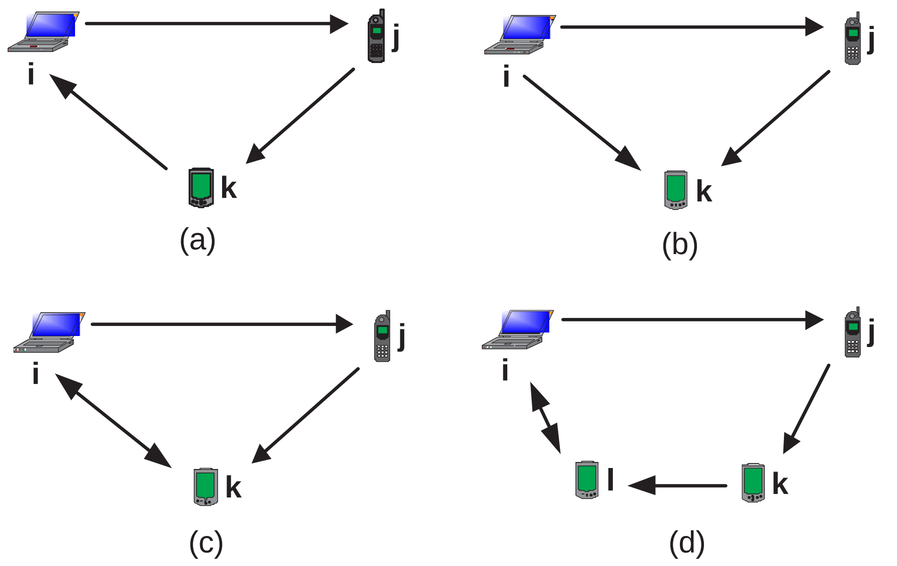

Figure 4.2: Three-party and four-party proxy sets. (a) An infeasible scenario for a three-party proxy set involving three unidirectional links. (b) A second infeasible scenario for a three-party proxy set involving three unidirectional links. (c) A feasible scenario for a three-party proxy set with only one bidirectional link. (d) A feasible scenario for a four-party proxy set with only one bidirectional link.

Figure 4.2(a) and 4.2(b) show two possible configurations of a three-party proxy set with unidirectional links only. The configuration in Figure 4.2(a) is infeasible according to Proposition 1, while the configuration in Figure 4.2(b) is infeasible because node k cannot reach either node i or node j.

Proposition 2: There is at least one configuration of an m-party proxy set with one bidirectional link.

The configuration in Figure 4.2(c) and any configuration obtained by a permutation of the identities of the nodes in the set has one bidirectional link. In this configuration, node i can reach node j and k directly, node j can reach node k directly and reach node i via node k, and finally node k can reach node i directly and node j via node i. The transmission ranges and distances among the nodes of the configuration in Figure 4.2(c) are:

$$\begin{cases} R_j < d_{ij} \leq R_i, \;\; R_k < d_{jk} \leq R_j; \\ d_{ik} \leq R_i, \;\; d_{ki} \leq R_k. \end{cases} \tag{4.7}$$

To show that there is at least one configuration of four-party proxy set with one bidirectional link we consider the configuration in Figure 4.2(d). Since there is a loop $i \rightarrow j \rightarrow k \rightarrow l \rightarrow i$, every node can reach the other nodes in the set. The transmission ranges and distances among the nodes of the configuration in Figure 4.2(d) must satisfy the following constraints:

$$\begin{cases} R_j < d_{ij} \leq R_i, \;\; R_k < d_{jk} \leq R_j, \;\; R_l < d_{kl} \leq R_k; \\ d_{li} \leq R_i, \;\; d_{li} \leq R_l; \\ d_{ik} > R_i, \;\; d_{jl} > R_j, \;\; d_{ki} > R_k, \;\; d_{lj} > R_l. \end{cases} \tag{4.8}$$

In the general case of an m-party proxy set consider the nodes $i_1, i_2, \ldots i_m \in \mathcal{N}$ connected as follows: nodes i_k and i_{k+1} $(1 \leq k \leq m-2)$ are connected by unidirectional links from node i_k to node i_{k+1}, and nodes i_1 and i_m are connected by a bidirectional link. Thus the ranges and distances among nodes must satisfy the following constraints

$$\begin{cases} R_{k+1} < d_{k,k+1} \leq R_k, \;\; \text{for } 1 \leq k \leq m-2; \\ d_{1m} \leq R_1, \;\; d_{m1} \leq R_m; \\ d_{k,(k+j \mod m)} > R_k, \;\; \text{for } 2 \leq j \leq m-1, \; 1 \leq k \leq m. \end{cases} \tag{4.9}$$

4.1.2 Topological Considerations for AsyMAC

The handling of the hidden nodes is an essential problem for wireless MAC layer protocols operating in the presence of asymmetric links. We introduce topological concepts necessary to define a hidden node of a network with asymmetric links.

We define a series of topological concepts related to communication in the presence of asymmetric links and illustrate for the simple scenario in Figure 4.3; the sender node s sends a packet to the receiver node r in the vicinity of nodes i, $1 \leq i \leq 9$. The circles centered at s and r show the transmission ranges of the sender and the receiver, respectively. The reachability information of the other nodes is shown by directed lines; to avoid cluttering the figure we do not include the links not relevant to the scenario. In this simple scenario we assume that the asymmetric links are caused by the nodes having different transmission ranges and the transmission range is a disk; this is not necessarily true in real life scenarios, and our definitions do not assume a unit disk model.

We have defined *m-party proxy set* in Section 4.1.1. In the scenario specified by Figure 4.3, the three party proxy sets are {r, 1, 6}, {r, 2, 6}, {r, 2, 7}, {r, 3, 7}, {r, 3, 8}, {r, 4, 8}, and {r, 4, 9}.

Definition 4: Call the *vicinity* of node i, V_i the set of nodes that could be reached from node i.

$$V_i = \{j \,|\mathcal{R}(i,j)\} \tag{4.10}$$

In our scenario, the vicinity of the receiver node r is $V_r = \{1, 2, 3, 4, 5\}$.

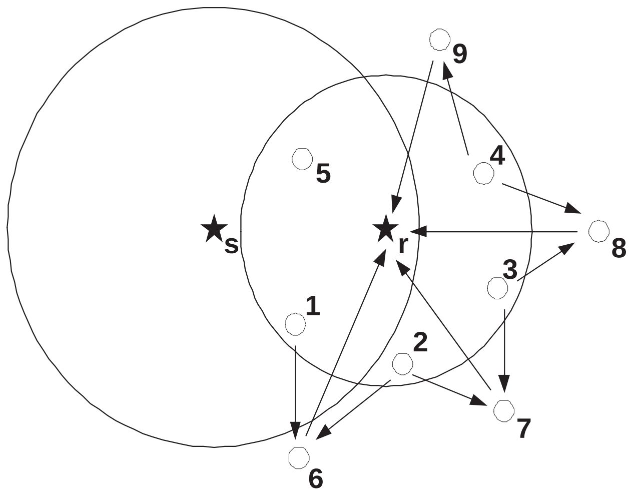

Figure 4.3: An illustration for topology concepts. The transmission ranges of the sender s and the receiver r are reflected by the circles centered at them. The partial reachability information of the other nodes is shown by directed lines.

Definition 5: Call H_{sr} the set of *hidden nodes of a transmission* T_{sr}. H_{sr} includes nodes that are not reachable from the sender, but from which the receiver is reachable:

$$H_{sr} = \{k \mid \neg\mathcal{R}(s,k) \wedge \mathcal{R}(k,r)\} \tag{4.11}$$

Note that H_{sr} are the hidden nodes for the transmission of the DATA packets, while H_{rs} are the hidden nodes for the transmission of ACK packets. In our scenario, the hidden nodes of the transmission from the source node s to the receiver node r are $H_{sr} = \{2, 3, 4, 6, 7, 8, 9\}$.

Definition 6: Call $P3_i$ the *three-party proxy set coverage* of node i. $P3_i$ is the set of nodes which are either reachable by node i directly or participate in a three-party proxy set with node i and a third node.

$$P3_i = \{k \mid \mathcal{R}(i,k) \vee \exists_j \ (\mathcal{R}(i,j) \wedge \mathcal{R}(j,k) \wedge \mathcal{R}(k,i))\} \tag{4.12}$$

In our scenario, the three-party proxy set coverage of node r is $P3_r = \{1, 2, 3, 4, 5, 6, 7, 8, 9\}$.

Definition 7: Call $H3_{sr}$ the ***hidden nodes*** of a transmission T_{sr} in the three-party proxy set coverage of node r. The set $H3_{sr}$ includes hidden nodes covered by $P3_r$.

$$H3_{sr} = H_{sr} \cap P3_r \tag{4.13}$$

In our scenario, the hidden nodes in the three-party proxy set coverage of r are $H3_{sr} = \{2, 3, 4, 6, 7, 8, 9\}$.

Definition 8: Call $XH3_{sr}$ the *extended hidden nodes* of a transmission T_{sr} in three-party proxy set coverage of node r. The set $XH3_{sr}$ includes nodes in $H3_{sr}$ not covered by V_r.

$$XH3_{sr} = H3_{sr} - V_r \tag{4.14}$$

In the scenario of Figure 4.3, the extended hidden nodes of the transmission from the source node s to the receiver node r are $XH3_{sr} = \{6, 7, 8, 9\}$.

Definition 9: Call $XHR3_{sr}$ the *extended hidden nodes relay set* of a transmission T_{sr} in three-party proxy set coverage of node r. $XHR3_{sr}$ includes *all* nodes in $P3_r$ that could relay traffic from node r to nodes belonging to $XH3_{sr}$.

$$XHR3_{sr} = \{j \mid j \in V_r \wedge \exists_{k \in XH3_{sr}}(\mathcal{R}(j, k))\} \tag{4.15}$$

The extended hidden nodes relay set of the transmission from s to r on the example scenario is $XHR3_{sr} = \{1, 2, 3, 4\}$.

Definition 10: Call $mXHR3_{sr}$ a *minimal extended hidden nodes relay set* of a transmission T_{sr} in three-party proxy set coverage of node r. $mXHR3_{sr}$ includes a subset of nodes from

$XHR3_r$ ($mXHR3_r \subseteq XHR3_r$) such that (i) the node r can relay traffic to any node in $XH3_{sr}$ through some nodes from $mXHR3_{sr}$ and (ii) the removal of any node from $mXHR3_{sr}$ makes some nodes in $XH3_{sr}$ unreacheable from r.

$$\forall_{k \in XH3_{sr}} \exists_{j \in mXHR3_{sr}} (\mathcal{R}(j,k)) \tag{4.16}$$

and

$$\forall_{j' \in mXHR3_{sr}} \exists_{k \in XH3_{sr}} \nexists_{j \in mXHR3_{sr} - \{j'\}} (\mathcal{R}(j,k)) \tag{4.17}$$

Note that $mXHR3_{sr}$ may not be unique, and different minimal extended hidden nodes relay sets could contain a different number of nodes. Call $\{mXHR3_{sr}\}$ the set that contains all possible sets of $mXHR3_{sr}$. For instance, in our scenario there are two possible minimal extended hidden nodes relay sets: $mXHR3_{sr} = \{2, 4\}$ and $mXHR3_{sr} = \{1, 3, 4\}$. Also note that the two sets have a different number of nodes.

Definition 11: Call $MXHR3_{sr}$ the *minimum extended hidden nodes relay set* of a transmission T_{sr} in three-party proxy set coverage of node r. $MXHR3_{sr}$ is the instance of $mXHR3_{sr}$ with the smallest number of nodes. Call $\{MXHR3_{sr}\}$ the set that contains all possible sets of $MXHR3_{sr}$.

In our scenario, we need to simply pick the smallest of the possible $mXHR3_{sr}$ sets, which in our case will be $MXHR3_{sr} = \{2, 4\}$.

We note that all the definitions provided above are *constructive*, providing their own implementation methodology. Every set is defined based on the cascade of definitions preceding it, and all of them can be reduced to the reachability matrix $\mathcal{R}(i, j)$.

4.1.3 Determination of the Sets in AsyMAC

The sets V_r and $P3_r$ of node r are the direct results of the neighbor discovery protocol of A^{4}LP, based on which we can determine the sets in AsyMAC.

(1) H_{sr} includes all the hidden nodes of a transmission T_{sr}, which might be outside of the three-party proxy coverage of node r ($P3_r$), thus the complete set of nodes of H_{sr} may not be found and is not maintained.

(2) The members of $H3_{sr}$ can be found by removing from the set $P3_r$ the nodes that can be reached by the other peer of the transmission. Note that in A^{4}LP/AsyMAC, the reachability information of two neighbors of a node can be calculated based on their locations and transmission ranges.

(3) $XH3_{sr}$ is obtained by $XH3_{sr} = H3_{sr} - V_r$.

(4) $XHR3_{sr}$ includes all nodes in V_r that can reach a node in set $XH3_{sr}$.

(5) The calculation of $\{mXHR3_{sr}\}$ is described in Figure 4.4.

(6) $\{MXHR3_{sr}\}$ includes the set(s) in $\{mXHR3_{sr}\}$ with the smallest cardinality. During the process of constructing $\{MXHR3_{sr}\}$, we can ignore the minimal extended hidden nodes set whose cardinality already exceeds the achieved minimum value, which becomes our incentive to improve the algorithm. The calculation of $\{MXHR3_{sr}\}$ is described in Figure 4.5.

Input: (1) The complete permutation of nodes in $XHR3_{sr}$, call it P.
(2) The super set $\{mXHR3_{sr}\} = \emptyset$.
Output: A superset that contains all minimal extended hidden nodes relay sets, $\{mXHR3_{sr}\}$.

```
1: /* Find $mXHR3_{sr}$ for each permutation node set $P_i \in P$.*/
2: for all permutations $P_i \in P$ do
3:     $mXHR3_{sr} = \emptyset$;
4:     $T = XH3_{sr}$;
5:     while $P_i \neq \emptyset \bigwedge T \neq \emptyset$ do
6:         remove the next node $p$ from $P_i$, $P_i = P_i - \{p\}$;
7:         $mXHR3_{sr} = mXHR3_{sr} \bigcup \{p\}$;
8:         for all nodes $t \in T$ do
9:             if $\mathcal{R}(p, t)$ then
10:                $T = T - \{t\}$;
11:            end if
12:        end for
13:    end while
14:    add $mXHR3_{sr}$ to $\{mXHR3_{sr}\}$;
15: end for
16:
17: /* Remove the set $M$ from $\{mXHR3_{sr}\}$ if there exists a set $M' \in \{mXHR3_{sr}\}$ such that
    $M' \subset M$. */
18: for all $M \in \{mXHR3_{sr}\}$ do
19:     for all $M\prime \in \{mXHR3_{sr}\}$ do
20:         if $M\prime \subset M$ then
21:             remove $M$ from $\{mXHR3_{sr}\}$;
22:             break;
23:         end if
24:     end for
25: end for
26:
27: return $\{mXHR3_{sr}\}$;
```

Figure 4.4: The algorithm for calculation of $\{mXHR3_{sr}\}$.

Input: (1) The complete permutation of nodes in $XHR3_{sr}$, call it P.
(2) The super set $\{MXHR3_{sr}\} = \emptyset$.
Output: A superset that contains all minimum extended hidden nodes relay set, $\{MXHR3_{sr}\}$.

```
$min\_cardinality = \mathbf{MAX}$;

/* Find $mXHR3_{sr}$ for each permutation node set $P_i \in P$. */
for all permutations $P_i \in P$ do
    $mXHR3_{sr} = \emptyset$;
    $T = XH3_{sr}$;
    while $P_i \neq \emptyset \bigwedge T \neq \emptyset \bigwedge |mXHR3_{sr}| < min\_cardinality$ do
        remove the next node $p$ from $P_i$, $P_i = P_i - \{p\}$;
        $mXHR3_{sr} = mXHR3_{sr} \bigcup \{p\}$;
        for all nodes $t \in T$ do
            if $\mathcal{R}(p, t)$ then
                $T = T - \{t\}$;
            end if
        end for
    end while

    /* If the number of nodes in $mXHR3_{sr}$ is less than the currently achieved minimum
    cardinality, update $min\_cardinality$, reset $\{MXHR3_{sr}\}$ to $\emptyset$, and add $mXHR3_{sr}$ into
    $\{MXHR3_{sr}\}$. */
    if $T = \emptyset$ then
        if $|mXHR3_{sr}| < min\_cardinality$ then
            $\{MXHR3_{sr}\} = \emptyset$;
            $min\_cardinality = |mXHR3_{sr}|$;
        end if
        add $mXHR3_{sr}$ to $\{MXHR3_{sr}\}$;
    end if
end for

return $\{MXHR3_{sr}\}$;
```

Figure 4.5: The algorithm for calculation of $\{MXHR3_{sr}\}$.

4.1.4 Accuracy Metrics for Node Classification

We introduce a set of metrics characterizing the ability of a MAC layer protocol to silence nodes which could cause collisions. Ideally, an algorithm should silence all nodes that have the potential to be hidden nodes, as well as nodes that could potentially be affected by the transmission T_{sr}. Assume there exists an algorithm I which constructs the set of all the nodes that should be silenced during a transmission T_{sr}:

$$\mathcal{S}_{sr}(I) = H_{sr} \cup H_{rs} \cup V_s \cup V_r \tag{4.18}$$

In practice, the set of nodes silenced by an algorithm F, $\mathcal{S}_{sr}(F)$, might contain nodes that are silenced unnecessarily (misclassified) and might lack nodes which should have been silenced (missed nodes).

Definition 12: Call the *misclassification ratio* of an algorithm F for a transmission T_{sr} as $Misc_{sr}(F)$, which measures the ratio of nodes that are incorrectly silenced by F.

$$Misc_{sr}(F) = \frac{|\mathcal{S}_{sr}(F) - \mathcal{S}_{sr}(I)|}{|\mathcal{S}_{sr}(I)|} \tag{4.19}$$

Definition 13: Call the *miss ratio* of an algorithm F for a transmission T_{sr} as $Miss_{sr}(F)$, which measures the ratio of nodes which are not silenced by the algorithm F, although they should have been.

$$Miss_{sr}(F) = \frac{|\mathcal{S}_{sr}(I) - \mathcal{S}_{sr}(F)|}{|\mathcal{S}_{sr}(I)|} \tag{4.20}$$

Let $\overline{Misc(F)}$ and $\overline{Miss(F)}$ be the *average misclassification* ratio and *average miss ratio* of an algorithm F, respectively. The averages are computed over a network $\mathcal{N}$.

$$\overline{Misc(F)} = \frac{\sum_{\forall_{s,r \in \mathcal{N}} \mathcal{R}(s,r)} |\mathcal{S}_{sr}(F) - \mathcal{S}_{sr}(I)|}{\sum_{\forall_{s,r \in \mathcal{N}} \mathcal{R}(s,r)} |\mathcal{S}_{sr}(I)|} \tag{4.21}$$

and

$$\overline{Miss(F)} = \frac{\sum_{\forall_{s,r \in \mathcal{N}} \mathcal{R}(s,r)} |\mathcal{S}_{sr}(I) - \mathcal{S}_{sr}(F)|}{\sum_{\forall_{s,r \in \mathcal{N}} \mathcal{R}(s,r)} |\mathcal{S}_{sr}(I)|} \tag{4.22}$$

4.2 The A^{4}LP Routing Protocol

The A^{4}LP protocol consists of a neighbor discovery protocol that each node discovers its In-, In/Out-, and Out-bound neighbors, a path discovery protocol with m-limited forwarding, and a path maintenance protocol.

4.2.1 Information maintained by a node and packet types

A node $i \in \mathcal{N}$ maintains several data structures, a routing table (see Table 4.1), a path request sequence number and a node sequence number. The information in different packet types used by the A^{4}LP protocol is summarized in Table 4.2, and abbreviations can be found in Table 4.3.

1. *Routing Table* (RT_i): caches information for all neighbors and for most recently used destination nodes (Table 4.1). The field *dstNBType* takes one of the following values: In-bound,

Table 4.1: The fields of a routing table used in the A^{4}LP protocol

Field	**Description**
dstId	the node id of the destination node
dstLoc	the location of the destination node
dstClass	the class of the destination node
dstPow	the residual power of the destination node
dstRange	the transmission range of the destination node
dstSeq	the node sequence number of the destination node
dstNBType	the neighbor type of the destination node
nextHop	the next hop to forward a packet
expTime	the expiration time

Table 4.2: The fields of packet types used in the A^{4}LP protocol

Packet Type	**Fields**					
Hello	srcId	srcLoc	srcPow	srcClass	srcRange	srcSeq
Convey	srcId	dstId	lowId	lowLoc	lowClass	lowPow
	lowRange	lowSeq				
Update	srcId	srcLoc	srcPow	srcClass	srcRange	srcSeq
PErr	srcId	dstId	srcSeq			
FwdReq	srcId	srcLoc	srcSeq	dstId	dstLoc	dstSeq
	reqSeq	cutoff	fwdPath	weakHops	powCons	
BackReq	srcId	srcLoc	srcSeq	dstId	dstLoc	dstSeq
	reqSeq	cutoff	fwdPath	backPath	weakHops	powCons
FwdReply	srcId	dstId	fwdPath	backPath		
BackReply	srcId	dstId	backPath			
FwdReqAck	srcId	dstId	fwdPath			
FwdReplyAck	srcId	dstId				

Out-bound, In/Out-bound, or Not-neighbor. *expTime* records the expiration time for an entry after which it is no longer valid.

2. *Request Sequence Number* (reqSeq): a counter, uniquely identifies a path request packet sent by the node i. reqSeq is incremented every time a route request is sent.

Table 4.3: The abbreviations used in A^{4}LP

Field	Description
srcId/dstId/lowId	the node id of the source/destination/L-node
srcLoc/dstLoc/lowLoc	the location of the source/destination/L-node
srcClass/lowClass	the class of the source/L-node
srcPow/lowPow	the residual power of the source/L-node
srcRange/lowRange	the transmission range of the source/L-node
srcSeq/dstSeq/lowSeq	the node sequence number of the source/destination/L-node
reqSeq	the path request sequence number
cutoff	the forward cutoff
fwdPath/backPath	the forward/backward path
powCons	the power consumption per packet
weakHops	the number of weak hops

3. *Node Sequence Number* (seq): a counter revealing the freshness of a node, incremented when the node detects the change of location, residual power, transmission range, and so on.

4.2.2 Neighbor Discovery Process

In-bound Neighbor Discovery Process

The In-bound neighbor discovery (which, incidentally, leads also to the discovery of neighbors which will later turn out to be In/Out-bound) is initiated when a node joins the network. Each node periodically broadcasts a *Hello* packet to inform all the neighbors in its range of its current location, residual power, and transmission range. The time between two such transmissions is called a *hello interval*.

Upon receiving a *Hello* packet a node either updates an existing entry in its routing table or creates a new one. Acknowledgements are not required (actually not possible for In-bound neighbors). A node deletes the entries of Out- and In/Out-bound neighbors if it does not receive their *Hello* packets for several hello intervals. A *Hello* packet is a broadcast packet with a life time of one hop. The *Hello* packet provides the location, the class, the residual power, and the transmission range of the sender, see Table 4.2.

Out-bound Neighbor Discovery Process

Due to the nature of asymmetric links, Out-bound neighbors are not detected directly as their signals cannot be heard. For example, in the three-party proxy set in Figure 4.2(c), the *Hello* packet from node j cannot reach node i, thus node i cannot know that node j is an Out-bound neighbor. However, node k, which is an In/Out-bound neighbor of node i and an Out-bound neighbor of node j, is aware that link L_{ij} is asymmetric with i as the H-node and j as the L-node. Thus, node k sends a *Convey* packet to node i with the information of node j, and, at the same time, records node i as the next hop to reach node j.

In the Out-bound neighbor discovery, a node periodically checks the link relationship between its neighbors, sets up the route to its In-bound neighbor if a three-party proxy set is detected, and informs the H-node of an asymmetric link, when it detects one. The time between two Out-bound neighbor discovery is called a *convey interval*. The *Convey* packet contains the Id of the sender and of the destination (the H-node of an asymmetric link), the Id, the location, the class, the residual power, the range, and the sequence number of the L-node of the asymmetric link, see Table 4.2.

4.2.3 Location and Power Update

Dissemination of the approximate location of a node as well as its residual power is critical for any location- and power-aware routing scheme, yet it is not the focus of this thesis. It can be achieved by (i) gossiping algorithms, (ii) a broadcast scheme, in which updates are sent infrequently and locally. (iii) a hierarchical scheme - nodes form clusters around *head of a cluster*, who covers a relative large area and is able to exchange information collected from members of the cluster, or some other scheme.

In A^{4}LP a node sends location and power updates only when (i) it joins the network, (ii) has moved significantly since the last reported location, (iii) its residual power goes below *low water mark*.

4.2.4 m-limited Forwarding

We use m-limited forwarding as the technique to disseminate information in the power-constrained ad hoc networks. The area-based function $\mathcal{F}^a$ is used for the selection of the candidate nodes to forward the packets. The details of the m-limited forwarding technique can be found in Chapter 3 thus are not discussed here.

4.2.5 Path Discovery

When the sender does not have a route to the destination, it initiates *path discovery*. Traditional reactive ad hoc protocols consider only symmetric links, thus, the *forward/backward path* from the source/destination node to the destination/source node consists of the same set of nodes, but in reverse order. Once a path is found as a result of a *path discovery*, an acknowledgment is sent to the node originating the request.

In A^{4}LP, the forward and backward paths are not necessary to be the same, thus we need four phases to find and confirm both paths: *forward path request*, *backward path request*, *forward path reply*, and *backward path reply*. Moreover, we need two additional phases, namely, *forward path request acknowledgement* and *forward path reply acknowledgement*, if the destination node has a current route to the source node, as can be seen in Figure 4.6. The fields of each packet type and their abbreviations can be found in Tables 4.2 and 4.3.

Forward Path Request. The source node initiates a forward path request (*FwdReq*) packet, and uses *m-limited forwarding* to send this packet to its Out- and In/Out-bound neighbors. *fwdPath* accumulates the sequence of hops taken by the *FwdReq* packet as it travels through the network. Each intermediate node appends its node id onto *forward path* before forwarding the *FwdReq* packet. *cutoff* is the *forwarding cutoff* as described in Section 3.1. *powCons* accumulates the power consumption rate of hops taken by the *FwdReq* packet. Both transmitting and receiving power rate are counted. *weakHops* accumulates the number of nodes that operate at *low-power*

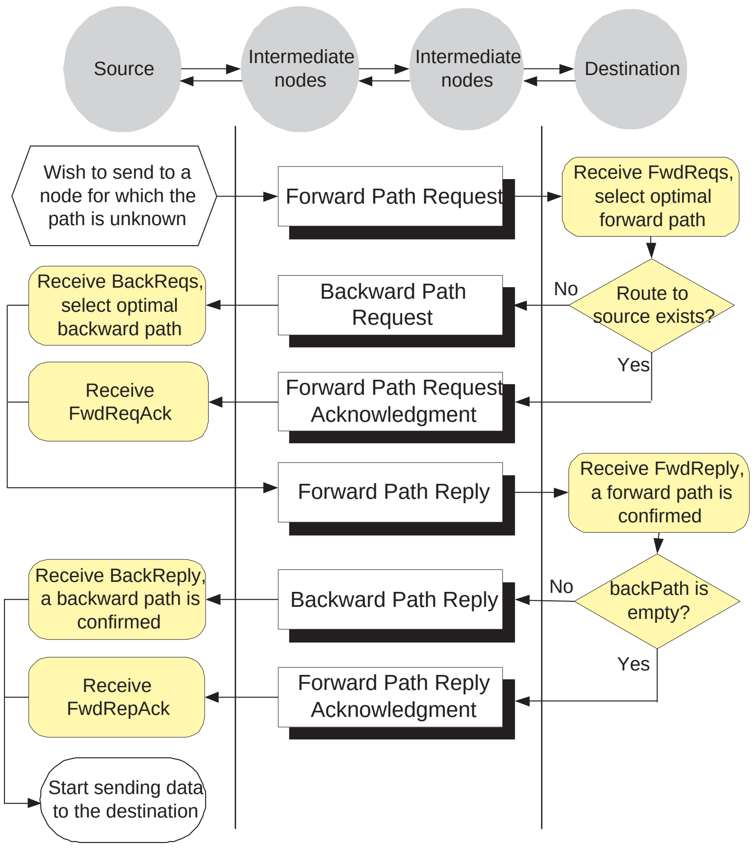

Source
Intermediate nodes
Intermediate nodes
Destination
Wish to send to a node for which the path is unknown
Forward Path Request
Receive FwdReqs, select optimal forward path
Route to source exists?
No
Yes
Backward Path Request
Receive BackReqs, select optimal backward path
Forward Path Request Acknowledgment
Receive FwdReqAck
Forward Path Reply
Receive FwdReply, a forward path is confirmed
backPath is empty?
No
Yes
Backward Path Reply
Receive BackReply, a backward path is confirmed
Forward Path Reply Acknowledgment
Receive FwdRepAck
Start sending data to the destination

Figure 4.6: The path discovery in A^{4}LP involves the following phases: Forward Path Request, Backward Path Request, Forward Path Reply, Backward Path Reply, Forward Path Request Acknowledgement, and Forward Path Reply Acknowledgement.

level, which is an indicator of the path quality. Upon receiving a *FwdReq* packet, an intermediate node synchronizes information of the source and destination node according to their sequence numbers, such that both the packet and the intermediate node contain up-to-date information about the source and destination node. If the intermediate node is allowed to forward the packet, *fwdPath*, *powCons*, *weakHops* may need to be modified. The destination node continues to accept *FwdReq* packets for a given time interval, after which it chooses a forward path from the set of received

FwdReq packets based on the power consumption per packet, arrival time, and quality of path. The destination node initiates either the forward path request acknowledgement phase if it has a valid route to the source node, or the backward path request phase otherwise.

Forward Path Request Acknowledgement. The destination node initiates a forward path request acknowledgement phase when it receives a *FwdReq* packet and has a route to the source. The forward path is piggybacked into a forward path request acknowledgement (*FwdReqAck*) packet. When the sender receives this packet, the forward path reply phase is triggered.

Backward Path Request. The destination initiates a backward path request (*BackReq*) packet, and uses *m-limited forwarding* to send the packet to its Out-, In/Out-bound neighbors, with the forward path piggybacked. Intermediate nodes handle a *BackReq* packet similar to a *FwdReq* packet. The source node chooses the best backward path based on the *BackReq*s received in a given interval, and initiates the forward path reply phase to confirm the forward path.

Forward Path Reply. The source node initiates a forward path reply phase by unicasting a *forward path reply* (*FwdReply*) packet along the forward path to the destination node. If the forward path reply phase is triggered by a *BackReq* packet, the source node piggybacks the backward path. *backPath* is set to be empty if the forward path reply phase is initiated by a *FwdReqAck* packet. A route to the destination node is established during the traversal of a *FwdReply* packet. Each node on the forward path updates its next hop neighbor towards the destination node in the *fwdPath* field of the *FwdReply* packet. To get the maximum benefit from the forward path, sub-paths can be established between intermediate nodes. For instance, suppose an intermediate node

N_i receives a *FwdReply* packet with the forward path as $[N_0, N_1, \cdots, N_i, N_{i+1}, \cdots, N_k]$ where node N_0 is the source node and node N_k is the destination node. Node N_i could establish route to $N_{i+1}, N_{i+2}, \cdots, N_k$ with next hop as N_{i+1}. The destination node initiates either the backward path reply phase if *backPath* is not empty, or initiates the forward path reply acknowledgement phase otherwise.

Backward Path Reply. The destination node initiates a backward path reply phase by unicasting a *backward path reply* (*BackReply*) packet along the backward path to the source node. A route to the source node is established during the traversal of a *BackReply* packet. All intermediate nodes handle a *BackReply* packet similar to a *FwdReply* packet. When the source node receives a *BackReply* packet, the path discovery process is completed successfully. Thus, the source node is capable of exchanging data packets with the destination node.

Forward Path Reply Acknowledgement. The destination node initiates a forward path reply acknowledgement phase when it receives a *FwdReply* packet in which *backPath* field is empty, and unicasts a forward path reply acknowledgement (*FwdReplyAck*) packet to the source node. The source node is informed the end of the path discovery phase by the *FwdReplyAck* packet and the transmission of data packets are triggered.

4.2.6 Path Maintenance

Movement of nodes lying along an active path may cause a route to become invalid. In case a route becomes invalid, at least one of the links on the route fails. A link ($L_{i,j}$) failure could be detected, if all attempts to forward a packet from node i to the next hop j fails. All packets at a failed link will be discarded. The link failure has to be reported to the source node to avoid massive retransmissions.

If the source node detects the link from it to the next hop becoming unreachable, it disables the routing entry to the destination node, and initiates a path discovery process to recover the route to the destination node. If the link failure happens at an intermediate node, it reports to the source node by sending a path error (*PErr*) packet. The source node recovers the route to the destination node by initiating a path discovery process.

4.3 The AsyMAC Protocol

4.3.1 A Solution to the Hidden Node Problem

In a wireless ad hoc network with asymmetric links, the sender may not be able to receive the CTS or ACK packets from the receiver. In such a case a DATA packet, or the next frame cannot be sent. The IEEE 802.11 protocol assumes that all the connections are symmetric. Our protocol relaxes this assumption, asymmetric links can be used provided that they are part of a *three-party proxy set* [WJM04].

Our protocol retains the use of RTS, CTS, DATA and ACK frames defined in the IEEE 802.11 standard. In addition, we introduce four new frames: XRTS (Extended RTS), XCTS (Extended CTS), TCTS (Tunneled CTS), and TACK (Tunneled ACK).

An ideal MAC layer protocol should be based upon a scheme that delivers the RTS and CTS packets to all hidden nodes in H_{rs} and H_{sr}, respectively. However, such a scheme can be impractical because (i) a node may not have the knowledge of all its In-bound neighbors; (ii) the number of hops needed to reach an In-bound neighbor might be large, thus the time penalty and the power consumption required for the RTS/CTS diffusion might outweigh the benefits of a reduced probability of collision.

Our solution is to send RTS and CTS packets to the nodes in $H3_{rs}$ and $H3_{sr}$ respectively. In this way, a considerable number of nodes that are misclassified as "hidden" nodes by [PKD01], referred to as protocol A, and [FTB02], referred to as protocol B, are allowed to transmit. Note that our approach does not identify all hidden nodes, but neither methods A or B are able to identify all hidden nodes.

4.3.2 Node Status

In IEEE 802.11, when a node overhears a RTS or a CTS packet, it becomes *silent* and cannot send any packet until its NAV expires. This way, nodes in the relay set cannot send XRTS/XCTS as they should be in a *silent* state after overhearing the RTS/CTS packet. To resolve this dilemma, we replace the *silent* state with a *quasi silent* state, in which a node is allowed to send control packets, except RTS and CTS.

The medium access control model proposed in this dissertation classifies a node as either *idle*, *active*, *quasi silent*, or *silent*. When a node is idle, it is able to send or receive any type of packets. When a node is active, it is either sending or receiving a packet. When a node is in the quasi silent state, it can either receive packets or send any packet type except RTS, CTS, or DATA. When a node is in the silent state, the node can receive packets but cannot send any packet.

4.3.3 Medium Access Control Model

The medium access control (MAC) model of our protocol is based upon an extended four-way handshake (Figure 4.7). For short data frames, there is no need to initiate a RTS/CTS handshake (see Figures 4.8(a) and 4.8(b)). For long data frames, we recognize several phases (see Figures 4.8(c) and 4.8(d)):

1. Sensing. The sender s senses the medium. If it does not detect any traffic for a DIFS period, the sender starts the contention phase; otherwise, it backs off for a random time before it senses again.

2. Contention. The sender s generates a random $\gamma \in$ [0, contention window] slot time. The sender s starts a transmission if it does not detect any traffic for γ slot time.

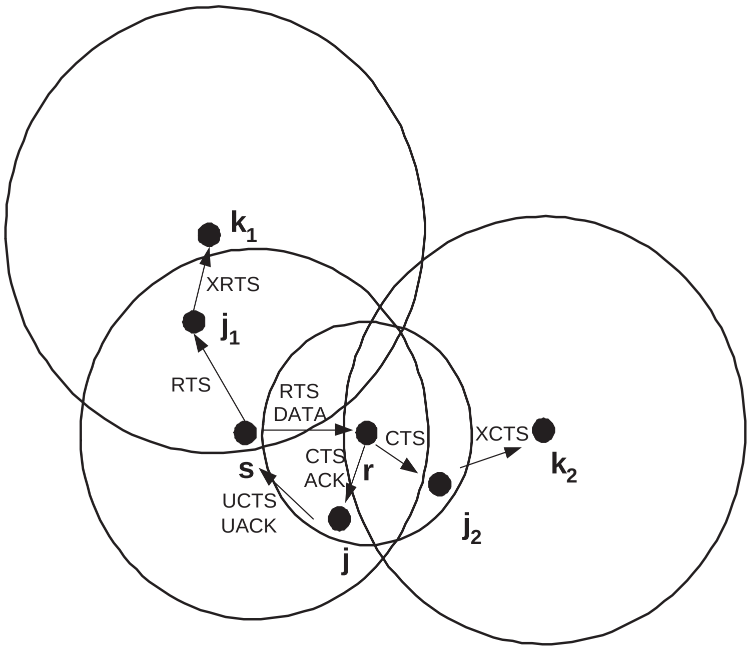

Figure 4.7: Routing over asymmetric links in a heterogeneous MANET. Node s is the sender, node r is the receiver, the link from node s to r is asymmetric, and node j is the proxy node that can relay traffic to s for r. Nodes k_1 and k_2 are hidden nodes for transmissions T_{rs} and T_{sr}, respectively. Nodes j_1 and j_2 are the proxy nodes that can relay traffic from s to k_1 and from r to k_2, respectively.

3. RTS transmission. The sender s sends a RTS packet to the receiver r. The RTS packet specifies the NAV(RTS), *link type* of L_{sr} and $MXHR3_{rs}$. The *link type* field is used to determine whether symmetric or asymmetric medium access control model is used.

4. CTS transmission. The receiver r checks whether the link is symmetric or not. If link L_{sr} is symmetric, node r sends a CTS packet back to node s; otherwise, node r sends a TCTS packet to node s. A TCTS packet specifies both the proxy node and the receiver r. The proxy node forwards the TCTS packet to the original sender s after receiving it. A CTS/TCTS packet can be sent only after sensing a free SIFS period. Instead of $MXHR3_{sr}$,

$MXHR3_{rs} - MXHR3_{sr}$ is specified in the CTS/TCTS packet so that every extended hidden node relay is included only once. Thus, the duration of XCTS/XRTS diffusion phase can be reduced.

5. XRTS/XCTS diffusion. All nodes that overhear a RTS/CTS/TCTS packet enters a *quasi silent* state. After the CTS transmission phase, all extended hidden node relays that are either specified in RTS or CTS/TCTS starts contention for broadcasting XRTS/XCTS to its neighbors. When a node captures the medium, all other nodes back-off for a random number of $(1 \ldots 4)$ SIFS periods, and continue the contention until the XRTS/XCTS diffusion phase finishes. An XRTS/XCTS diffusion phase lasts for 6 SIFS periods, after which all nodes except the proxy node become *silent*.

6. Data transmission. When the XRTS/XCTS diffusion phase finishes, the sender s starts sending DATA packets to the receiver r after sensing a free SIFS period.

7. Acknowledgement. Once the receiver r successfully received the DATA packet from the sender s, it replies with an ACK if link L_{sr} is symmetric, or a TACK packet if link L_{sr} is asymmetric. An ACK/TACK packet can be sent only after sensing a free SIFS period. When the sender s receives an ACK/TACK packet, it starts contending the medium for the next frame. Meanwhile, the NAVs that are reserved for this transmission should expire.

At any moment, if a node overhears a packet containing new NAV information, it compares it with the currently stored NAV, and retains the NAV which expires later.

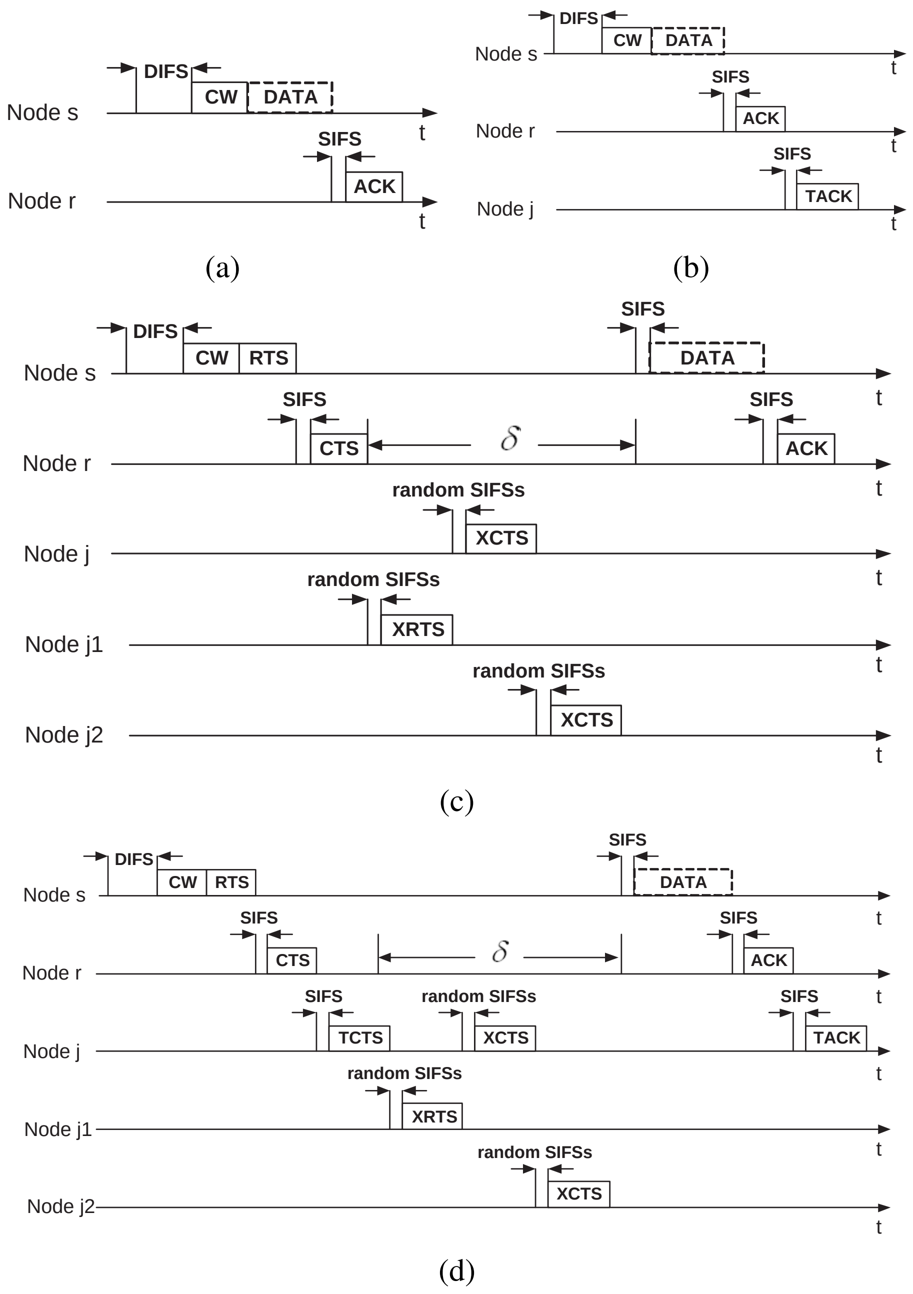

Figure 4.8: The medium access model of AsyMAC for the scenario in Figure 4.7. (a) The medium access model of AsyMAC for short data frames over a symmetric link. (b) The medium access model of AsyMAC for short data frames over an asymmetric link. (c) The medium access model of AsyMAC for long data frames over a symmetric link. (d) The medium access model of AsyMAC for long data frames over an asymmetric link.

4.4 Simulation and Case Study

We have implemented the AsyMAC protocol in NS-2 [BEF00, VIN], an object-oriented event-driven simulator developed at the Lawrence Berkeley National Laboratory, with the CMU wireless extensions [CMU]. As AsyMAC requires a routing protocol able to handle asymmetric links, we paired it with the A^4LP routing protocol to form a complete ad hoc networking stack. In our experiments, we compare the A^4LP/AsyMAC pair against the standard IEEE 802.11 protocol coupled with AODV [PR99], a widely used on-demand ad hoc routing protocol and the more recent OLSR [CJL01] protocol.

The simulation results reflect the performance of the pair of the corresponding MAC layer and routing protocols rather than the performance of the MAC layer or routing protocol alone. We had chosen this experimental setup because it provides the most informative comparison of real scenarios. We cannot run a routing protocol which does not support asymmetric links on top of AsyMAC. On the other hand, A^4LP can be run on top of MAC layer protocols which do not support asymmetric links. However, A^4LP has a higher overhead than routing protocols which assume symmetric connections, thus an A^4LP/802.11 combination would always perform somewhat worse than combinations such as OLSR/802.11, because we can take advantage of the existence of asymmetric links only if they are supported throughout the stack. Thus, the only reasonable choices are to use either all symmetric protocols or all asymmetric-link aware ones in the full stack.

A possible study would involve the comparison between asymmetric stacks, by substituting for AsyMAC the protocols described by [FTB02] and [PKD01]. In Section 4.4.3, we have implemented the core decision algorithms of these protocols for a comparison of the classification accuracy. However, there is no publicly available NS-2 implementation of these protocols, and a fully functional implementation of these protocols is beyond the scope of this thesis.

First, we analyze the benefits of algorithms able to take advantage of asymmetric links in the maintaining the connectivity of a network. Through the study of a specific scenario, we show that a protocol stack composed by the A^{4}LP/AsyMAC protocol is able to maintain connectivity where the standard IEEE 802.11 MAC layer protocol coupled with AODV or OLSR loses connectivity.

Second, we carry out a simulation study in which we evaluate the performance of the A^{4}LP/ AsyMAC stack against the AODV/802.11 and OLSR/802.11 stacks in a series of randomized networking scenarios with realistic traffic patterns.

Finally, we compare the AsyMAC protocol against two previously proposed asymmetric MAC layer protocols in terms of the accuracy of the hidden node classification.

4.4.1 A Connectivity Scenario

In this section, we briefly discuss an example when A^{4}LP/AsyMAC uses asymmetric links to route packets from each pair of nodes while both AODV/802.11 and OLSR/802.11 fail to route packets. The connectivity scenario is given in Figure 4.9. The initial position of nodes is depicted in the graph (a), which shows also the transmission range and the distance between the nodes. The graph

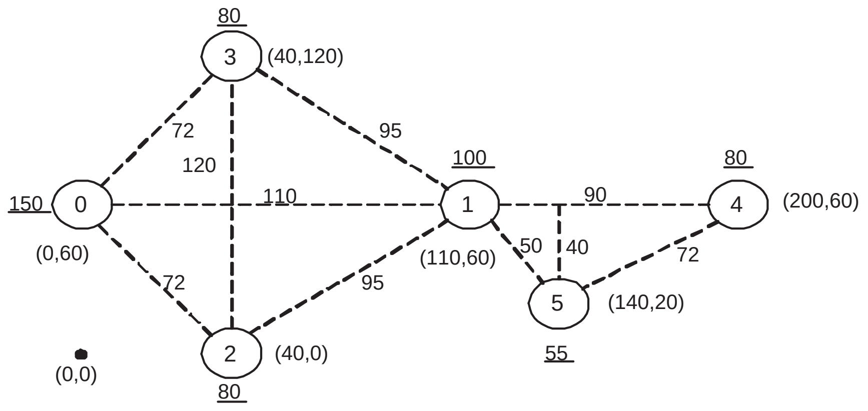

(a) Physical topology of the network

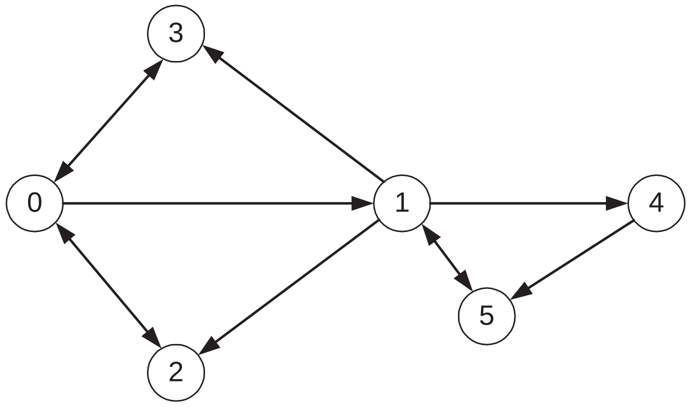

(b) Logical topology of the network

Figure 4.9: (a) The physical topology of the network, where node 0 and 4 are exchanging packets. The numbers next to the nodes indicate the position in the (x,y) format and the transmission range (underlined). The numbers on the links represent the distance between the nodes. (b) The logical topology of the network.

(b) is a logical view of the above scenario. The nodes do not move during the simulation. The forward and reverse routes are found and established by A^{4}LP, and MAC layer acknowledgements are assured by AsyMAC. For instance, node 5 is a proxy node that forwards CTS and ACK packets for a unidirectional transmission from node 1 to node 4 at the MAC layer. In this scenario, the two far-most nodes 0 and 4 are exchanging packets. The packets are successfully delivered and acknowledged by A^{4}LP/AsyMAC, while all packets are lost by AODV/802.11 or OLSR/802.11 during the transmission.

4.4.2 A Study of Alternative Protocol Stacks in Mobile Ad Hoc Networks

The previous scenario provided an example when the A^{4}LP/AsyMAC protocol maintained connectivity, while the AODV/802.11 and OLSR/802.11 stacks did not. However, these extreme cases might be relatively rare. In the following, we compare these protocol stacks in a series of simulations involving a heterogeneous MANET in a more realistic setup. To describe the movement of nodes in the system, we use the "random waypoint" model [BMJ98], which has been described in Section 3.2. The nodes are classified into four classes *C1, C2, C3* and *C4* with different transmission ranges.

The traffic patterns are generated by CBR sources sending UDP packets. Each CBR source resides at one node and generates packets for another node. Each CBR source is active for a time interval called *CBR duration*. Our simulation allows a *setup time* to allow nodes gather certain routing information before generating any traffic. After the *setup time*, the simulation time is divided into equal time slices, called *switching intervals*. During each switching interval, we generate CBR sources for different pairs of senders and receivers. Table 4.4 illustrates the default settings and the range of the parameters for our simulation experiments.

To construct 95% confidence intervals, each experiment was repeated 20 times for a pair of scenario and traffic pattern, the two elements affecting the results of a performance study. This

Table 4.4: The default values and the range of the parameters for our simulation studies

Field	**Value**	**Range**
simulation area	500×500 (m^2)	
number of nodes	8(*C1*), 16(*C2*), 24(*C3*), 32(*C4*)	30-110
ratio of nodes	C1:C2:C3:C4 = 1:2:3:4	
transmission ranges	200(*C1*),150(*C2*), 100(*C3*),50(*C4*)(m)	
speed	1 (m/s)	1-10 (m/s)
pause time	15 (s)	
simulation time	300 (s)	
setup time	20 (s)	
switching interval	10 (s)	
number of CBR sources	10	4-40
CBR packet size	64 (bytes)	
CBR sending rate	512 (bps)	
CBR duration	5 (s)	

involves 200 individual runs for the each of the 3 studies. The average execution time for a single experiment was about 3 hours, for a total of 1800 hours of computation time. By observing the evolution of the average values and the calculated confidence intervals after 5, 10 and 20 repetitions, we notice that at 20 repetitions the values reach quiescence, and future repetitions would provide only insignificant changes on the overall shape of the graphs.

We are concerned with the impact of node mobility, network load, and network density upon packet loss ratio, and latency. For each randomly generated scenario and traffic patterns, we run simulation experiments covering AODV with IEEE 802.11, OLSR with IEEE 802.11, A^{4}LP using 3-limited forwarding with the distance-based fitness function (A^{4}LP-M3-F1/AsyMAC) with AsyMAC, and A^{4}LP using 3-limited forwarding with the area-based fitness function (A^{4}LP-M3-F2) with AsyMAC.

The influence of network load

The effect of the network load upon the packet loss ratio for two standard protocol stacks AODV/802.11, OLSR/802.11 and for A^{4}LP-M3-F1/AsyMAC and A^{4}LP-M3-F2/AsyMAC is summarized by Figure 4.10. The ratio of the packets lost by AODV/802.11 is roughly twice the rate of the packets lost by the other protocols. The major reason is that flooding, an inefficient broadcast solution, is used in AODV/802.11 for finding a route. Among the other protocols, A^{4}LP-M3-F2/AsyMAC performs the best, followed by OLSR/802.11, which delivers more packets than A^{4}LP-M3-F1/AsyMAC for similar scenarios and traffic patterns. OLSR/802.11 is able to deliver packets only via symmetric links, thus packets are dropped if at least one asymmetric link is on the *critical* path; however, A^{4}LP/AsyMAC is able to deliver those packets. Our experiments also show the metric we proposed in [WJM04] (A^{4}LP-M3-F2), a combined metric with distance, power level and class information, provides better performance than the distance only metric (A^{4}LP-M3-F1) in heterogeneous MANETs.

In our study, the measured values have relatively large confidence intervals, and most of these confidence intervals overlap. This means that we do not have 95% confidence that for any particular experimental instance the given protocol will perform better than the other protocol. Indeed, if there are no (or very few) asymmetric links, the symmetric protocols will likely outperform the asymmetric ones, due to the higher overhead of the asymmetric protocol. Unfortunately, the range of the measurable values for metrics such as packet loss is very wide – in some scenarios there might be no packet loss, in other ones, many of packets are lost. This variability is reflected in

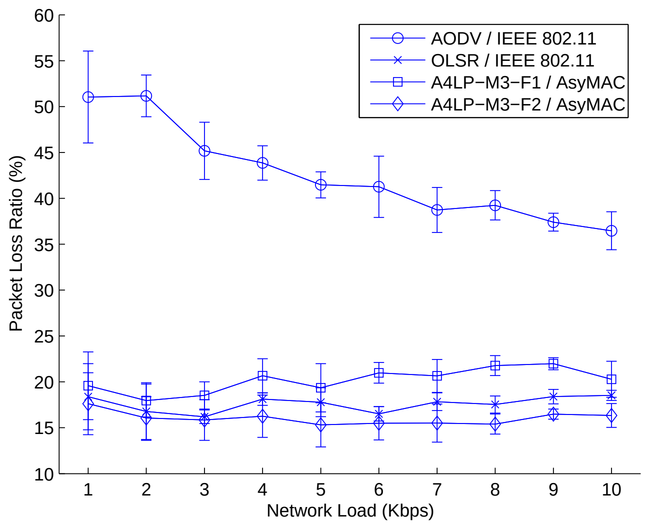

Figure 4.10: Packet loss ratio versus network load. The ratio of packets lost by AODV/802.11 is roughly twice the ratio of packets lost by the other protocols. Among the other protocols, A^{4}LP-M3-F2/AsyMAC performs the best, followed by OLSR/802.11, which delivers more packets than A^{4}LP-M3-F1/AsyMAC for similar scenarios and traffic patterns.

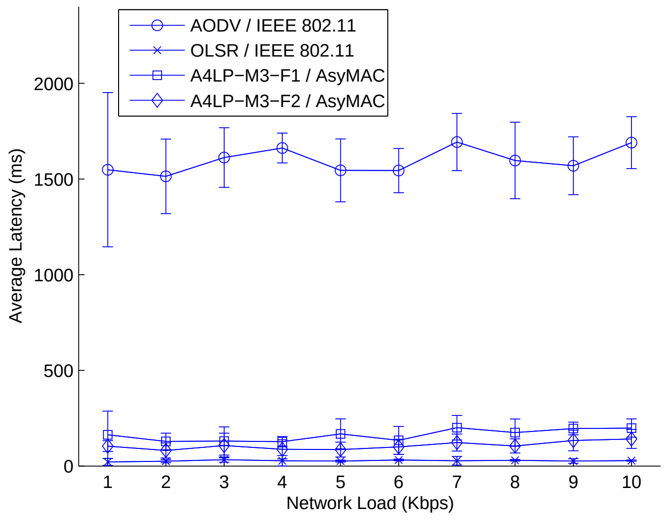

Figure 4.11: Average latency versus network load. The average latency of AODV/802.11 is much higher than the other protocols. Among the other protocols, OLSR/802.11 has the shortest latency.

relatively large confidence intervals. We believe that often when the average value of packet loss is lower for one of the protocols, the protocol will perform *in average* better than the other ones.

The effect of the network load upon the average latency for two standard protocol stacks AODV/802.11, OLSR/802.11 and for A^{4}LP-M3-F1/AsyMAC and A^{4}LP-M3-F2/AsyMAC is summarized by Figure 4.11. The average latency of AODV/802.11 is much higher than that of the other protocols. AODV is a reactive protocol which finds routes only when needed. A^{4}LP is a hybrid protocol, routes to non-neighbors are still discovered when needed, however, routes to certain In-, Out-, and In/Out-bound neighbors are maintained proactively in a routing table; this fact contributes to the reduction of the average packet delivery latency.

The OLSR/802.11 stack has the lowest average packet delivery latency, followed by A^{4}LP-M3-F2/AsyMAC, and A^{4}LP-M3-F1/AsyMAC. Note, however, that the average packet delivery latency is based only on the delivered packets. The OLSR/802.11 stack drops more packets than A^{4}LP-M3-F2/AsyMAC; these are the packets which require a protocol able to deal with asymmetric links. The packets that could be delivered by A^{4}LP-M3-F2/AsyMAC but not by OLSR/802.11 generally have higher latency, and this could explain why the average packet delivery latency of A^{4}LP-M3-F2/AsyMAC is higher than that of OLSR/802.11.

The influence of node mobility

The average packet loss ratio versus node mobility is summarized in Figure 4.12. With the node mobility increasing, the performances of A^{4}LP-M3-F2/AsyMAC and OLSR/802.11 are degraded, while the performance of AODV/802.11 fluctuates between 35% to 45%. AODV/802.11 performs

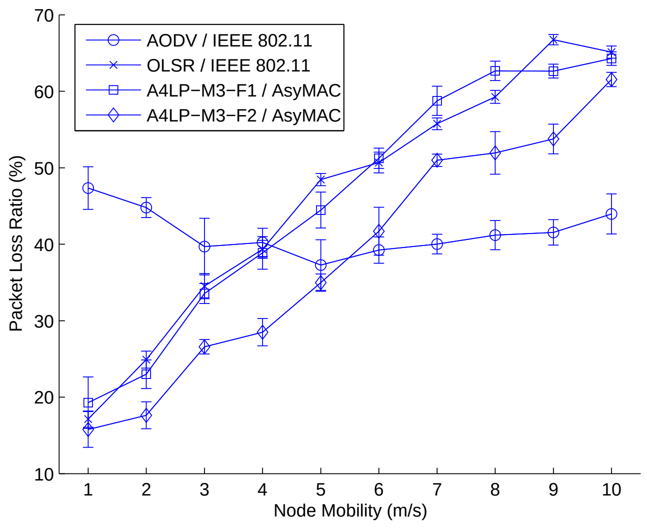

Figure 4.12: Packet loss ratio versus node mobility. With the node mobility increasing, the performances of A^{4}LP-M3-F2 and OLSR/802.11 are degraded while the performance of AODV/802.11 fluctuates between 35% and 45%. AODV/802.11 performs the worst in case of ad hoc networks with low mobility, but it outperforms the other protocols for highly mobile ad hoc networks.

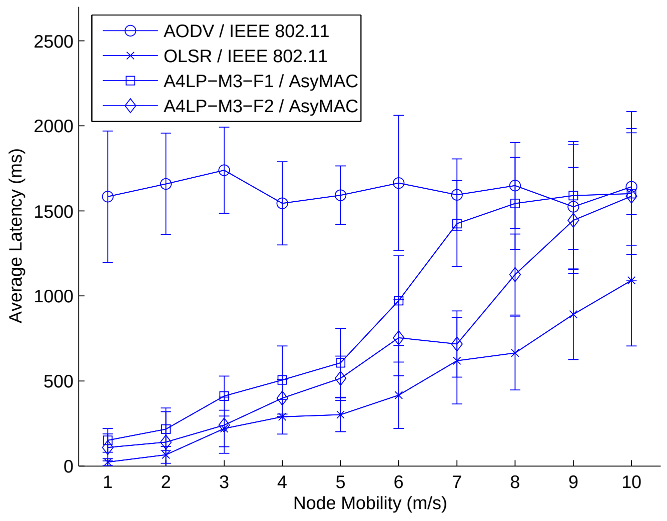

Figure 4.13: Average latency versus node mobility. The average latency of AODV/802.11 is much higher than the other protocols that perform similarly.

the worst in case of ad hoc networks with low mobility, but it outperforms the other protocols for highly mobile ad hoc networks. The reason for this is that for ad hoc networks with relatively high mobility, cached routes and neighbor information becomes stale rapidly, which degrades the performance of proactive (OLSR) or hybrid (A^4LP) protocols but not reactive (AODV) protocols. However, A^4LP-M3-F2/AsyMAC always outperforms OLSR/802.11 and A^4LP-M3-F1/AsyMAC at any node mobility in terms of packet loss ratio.

Figure 4.13 presents the average packet delivery latency versus node mobility. AODV, which is an on-demand protocol, shows about the same relatively long latency irrespective of the mobility of the nodes. For A^4LP/AsyMAC and OLSR/802.11, the average latency increases with the mobility since the protocols require additional overhead to keep the topology of the network up-to-date. At the mobility of about 10 m/s, AODV/802.11, A^4LP-M3-F1/AsyMAC and A^4LP-M3-F2/AsyMAC delivers packets with about the same latency. In these tests, OLSR/802.11 outperforms A^4LP/AsyMAC because the amount of topology data it needs to maintain is lower, being restricted to the symmetric links only. This latency advantage comes at the cost of ignoring asymmetric links, therefore, potentially disconnecting nodes which would maintain connectivity with the A^4LP/AsyMAC solution.

The influence of the number of nodes

In the following set of experiments, we vary the number of nodes moving in the measurement area. As the nodes have a limited range, when the number of nodes is too low, some nodes might lose connectivity.

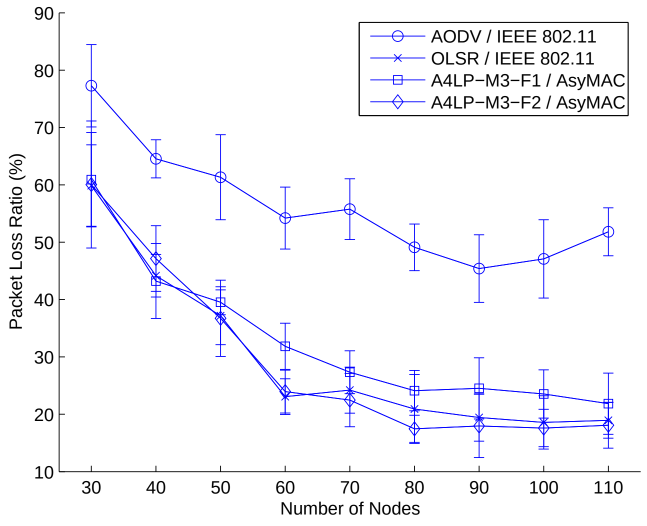

Figure 4.14: Packet loss ratio versus number of nodes. A^{4}LP-M3-F2/AsyMAC delivers most packets, followed by OLSR/802.11, A^{4}LP-M3-F1/AsyMAC and AODV/802.11 for similar scenarios and traffic patterns. The packet loss ratio decreases when the number of nodes increases.

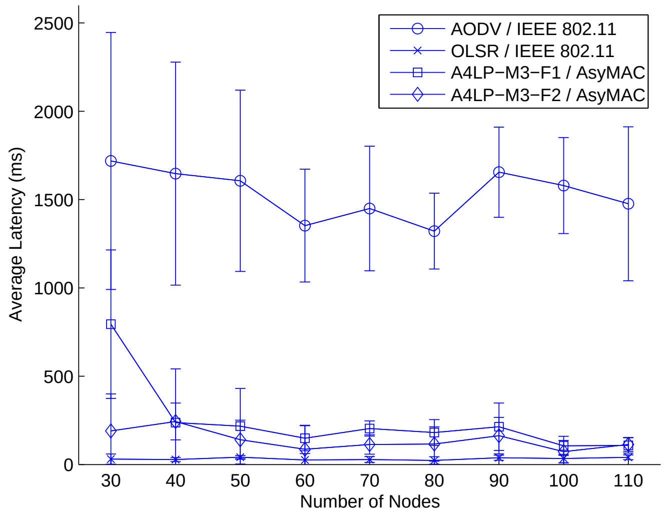

Figure 4.15: Average latency versus number of nodes. The average latency of AODV/802.11 is much higher than the other protocols. The packet delivery latency tends to decrease as the number of nodes increases for A^{4}LP/AsyMAC and OLSR/802.11.

Figure 4.14 illustrates the packet loss ratio versus the number of nodes. For similar scenarios and traffic patterns, A^{4}LP-M3-F2/AsyMAC delivers most packets, followed by OLSR/802.11, A^{4}LP-M3-F1/AsyMAC, and AODV/802.11. As the number of nodes in the network increases, the network connectivity increases as well, thus the packet loss ratio decreases. Figure 4.14 shows that the packet loss ratio decreases from roughly 60% to about 20% as the number of nodes increases from 30 to 110.

Figure 4.15 shows the average packet delivery latency versus the number of nodes. The average latency of AODV/802.11 is much higher than the other protocols. For A^{4}LP/AsyMAC and OLSR/802.11 the packet delivery latency tends to decrease as the number of nodes increases. As the number of nodes in the network increases, more neighbors and routes are found during the neighbor information exchange process, thus the packet delivery latency decreases.

4.4.3 The Accuracy of Hidden Node Classification

A node is *misclassified* as a hidden node if it is silenced by the algorithm while it should not be silenced. Misclassification reduces bandwidth utilization because it leads to unnecessary silencing of nodes which could have been transmitting. A node is *missed* by the algorithm if it was not silenced although it should have been. Missed nodes lead to collisions. The more accurate is a protocol in classifying the nodes, the better the bandwidth utilization. A useful measure of the global performance of an algorithm is the number of incorrect silencing decisions per transmission - defined as the sum of misclassified and missed nodes.

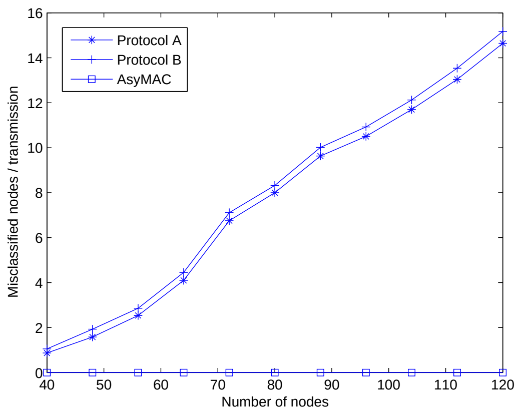

(a) Misclassified nodes

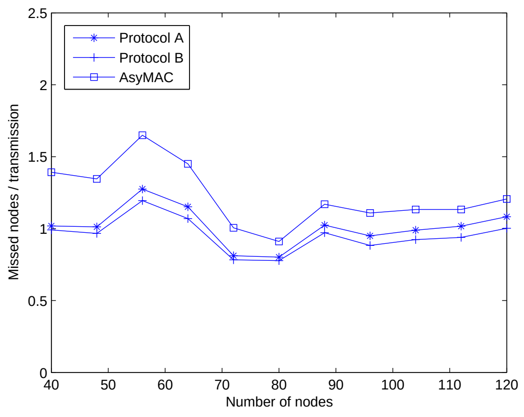

(b) Missed nodes

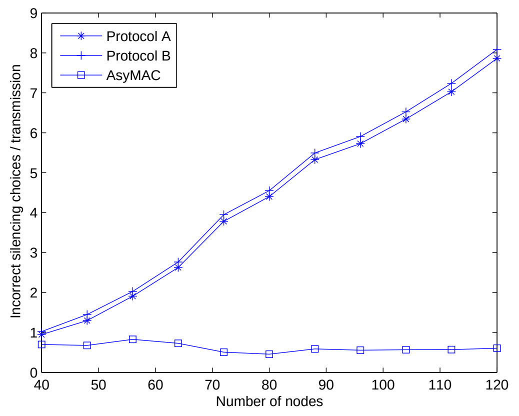

(c) Incorrectly classified nodes

Figure 4.16: (a) The average misclassified nodes per transmission as a function of the number of nodes. AsyMAC does not misclassify nodes in a static network. (b) The average missed nodes per transmission for protocols A, B, and our approach, as a function of the number of nodes. (c) The average number of incorrect silencing decisions per transmission for protocols A, B, and for our approach.

We compare the accuracy of the classification of our proposed AsyMAC protocol with the accuracy of two known protocols which are performing the same classification [FTB02, PKD01]. The simulation environment is an area of 500×500 meters. We populate our environment with a heterogeneous collection of nodes belonging to the four main classes of wireless nodes *C1, C2,* *C3*, and *C4* (see [MMJ03, WJM04]). The transmission ranges are normally distributed random variables with the mean $100, 75, 50$, and 25 meters, respectively and the standard deviations for each class is 5 meters. The simulation scenarios are created using a set of 40 to 120 nodes including an equal number of nodes for each class, uniformly distributed in the area. For each generated scenario, we repeat the experiment 1000 times. The displacement of nodes are distributed around an initial position and the standard deviation is 20% of its transmission range.

The results of the simulation are shown in Figure 4.16. The graph (a) shows the number of misclassified nodes per transmission. The AsyMAC algorithm does not misclassify nodes in a static network, because in the process of three-party proxy set formation, the nodes whose transmission ranges do not reach the current node are filtered out. However, misclassified nodes can appear with the AsyMAC protocol if the nodes are highly mobile and the current configuration does not reflect the one detected when the three-party proxy set was established. The graph (b) shows the missed nodes per transmission. Here the AsyMAC protocol performs worse than the other two protocols considered, as it is considering only the three-party proxy sets, and ignores possible higher order proxy sets. However, the number of missed nodes is very small for all the three protocols. Graph (c) shows the number of incorrect silencing decisions per transmission. Here, the AsyMAC protocol emerges with the lowest number of incorrect decisions, as its better performance at misclassification compensates for the lower performance in regards to missed nodes.

4.5 Summary

In this chapter, we argue that asymmetry of the transmission ranges in wireless networks is a reality and should be treated as such. This asymmetry makes reliable communication more difficult and requires special medium access control and routing protocols to handle it.

The models of traditional multiple access networks assumes that all nodes share a single communication channel and have access to the feedback (success, idle slot, collision) from any transmission. In this case, splitting algorithms allow sharing of the communication channel in a cooperative environment with reasonable efficiency and fairness. This is no longer the case for wireless networks with asymmetric or unidirectional links, where the sender and the receiver do not share the feedback channel and hidden nodes may interfere with ongoing transmissions.

In case of networks with asymmetric links, hidden nodes may be out of the reach for the sender and the receiver, but their transmissions may interfere with the reception of a packet by the intended destination. The hidden node problem is further complicated due to the fact that the feedback from the receiver in a RTS/CTS exchange may have to pass through several relay stations before reaching all the nodes which are expected to be silent.

Some of the solutions proposed in the literature reduce the probability of a collision by requiring a larger set of nodes to be silent unnecessarily. In turn, this has negative effects upon the communication latency and the overall throughput. We propose a MAC layer protocol, AsyMAC, which reduces the number of nodes to be silenced and at the same time, it may miss some of the nodes which should have been classified as “hidden”.

IEEE 802.11 assumes symmetric links between each pair of nodes while AsyMAC does not. For traffic over asymmetric links, AsyMAC relies on a proxy node in the three-party proxy set to relay acknowledgements back to the sender so that the reliability is assured. Our MAC protocol reduces average packet loss ratio and average latency as asymmetric links are comprehensively utilized which dominate the routing in heterogeneous MANETs.

We conducted a simulation experiment using the NS-2 simulator and compared the performance of AODV/802.11, OLSR/802.11, A^{4}LP using 3-limited forwarding with distance metric (A^{4}LP-M3-F1) with AsyMAC, and A^{4}LP using 3-limited forwarding with the metric proposed in [WJM04] (A^{4}LP-M3-F2) with AsyMAC. It is reported that A^{4}LP/AsyMAC performs much better than AODV/802.11 in the aspects of average packet loss ratio and average latency. A^{4}LP-M3-F2 with AsyMAC incurs much less average packet loss ratio compared to OLSR/802.11. Our simulation results also indicate that the fitness function proposed in [WJM04] is more proper than the traditional distance function used in heterogeneous MANETs.

CHAPTER 5
THE TIME-PARALLEL SIMULATION OF WIRELESS AD HOC NETWORKS

The development of communication systems requires rigorous performance studies. Analytical performance studies can only be carried for simple models of complex systems; such studies tend to provide a basic understanding of system behaviors and qualitative results. Simulation, on the other hand, is often used for quantitative performance study of more realistic models of complex systems.

Wireless ad hoc networks are rarely amenable to analytical performance analysis due to the complexity of the models involved. Simulation has emerged as an important tool for the study of wireless ad hoc networks, but it is commonly used to study networks with a few hundred nodes for a relatively short period of time.

There are many high quality simulators either developed in academic environments such as NS-2 [VIN], GloMoSim [ZBG98] or commercial offerings such as OpNet [OPN] and QualNet [QN]. However, we find that the recent evolution of wireless systems are creating environments with thousands of nodes and/or very high density of wireless resources, and these scenarios are pushing the limits of serial simulators such as NS-2. Even when feasible, such simulations require a significant computing power and can take a very long time. Although there is a clearly perceived need to develop simulators which can take advantage of parallel or cluster computers, the problem of parallelizing simulations through spatial partitioning turned out to be very difficult, due to the heavy interaction between the spatial partitions.

In this dissertation, we present an approach for time-parallel simulation of wireless ad hoc networks. Time-parallel simulation has been used for some time; its applicability is strongly dependent on the simulated phenomena and can yield exact results only for systems whose behavior is modeled by regenerative stochastic processes. However, as we will show, good approximations can be obtained quickly, and the quality of the approximation can be improved through iteration.

Our time-parallel simulation of wireless ad hoc networks uses a traditional simulation package coupled with new techniques for the practical implementation of the simulation. We develop a methodology to analyze the accuracy of the simulation and introduce the notion of perturbation of measurements; then we present a layer-by-layer analysis of the impact of the perturbations on the performance of the network. This approach allows us to predict the accuracy of the simulation results through an analysis of the protocols involved at each layer.

This chapter is organized as follows. We present a one-step time-parallel simulation model in Section 5.1, then in Section 5.2 we presents our model of the propagation of perturbations in wireless networks, the impact of the protocols at the various layers of the networking stack, and the application for time-parallel simulation. We apply these considerations to propose several methods for improving the speed and accuracy of time-parallel simulation. Section 5.3 presents the implementation of the theoretical models developed in the previous section with the widely used

NS-2 simulator. A series of simulation studies that investigate the speedup and precision of the proposed methods for typical wireless network simulation scenarios are presented in Section 5.4. We summarize our results in Section 5.5.

5.1 The One-step Time-parallel Simulation Model

A simulation S of an ad hoc network is specified by a six-tuple $(A, \tau, \mathcal{E}, \mathcal{I}, \mathcal{F}, \mathcal{T})$ where $\mathcal{A}$ is the geographic area, $\tau = [\tau^s, \tau^e]$ is the time interval, $\mathcal{E} = \{e_1, e_2, \ldots\}$ is the set of *planned events* and $\mathcal{I}$ is the initial state of the network at time τ^s. The output of the simulation is the simulation trace $\mathcal{T} = \{t_1, t_2, \ldots\}$ and the final state $\mathcal{F}$ at time τ^e. The simulation trace is a series of events which includes the planned events ($\mathcal{E} \subset \mathcal{T}$) as well as events which are consequences of the planned events.

The idea behind the time-parallel simulation is to replace the simulation S with a number of smaller *simulation segments*, which operate on the full area $\mathcal{A}$, but on subsets of the time interval τ. First, we describe the most straightforward way for implementing time-parallel simulation through disjoint time intervals of equal duration. In the following sections, we consider modifications to this basic model in order to achieve higher accuracy and/or speedup. In this basic model, we partition the time interval into m equal-length disjoint intervals:

$$\tau_i = [\tau_i^s, \tau_i^e] = [(i-1)\frac{\mid \tau \mid}{m}, i \cdot \frac{\mid \tau \mid}{m}], \;\; i \in \{1, .., m\} \tag{5.1}$$

where $|\tau|$ calculates the duration of time interval τ.

Let $t(e)$ be the firing time of an event e, this also implies the partitioning of the planned event set:

$$\mathcal{E}_i = \{e_i \mid e_i \in \mathcal{E},\ \ \tau_i^s \leq t(e_i) < \tau_i^e\} \tag{5.2}$$

The segments of the time-parallel simulation are specified by the six-tuple $(\mathcal{A}, \tau_i, \mathcal{E}_i, \mathcal{I}_i, \mathcal{F}_i, \mathcal{T}_i)$. As the segments are m times shorter than in the original simulation, their execution will take roughly m times shorter time, and they can be executed in parallel on m independent processors. The simulation trace of the full simulation will be the union of the simulation traces $\mathcal{T} = \mathcal{T}_1 \bigcup \ldots \bigcup \mathcal{T}_m$, while the final state of the network will be $\mathcal{F} = \mathcal{F}_m$.

The main difficulty pertains the calculation of the initial state $\mathcal{I}_i$. For the first segment, we have $\mathcal{I}_1 = \mathcal{I}$. For the other segments, the correct initial state is the final state of the previous segment $\mathcal{I}_i = \mathcal{F}_{i-1}$. However, using the final state of the previous simulation segment would require the in-order simulation of the segments, preventing any parallelism.

One crude approximation would be to assume that every simulation segment starts with the original state of the network ($\mathcal{I}$). In this *one-step time-parallel simulation model*, the simulation segments are specified by $(\mathcal{A}, \tau_i, \mathcal{E}_i, \mathcal{I}, \mathcal{F}_i, \mathcal{T}_i)$.

Experiments show that the accuracy of the one-step time-parallel simulation is not sufficient for the practical purposes of wireless ad hoc network simulation. In the following, we analyze the source of errors in the time-parallel simulation of wireless ad hoc networks, estimate the magnitude of these errors, and propose methods to improve the accuracy of the simulation.

5.2 Perturbation Analysis and Improving Accuracy of Time-Parallel Simulation

A simulation trace includes *planned events*, ($\mathcal{E} \subset \mathcal{T}$), as well as *new events* triggered by the planned events and calculated by the simulation process. For example the event corresponding to sending a packet may trigger a new event indicating a collision with with another transmission. Every event e_i has a set of *properties*, e.g, the firing time of the event $t(e_i)$, the type of the event, the packet size, etc. Such information allows us to determine important measures of performance such as packet delay, packet loss ratio, throughput, and so on.

The purpose of running a simulation is to collect the information associated to the events in the trace. However, we are rarely interested in individual events, we are concerned with observations, or measurements, spanning longer time intervals, or the entire trace.

5.2.1 Measurements on the Simulation Trace

Measurements can be:

(a) *instantaneous* $M^i(t_c)$, reflecting the situation at the current time t_c.

(b) *cumulative* $M^c(t_c)$, reflecting the evolution of the measurement from the beginning of the simulation to the current time t_c. For every instantaneous measurement M^i, there is an associated cumulative measurement M^c:

$$M^c(t_c) = \int_0^{t_c} M^i(t)dt \tag{5.3}$$

(c) *average* $M^a(t_c)$. For every instantaneous measurement M^i, there is an associated average measurement M^a defined by:

$$M^a(t_c) = \frac{\int_0^{t_c} M^i(t)dt}{t_c} \tag{5.4}$$

An example is of instantaneous measurement is the *current transmission rate*, with the associated cumulative measurement *total transmitted data*, and the associated average measurement *average transmission rate*.

Many average measurements are expressed as *ratios* of measured quantities. For some of these measurements, we find it useful to define the complementary measure $C(M^a) = 1 - M^a$. For instance the ratio measure *average packet loss ratio* has its complement *average packet delivery ratio*.

5.2.2 Perturbations on a Measurement

In the following, we investigate how an event *perturbs* the measurements of a simulation of wireless ad hoc networks. Our model accurately captures the underlying phenomena and provides a framework in which observations can be analyzed and predictions can be made.

We call an *approximate simulation for the measurement* M, related to simulation S, a simulation S' which generates a trace $\mathcal{T}'$ such that $M(\mathcal{T}') \approx M(\mathcal{T})$.

The *absolute error of simulation* for measurement M is

$$\delta_M = |M(\mathcal{T}) - M(\mathcal{T}')| \tag{5.5}$$

The *relative error of simulation* for measurement M is

$$\varepsilon_M = \frac{|M(\mathcal{T}) - M(\mathcal{T}')|}{|M(\mathcal{T})|} \tag{5.6}$$

We define the relative accuracy for measurement M as $1 - \varepsilon_M$. In most cases, the relative accuracy, expressed in percentages, is the most intuitive measure of the quality of an approximate simulation. For instance, a statement such as "the simulation has an accuracy of 98%" can conveniently express the fact that the relative error of the measurement is smaller than 2%. The relative accuracy is a non-dimensional quantity, allowing us to compare the accuracy of different measurements.

However, the relative error suffers from the phenomena of error amplification for measurements which represent the average ratios for rare events. Let us consider a simulation scenario where out of 1000 packets sent 2 are lost; then we say that the packet loss ratio is $M_{\text{PLR}} = 0.002$. If we have an approximate simulation which finds only one lost packet, the relative error will be:

$$\varepsilon_{\text{PLR}} = \frac{|M'_{\text{PLR}} - M_{\text{PLR}}|}{|M_{\text{PLR}}|} = \frac{|0.002 - 0.001|}{|0.002|} = 50\% \tag{5.7}$$

However, repeating the same calculation for the complementary measure packet delivery ratio $M_{\text{PDR}} = C(M_{\text{PLR}}) = 1 - M_{\text{PLR}}$:

$$\varepsilon_{\text{PDR}} = \frac{|M'_{\text{PDR}} - M_{\text{PDR}}|}{|M_{\text{PDR}}|} = \frac{|0.998 - 0.999|}{|0.998|} \approx 0.1\% \tag{5.8}$$

Thus, the simulation appears very inaccurate for one measurement and very accurate for the complementary measurement. The physical phenomenon behind is that the appearance of a rare event, e.g. a packet loss in a lightly loaded network, is dependent on the coincidence of a number of factors. An approximate simulation might approximate well the probability of occurrence of those factors, but not the exact location and time where the event will take place. Therefore, the absolute error might be a better indicator of the accuracy of simulation for the measurements on rare events. The absolute error has the additional advantage that the absolute error of the measurement and the complementary measurement is identical:

$$\delta_M = |M(\mathcal{T}) - M(\mathcal{T}')| = |(1 - M(\mathcal{T})) - (1 - M(\mathcal{T}'))| = \delta_{C(M)} \tag{5.9}$$

Now we introduce the notion of a *perturbing event* e_p. We consider a simulation with the planned events $\mathcal{E} = \{e_1, e_2, \ldots\}$ and a perturbed set $\mathcal{E}' = \mathcal{E} \bigcup e_p$. The perturbed set of planned events will lead to a simulation trace $\mathcal{T}'$ and, obviously, to perturbed measurements $M'(t)$. We are interested in the size and the temporal extent of the perturbations $\Delta M(t) = M'(t) - M(t)$. We say that:

- The perturbation has *no effect* on measurement M if $\Delta M(t) = 0, \ \forall t$.
- The event e_p creates a *time limited perturbation* in the measurement M which lasts until the *extinction time* t_e if $\Delta M(t) = 0, \ \forall t > t_e$.
- The event e_p has a *shift effect perturbation* on the measurement M if $\lim_{t \to \infty}(\Delta M(t)) = c$, with c being the *shift constant*. If there exists a time point t_s with the property that $\Delta M(t) = c, \ \forall t > t_s$, we call t_s the *stabilization point*.

Property 1: If an event e_p causes a time-limited perturbation on the instantaneous measurement M^i with the extinction time t_e, it creates a shift effect perturbation on the corresponding cumulative measurement M^c, with the stabilization point $t_s = t_e$. The shift constant can be expressed as:

$$c = \int_{t(e_p)}^{t_e} \Delta M^i(t) dt \tag{5.10}$$

- We say that an event causes a *destabilizing perturbation* of measurement M if $\nexists\, t_s > t(e_p)$ such that $\Delta M = c, \ \forall t > t_s$.

5.2.3 Propagation of Perturbations in Wireless Ad Hoc Networks

As a first approximation, the events in a wireless ad hoc network are caused by individual transmissions of packets. We consider the perturbing event to be the insertion of a new packet in the network. The removal of the packet is not considered separately, because it is equivalent to simply reversing the perturbed and the original system. As we are concerned about the absolute values of the difference on the measurements of these systems, the reversed system will yield the same conclusions. An additional type of perturbation we consider is the perturbation of the initial state, that is, the simulation starts with a different initial state than expected. We discuss this type of perturbation separately.

For events representing the addition or removal of a single packet, the immediate affect of the perturbations is usually minimal. However, the networking protocols deployed at various levels of the networking stack can amplify or (in some cases) reduce the impact of the perturbations.

In the following, we investigate the impact of the protocols deployed at the various layers of the networking stack on the perturbation produced by the insertion of a single packet.

Physical layer. An inserted packet will perturb the physical layer measurements only for the duration of the packet transmission. The time it takes to transmit a packet can be calculated as follows. Assume that we send a packet of 1536 bit, the maximum length supported by the 802.11b protocol. The transmission rate of 802.11b is 1.375 Mbps. The time required to send this packet is composed of:

- Distributed Inter-Frame Space (DIFS), set to 50μs
- Data packet transmission: 192μs for the preamble + $1536/\ 1.375Mbps = 192\mu s + 1118\mu s$
- Short Inter-Frame Space (SIFS), set to 10μs
- 802.11 ACK packet: $192\mu s + 14/1.375Mbps = 203\mu s$

Thus, the total transmission time becomes $2084\mu s$, or approximately, 2 ms. This might change slightly for different protocols, but the order of magnitude remains the same. We conclude that the perturbation at the physical layer due to a new packet is time-limited, with a very short (2 ms) extinction time.

MAC layer. The perturbation caused by an inserted packet at the MAC layer depends on the load of the network, and the type of the inserted packet. If the packet is a control packet such as RTS, CTS, or ACK, its influence extends beyond the time frame covered. For instance, receiving an RTS packet in a CSMA/CA network forces the node to refrain from transmitting for the duration specified in the packet. The size of this interval can be as long as the maximum packet transmission time, on the order of magnitude of 2μs.

Delaying the sending of a packet can in its turn delay the sending of the response or follow-up packets, creating a ripple effect. Normally, this will appear as a time-limited perturbation. For a TDMA (Time Division Multiple Access) type protocol, for a channel with the capacity of n bps, with a load of $\nu \leq 1$, and a packet size of l, the extinction time can be estimated as:

$$t_e = \frac{l}{n \cdot (1 - \nu)} \tag{5.11}$$

Note that for a full channel, $\nu = 1$, the perturbation becomes a shift effect perturbation.

For CSMA/CD (Carrier Sense Multiple Access with Collision Detection) protocols, the perturbation will extend to the length of the contention window. IEEE 802.11b uses an exponential back-off algorithm where the contention window (CW) can vary between CW_{MIN} and CW_{MAX}. Typical values of CW_{MIN} are between 7-15 and of CW_{MAX} are between 7-255 with the numbers being multiples of a slot time which is 20μs in IEEE 802.11b. Thus, the influence of the initial collision can extend to 5000μs. However, if the channel is very busy, the initial collision can lead to further collisions down the line. Furthermore, every collision extends the collision window through exponential back-off, which will be only gradually reduced.

In conclusion, for highly loaded networks, the insertion of a packet that creates a collision can cause perturbations for up to several seconds in the worst case.

Network layer. Perturbations triggered by packet insertion at the network layer are heavily dependent on the nature of the protocol and the inserted packet. The critical question is whether the packet will change the routing of future packets or not. If the packet is part of an established flow of application layer data, it will most likely not affect the routing of the other packets. If the packet is the first packet of a new flow, and the routing protocol is a reactive one, the packet will establish a new route. This frequently requires broadcast of routing information, which in its turn triggers the transmission of additional packets. Although this appears to be a destabilizing perturbation, the extent of this flooding is carefully constrained by the routing protocol and it will last at most several seconds.

Proactive routing algorithms deploy a routing table periodically updated by routing packets. The insertion of a routing packet triggers a perturbation in the network by changing the routing table of a node, and this will affect the routing of future packets. This is a major perturbation, affecting a large number of packets and a time interval on the order of minutes. A routing table perturbation is extinct when the routing tables of the original and the perturbed system re-converge. This situation occurs when:

- The modified routes are superseded by new, independently discovered routes, in both the original and the perturbed system (for instance, as a result of node mobility).
- The original system acquires the same routes as the perturbed one.
- The modified routes expire through a timeout and the routing table returns to the unperturbed version.

- An external command or a predetermined timeout flushes partially or completely the routing tables, forcing the recomputing of all routes.

Although it is technically possible to imagine a routing protocol where the loss or addition of a single routing packet would change the routes indefinitely, virtually all protocol designers, in their quest to make the protocols more reliable, have adapted features which make the routing tables converge; this has the indirect effect of limiting the perturbations and improve the accuracy of time-parallel simulations.

Transport layer and application layer. Finally, we investigate how a perturbing event affects the transport layer and the application layer protocols. The major difference here is between reliable or non-reliable protocols. Let us consider the case of the most frequently used reliable transport protocol, TCP. The loss of a single TCP packet can significantly perturb the subsequent TCP flow: the packet will be retransmitted, the transmission window reset to its minimal value, which will then extend through the slow start algorithm. Thus, the loss of a single packet can exert an influence over the network for several tens of seconds.

In the case of the UDP protocol, which does not implement reliable transmission, the perturbation is minimal or nonexistent at the transport layer. However, applications which deploy UDP at the transport layer frequently use application layer protocols to control the flow of data. For instance, the multimedia streaming application RealPlayer is using an application level byte stream protocol RTP (Real-time Transport Protocol, specified in RFC 1889) for the transfer of multimedia information, with UDP being the transport protocol. Packet losses are handled by a complex logic and actions involving the RTSP (Real Time Streaming Protocol), RTCP (Real Time Control Protocol), SDP (Session Description Protocol) and, of course RTP.

We conclude that perturbations have effects up to the application layer. However, at the application layer, the behavior of the system becomes very complex, and in some cases, small perturbations can have major effects on the state of the system. This problem is not specific to time-parallel simulation. Most simulation studies of wireless ad hoc networks consider scenarios with constant or variable bit rate generic UDP sources, without application level protocols deployed in the simulator. When application level flow is simulated, it is done by an artificially generated stream which replicates the properties of a packet stream generated by the application level protocol, without actually deploying the application in the simulator [WAH06]. In these types of models perturbations propagate only over very short time frames, thus creating an environment favorable for time-parallel simulation.

Up to this moment we have considered only perturbations caused by a single perturbing event. In the following, we discuss the possible inter-event perturbations, that is, the perturbations which arise from the interaction between two or more independent perturbing events. There can be several ways in which the perturbations caused by several events can be are composed:

Dual events. Dual events cancel each other; their successive occurrence does not change the state of the system. For instance, a reboot sequence is represented by two events: a node failure, followed after a short time by the node recovery. Individually, each event causes a perturbation, however, their effects cancel each other. The state of the system will be the same as if none of the events occurred. This favorable case rarely occurs in practice.

Idempotent events. Idempotent events lead to the same state regardless if only one, a subset, or all of them occur. For instance, two subsequent missed routing table updates create the same effect – an incorrect routing table entry, which requires the need to run a path discovery process. Idempotent events appear whenever some component of the system has a special "correct" state, while the other, "incorrect" states are functionally identical. Such system components are relatively frequent; examples are routing table entries or established end-to-end connections.

Independent events. Independent events lead to the same state of the system regardless of the order in which they occur; the overall perturbation of state caused by the events is additive. Their compound effect can be studied considering the perturbations caused by the individual events independently.

Mutually amplifying events. Such events lead to drastic alteration of state; the perturbation caused by the a sequence of such events is significantly larger than the perturbations caused by the individual events occurring independently. For example, an event that causes a routing table to be overwritten with incorrect values and the second event that propagates the incorrect routing table to all the nodes in the network, will cause the network failure.

Naturally, mutually amplifying events are the worst scenario from the point of view of the accuracy of the time-parallel simulation. We need to carefully consider whether they can occur in the considered scenarios. Note that in our hypothetical example, the mutually amplifying events caused a total interruption of the communication in the simulation. Practically deployed networking stacks contain build-in guards against such types of unstable behavior. Mutually amplifying events are clearly possible during the experimental testing of new routing or MAC protocols. The observation of such an unstable behavior is an important feedback to the developers; at the same time, they need to be aware that the errors in the time-parallel simulation of such unstable systems are significantly higher.

We conclude that inter-event interactions yield perturbations which are identical or smaller than the perturbations considered individually, for most practically deployed, stable protocols. Mutually amplifying events, however, are possible if the deployed protocol stack shows unstable behavior (most frequently, as a result of experimental code). In these cases the accuracy of the simulation will be much lower.

5.2.4 Techniques for Improving the Accuracy of Time-Parallel Simulation

Let us now return to the one-step time-parallel simulation described in Section 5.1, and consider the sources of errors in the approximation. For instance, in Figure 5.1(a) we see a partitioning of the simulation interval $[0, t]$ into three equal time intervals: $[0, t_1 = t/3]$, $[t_1 = t/3, t_2 = 2t/3]$ and $[t_2 = 2t/3, t]$. The event e_1, in the first segment is creating a perturbation which is not extinguished until the middle of the second segment. As the two segments are simulated independently, the processor simulating the second segment does not know about the perturbation which leads to an

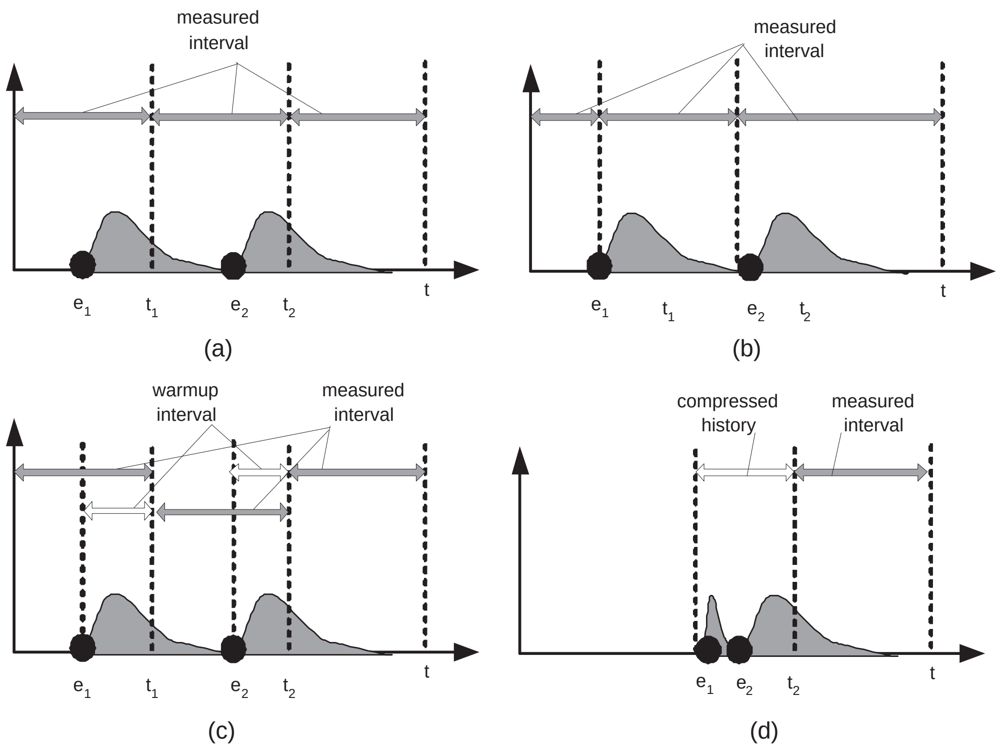

Figure 5.1: An illustration of techniques for improving the accuracy of time-parallel simulation. (a) Equal length batches without improvement. (b) Time interval shift. (c) Warmup intervals. (d) Warm up with compressed history.

inaccurate simulation. Let us now review several techniques through which this inaccuracy can be reduced or eliminated.

Time interval shift. One way to increase the accuracy of the simulation is to select the boundaries of the simulation intervals such that the perturbations are completely contained in the segments, as shown in Figure 5.1(b). These points are the equivalent of the regenerative states of stochastic processes. If we cannot find states where all the perturbations are extinguished, we can search for points where there are a comparatively smaller number of ongoing perturbations (partial regenerative states).

There are several problems with this approach. First, there might not be any regenerative states in the simulation, or their distribution might not lead to segments of size appropriate for parallelization. The most difficult problem, however, is to find regenerative or partially regenerative states in a simulation without first running the simulation itself. There are certain circumstances that the identification of such points is possible. If a routing protocol periodically flushes the complete set of routing information, that instance corresponds to a regenerative state. Similarly, long periods of silence can be used as regenerative states, and they can be identified with an initial analysis of the scenario.

Warmup interval. This technique relies on separating the time span of the simulation segment into a *warmup interval* followed by the *measurement interval*. During the warmup interval, we perform the simulation but do not perform any measurements. Thus, the simulation performed during the measurement interval will be more accurate, since it considers not only the events occurring during the measurement interval, but also the perturbations caused by events generated during the warmup interval.

The ideal size of the warmup interval is the shortest period which contains all the perturbing events that generate perturbations extending to the measurement interval (see Figure 5.1(c)). The size of the required warmup interval can vary between various segments, the first segment does not require a warmup interval. Unfortunately, for practical cases we cannot accurately compute the ideal duration of the warmup interval without first running the simulation.

Warmup with compressed history. In a practical run of time-parallel simulation with warmup interval, the size of the warmup interval can be significantly longer than the measurement interval; thus most of the computation time is spent into the simulation of the warmup interval, which does not contribute to the measurements. Traditionally, the warmup interval is the exact copy of the simulation scenario for a period before the measurement interval. We can replace the warmup interval with a shorter and/or simpler simulation interval which, however, would yield the same results. For instance, we can remove all the events from the warmup interval which do not produce perturbations at the measured point. For the events which produce perturbations, we might be able to replace them with events that are easier and faster to simulate. We call this modified warmup interval a *compressed history* (see Figure 5.1(d)).

Initial state approximation (ISA). In this technique, we are computing an approximation of the initial state of the simulation segments without previous execution of the simulation. We had seen that for a typical simulation of a wireless ad hoc network the perturbation with the largest impact on the measurements relates to the changes in the routing tables. As most simulations start with an empty routing table which will be filled in during the initial phase of the simulation, which becomes a major source of errors. Approximating the routing table at the beginning of each simulated segment can thus significantly increase the accuracy of the simulation.

Composite methods. The methods of improving the precision of the time-parallel simulation can be used in conjunction with one another. The warmup interval can be composed of two phases: one compressed history (for instance, covering the complete time frame from the beginning of the simulation), followed by a warmup interval operating on the original planned event list. The initial state approximation method can be used to approximate the state at the beginning of the warmup interval. The time interval shift method can also be deployed in conjunction with any of the methods.

5.3 Implementation of Time-parallel Simulation for Ad Hoc Networks

In the following, we present our implementation of the time-parallel simulation using the NS-2 simulator [VIN]. The first method, based on the iteratively extended warmup of the simulation segments, can be deployed without changes to the NS-2 implementation of the protocols. An alternative method that combines iteratively extended warmup and initial state approximation produces better results; this method requires some knowledge of the implementation of the routing protocol and additional code to allow the initialization of the routing tables.

Let us now highlight the relevant features of the NS-2 simulator. We defined a simulation as the transformation of the six-tuple $(\mathcal{A}, \tau, \mathcal{E}, \mathcal{I}, \mathcal{F}, \mathcal{T})$ into the output consisting of the final state $\mathcal{F}$ and the simulation trace $\mathcal{T}$. While NS-2 is compatible to this definition, there are differences in our ability to extract, interpret and modify the different components.

The NS-2 script and trace files, $\mathcal{E}$ and $\mathcal{T}$, are very easy to create, parse and filter; they consist of lines of text, one event per line. Once the simulation passes a given time line, the output at that time point immediately becomes available, thus the data can be extracted while the simulation is still in progress.

In contrast, it is relatively difficult to generate and extract the initial and final state of the simulation. The data associated with the state is distributed across the protocol implementations; there is no standard format and API through which this information can be accessed. While there is no obstacle in principle to access this information, this task needs to be handled case by case, and it requires extensive knowledge of the implementation details of the protocols involved. We proposed an alternative method that relaxes the need for state saving and restoration such that we can use the stock unpatched simulator for simulation of arbitrary protocols.

5.3.1 Time-parallel Simulation with Iteratively Extended Warmup Interval

Our first method for implementing time-parallel simulation relies on iterative extension of the warmup interval. The approach allows us to obtain simulation results with increasingly higher accuracy *during the runtime of the simulation*. The simulation can be stopped when the desired accuracy is reached. This approach does not require the manipulation of the initial or the final state of the simulation, thus it is independent of the simulated protocols. Nevertheless, different protocols might converge at a different speed to the correct solution.

We partition the temporal dimension of a simulation $S = (\mathcal{A}, \tau, \mathcal{E}, \mathcal{I}, \mathcal{F}, \mathcal{T})$ into m time intervals $\{\tau_i | \tau_i = [(i-1)\frac{|\tau|}{m}, i\frac{|\tau|}{m}], 1 \leq i \leq m\}$. Then, we obtain a time-parallel simulation set $L^{(0)} = \{S_i^{(0)} | S_i^{(0)} = (\mathcal{A}, \tau_i, \mathcal{E}_i^{(0)}, \mathcal{I}, \mathcal{F}_i^{(0)}, \mathcal{T}_i^{(0)}), 1 \leq i \leq m\}$, in which all simulation segments start with the initial state of the network ($\mathcal{I}$). Thus the time-parallel simulation set will operate on the full spatial component $\mathcal{A}$, but a subset of the temporal span τ_i. We call this raw time-parallel simulation method as the TPS algorithm. In case of an exact simulation, the final state of $S_i^{(0)}$ needs to match the initial state of $S_{i+1}^{(0)}$, $1 \leq i \leq m-1$. However, since there is no prior knowledge for the initial states of $S_2^{(0)}, \ldots, S_m^{(0)}$, when they are parallelized, the combined simulation trace $\mathcal{T}^{(0)} = \mathcal{T}_1^{(0)} \cup \mathcal{T}_2^{(0)} \cup \ldots \cup \mathcal{T}_m^{(0)}$ is far from being approximate.

We notice that the simulation trace of $S_1^{(0)}$ becomes an accurate trace after the execution of $L^{(0)}$. As we discussed in Section 5.2.4, a solution to refine the other simulation traces is to apply a warmup interval before the measurement interval, or say, to apply the final state of a simulation interval to the initial state of its successive simulation interval. The new simulation set becomes $L^{(1)} = \{S_i^{(1)} | S_i^{(1)} = (\mathcal{A}, \tau_i, \mathcal{E}_i^{(1)}, \mathcal{F}_{i-1}^{(0)}, \mathcal{F}_i^{(1)}, \mathcal{T}_i^{(1)}), 2 \leq i \leq m\}\}$. The causality dependencies of events of two consecutive time intervals are now removed, meanwhile the dependencies for events in a time interval to affect later time intervals are weakened, since the strongest causality dependencies (dependencies of two consecutive time intervals) are already removed. The combined simulation trace after the first iteration, $\mathcal{T}^{(1)} = \mathcal{T}_1^{(0)} \cup \mathcal{T}_2^{(1)} \cup \mathcal{T}_3^{(1)} \cup \ldots \cup \mathcal{T}_m^{(1)}$, should become more accurate, compared to $\mathcal{T}^{(0)}$.

As we repeat this process, all strong dependencies between consecutive simulation intervals are further removed and the simulation trace becomes more accurate. The parallel simulation continues until the error of simulation results in all relevant metrics is lower than a pre-defined threshold. The k-thiteration contains $m-k$ simulation segments

$$L^{(k)} = \{S_i^{(k)} | S_i^{(k)} = (\mathcal{A}, \tau_i, \mathcal{E}_i^{(k)}, \mathcal{F}_{i-1}^{(k-1)}, \mathcal{F}_i^{(k)}, \mathcal{T}_i^{(k)}), i \in \{k+1, \dots, m\}\} \tag{5.12}$$

After the k-th iteration, the traces of simulation intervals $S_1^{(0)}, S_2^{(1)}, \dots, S_{k+1}^{(k)}$ become accurate. The combined simulation trace of $L^{(k)}$ can be obtained by

$$\mathcal{T}^{(k)} = \mathcal{T}_1^{(0)} \cup \mathcal{T}_2^{(1)} \cup \mathcal{T}_3^{(2)} \cup \dots \cup \mathcal{T}_k^{(k-1)} \cup \mathcal{T}_{k+1}^{(k)} \cup \mathcal{T}_{k+2}^{(k)} \cup \dots \cup \mathcal{T}_m^{(k)} \tag{5.13}$$

We illustrate the approximate simulation in the following example, see Figure 5.2. Assume a simulation $S = (500 \times 500, [0, 180], \mathcal{E}, \mathcal{I}, \mathcal{F}, \mathcal{T})$ is segmented into 9 equal-duration time intervals, with $\tau_i = [20(i-1), 20i], i \in \{1, \dots, 9\}$. The simulation sets of iteration 0, 1, 2 are as follows

$$\begin{aligned}
L^{(0)} &= S_1^{(0)} \cup S_2^{(0)} \cup S_3^{(0)} \cup S_4^{(0)} \cup S_5^{(0)} \cup S_6^{(0)} \cup S_7^{(0)} \cup S_8^{(0)} \cup S_9^{(0)} \cup S_9^{(0)};\\
L^{(1)} &= S_2^{(1)} \cup S_3^{(1)} \cup S_4^{(1)} \cup S_5^{(1)} \cup S_6^{(1)} \cup S_7^{(1)} \cup S_8^{(1)} \cup S_9^{(1)} \cup S_9^{(1)};\\
L^{(2)} &= S_3^{(2)} \cup S_4^{(2)} \cup S_5^{(2)} \cup S_6^{(2)} \cup S_7^{(2)} \cup S_8^{(2)} \cup S_9^{(2)} \cup S_9^{(2)}.
\end{aligned} \tag{5.14}$$

The simulation traces after iterations 0, 1, 2 are as follows

$$\begin{aligned}
\mathcal{T}^{(0)} &= \mathcal{T}_1^{(0)} \cup \mathcal{T}_2^{(0)} \cup \mathcal{T}_3^{(0)} \cup \mathcal{T}_4^{(0)} \cup \mathcal{T}_5^{(0)} \cup \mathcal{T}_6^{(0)} \cup \mathcal{T}_7^{(0)} \cup \mathcal{T}_8^{(0)} \cup \mathcal{T}_9^{(0)};\\
\mathcal{T}^{(1)} &= \mathcal{T}_1^{(0)} \cup \mathcal{T}_2^{(1)} \cup \mathcal{T}_3^{(1)} \cup \mathcal{T}_4^{(1)} \cup \mathcal{T}_5^{(1)} \cup \mathcal{T}_6^{(1)} \cup \mathcal{T}_7^{(1)} \cup \mathcal{T}_8^{(1)} \cup \mathcal{T}_9^{(1)};\\
\mathcal{T}^{(2)} &= \mathcal{T}_1^{(0)} \cup \mathcal{T}_2^{(1)} \cup \mathcal{T}_3^{(2)} \cup \mathcal{T}_4^{(2)} \cup \mathcal{T}_5^{(2)} \cup \mathcal{T}_6^{(2)} \cup \mathcal{T}_7^{(2)} \cup \mathcal{T}_8^{(2)} \cup \mathcal{T}_9^{(2)}.
\end{aligned} \tag{5.15}$$

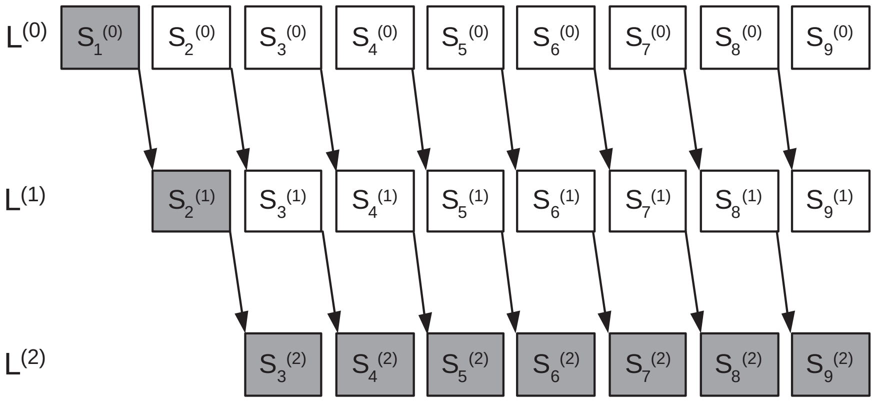

$L^{(0)}$
$L^{(1)}$
$L^{(2)}$
$S_1^{(0)}$ $S_2^{(0)}$ $S_3^{(0)}$ $S_4^{(0)}$ $S_5^{(0)}$ $S_6^{(0)}$ $S_7^{(0)}$ $S_8^{(0)}$ $S_9^{(0)}$
$S_2^{(1)}$ $S_3^{(1)}$ $S_4^{(1)}$ $S_5^{(1)}$ $S_6^{(1)}$ $S_7^{(1)}$ $S_8^{(1)}$ $S_9^{(1)}$
$S_3^{(2)}$ $S_4^{(2)}$ $S_5^{(2)}$ $S_6^{(2)}$ $S_7^{(2)}$ $S_8^{(2)}$ $S_9^{(2)}$

Figure 5.2: The time-parallel simulation with iteratively extended warmup interval (TPS-I). The duration of the simulation S is 180 sec. It is segmented into 9 equal-duration simulation intervals. The shaded simulation segments are used to compose the final simulation trace after 3 iterations.

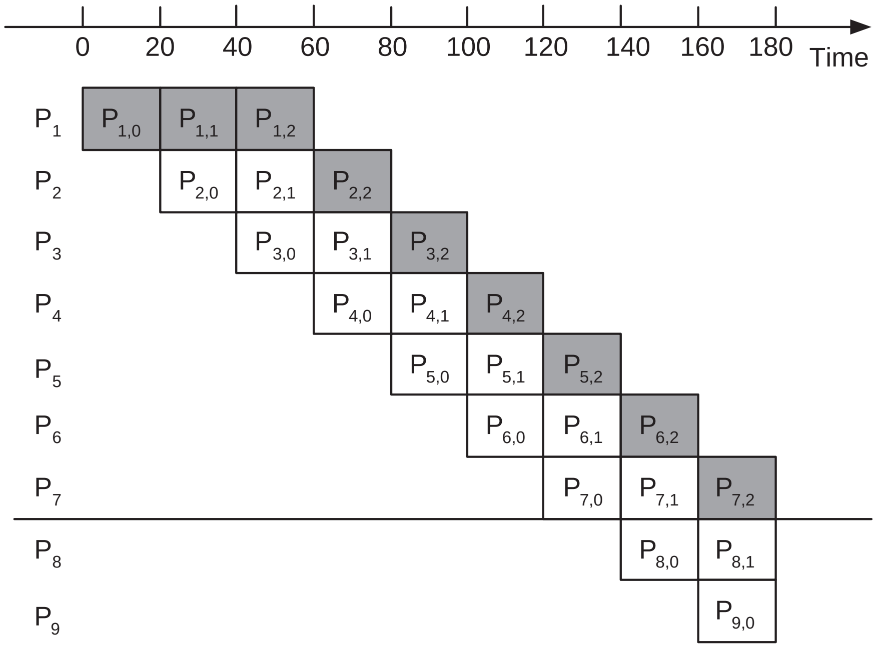

0
20
40
60
80
100
120
140
160
180
Time
P_1 $P_{1,0}$ $P_{1,1}$ $P_{1,2}$
P_2 $P_{2,0}$ $P_{2,1}$ $P_{2,2}$
P_3 $P_{3,0}$ $P_{3,1}$ $P_{3,2}$
P_4 $P_{4,0}$ $P_{4,1}$ $P_{4,2}$
P_5 $P_{5,0}$ $P_{5,1}$ $P_{5,2}$
P_6 $P_{6,0}$ $P_{6,1}$ $P_{6,2}$
P_7 $P_{7,0}$ $P_{7,1}$ $P_{7,2}$
P_8 $P_{8,0}$ $P_{8,1}$
P_9 $P_{9,0}$

Figure 5.3: An alternative approach to the time-parallel simulation in Figure 5.2. $m = 9$, $k = 2$. Shaded blocks correspond to partial results used to construct the final simulation results.

The proposed approach requires the ability to accurately capture the complete state of a simulation, and to restart the simulator with an arbitrary initial state. For instance, to accurately capture the state of the simulation at the MAC layer, we need to store information such as the packets in the priority queue, the status of timers for NAV, RTS, CTS and all the other MAC related information. In addition, the simulator is required to have the ability to start a simulation with an arbitrary value of these parameters. This is not possible with the stock NS-2 distribution. Furthermore, as different protocols require different state data, we would need to develop new patches for every new protocol considered.

In the following, we present a method (refer to Figure 5.3) to rearrange the calculations in such a way that the state saving and restoration is not necessary, and we can use the stock, unpatched simulator for arbitrary protocols. Let us consider the approximate simulation trace obtained after the k-th iteration. We partition the simulation interval into m overlapping time intervals:

$$\pi_i = \begin{cases} [(i-1)\frac{|\tau|}{m}, (i+k)\frac{|\tau|}{m}], \ i \in \{1, \ldots, m-k\}; \\ [(i-1)\frac{|\tau|}{m}, |\tau|], \qquad i \in \{m-k\ +1, \ldots, m\}. \end{cases} \tag{5.16}$$

The time interval π_i starts at the same time with τ_i, but it lasts for $(k+1)$ times the duration of τ_i for the first $(m-k)$ time intervals; π_i ends at τ_e for later time intervals. We obtain a time-parallel simulation set $L = \{P_i | P_i = (\mathcal{A}, \pi_i, \mathcal{E}_i, \mathcal{I}, \mathcal{F}_i, \mathcal{T}_i), i \in \{1, \ldots, m\}\}$. π_i can be divided into a set of sub time intervals, each with a duration of $\dfrac{|\tau|}{m}$:

$$\pi_{i,j} = [(i-1+j)\frac{|\tau|}{m}, (i+j)\frac{|\tau|}{m}] = \tau_{i+j} \tag{5.17}$$

Call $P_{i,j}$ the j-th sub-interval of P_i (enumeration starts at 0):

$$P_{i,j} = (\mathcal{A}, \pi_{i,j}, \mathcal{E}_{i,j}, \mathcal{I}_{i,j}, \mathcal{F}_{i,j}, \mathcal{T}_{i,j}), \quad 1 \leq i \leq m,\ 0 \leq j \leq \min\{k, m-i\} \tag{5.18}$$

where

$$\mathcal{I}_{i,j} = \begin{cases} \mathcal{I}, & \text{for } j = 0; \\ \mathcal{F}_{i,j-1}, & \text{for } j > 1. \end{cases} \tag{5.19}$$

Then,

$$P_i = \begin{cases} P_{i,0} + P_{i,1} + \ldots + P_{i,k},\ i \in \{1, \ldots, m-k\}; \\ P_{i,0} + P_{i,1} + \ldots + P_{i,m-i}, i \in \{m-k\ +1, \ldots, m\}. \end{cases} \tag{5.20}$$

$P_{i,j}$ simulates the same simulation interval as S_{i+j} ($\pi_{i,j} = \tau_{i+j}$). For instance, in Figures 5.2 and 5.3, $P_{3,2}$, $P_{4,1}$ and S_5 all simulate the simulation interval [80, 100].

We assume the same simulation S in Figure 5.2 as our example, $m = 9, k = 2$. The new simulation set $L = \{P_1, P_2, \ldots, P_9\}$ is shown in Figure 5.3. We observe that $P_{i,0}$ and S_i are essentially equivalent since they simulate the same time interval as well as the same set of events, without prior knowledge of the initial states (see Figures 5.2 and 5.3). Thus, $L^{(0)}$ can be rewritten as

$$L^{(0)} = \{S_i^{(0)} | i \in \{1, \ldots, m\}\} = \{P_{i,0} | i \in \{1, \ldots, m\}\} \tag{5.21}$$

The final state of simulation $P_{i,0}$ is naturally transferred as the initial state of simulation $P_{i,1}$, thus $P_{i,1}$ and $S_{i+1}^{(1)}$ are essentially equivalent since they simulate the same time interval and the same set of events with the same initial states. Thus, $I^{(1)}$ can be rewritten as

$$L^{(1)} = \{S_i^{(1)} | i \in \{2, \ldots, m\}\} = \{P_{i,1} | i \in \{1, \ldots, m-1\}\} \tag{5.22}$$

Similarly,

$$L^{(k)} = \{S_i^{(k)} | i \in \{k+1, \dots, m\}\} = \{P_{i,k} | i \in \{1, \dots, m-k\}\} \tag{5.23}$$

The alternative simulation algorithm has several desirable properties: (i) the final state corresponding to time interval τ_i is naturally and accurately accepted as the initial state of its successive time interval, τ_{i+1}, and the obstacle to save the state information is removed; (ii) if the number of iterations $(k+1)$ to obtain the approximate simulation trace is known, the subset $\{P_i | i \in \{m-k+1, \dots, m\}\}$ is not needed in the computation of $\mathcal{T}^{(k)}$, thus the required number of computational nodes can be reduced from m to $m-k$. In our example, the simulation set $\{P_8, P_9\}$ is not needed, and the required number of cluster nodes can be reduced from 9 to 7.

5.3.2 Time-parallel Algorithm with Initial State Approximation

In the previous section, we have seen how our implementation of iteratively extended warmup involves the threads of simulation specified by the six-tuple $S_i = (\mathcal{A}, \tau_i, \mathcal{E}_i, \mathcal{I}_i, \mathcal{F}_i, \mathcal{T}_i)$, that is, the simulation threads start with the same initial state $\mathcal{I}$, which is accurate only for S_1 and is one of the major source of errors for other simulation threads. To obtain an accurate simulation, we would need to start the simulation with an initial state $\mathcal{I}_i$ which describes the state of the simulation as would appear at the corresponding moment in a linear simulation run.

The initial state approximation method relies on running the simulation threads specified by $(\mathcal{A}, \tau_i, \mathcal{E}_i, \mathcal{I}'_i, \mathcal{F}'_i, \mathcal{T}_i')$ where $\mathcal{I}'_i$ is an approximation of the initial state. The whole point of the method is that $\mathcal{I}'_i$ is computable without the need to run a serial simulation to the corresponding time point.

The analysis of Section 5.2.3 shows that the perturbations with the largest effect on the behavior of the network are the changes in the routing tables. Therefore, in our implementation of the initial state approximation, we will concentrate on the estimation of the state of the routing table at the simulated time point. Naturally, this method can be applied only to the routing protocols which use a routing table. The method cannot be applied to purely reactive routing protocols such as AODV. On the other hand, reactive routing protocols maintain less state information, and approximating their initial state with an empty state yields less error. This conjecture is supported by our experiments in Section 5.4.

The approximation of the routing table needs to be implemented separately for every routing protocol, as both the routing table and its representation in the simulation code can vary among different protocols. In the following, we describe our implementation for the DSDV routing protocol.

The implementation requires the understanding of the procedure used by the protocol to build its routing table. In DSDV, every node maintains a routing table which contains all available destinations, the next node to reach a given destination and the number of nodes necessary to reach that destination. In essence, this is a shortest path problem, complicated by the fact that (a) no global view of the network is available and (b) the mobility of the nodes can change the network connectivity and make the routing tables obsolete. DSDV solves the first problem by deploying a distributed version of the Bellman-Ford algorithm. This algorithm relies on the iterative improvement of the routing tables through periodic or event-triggered broadcast of the routes to the immediate neighbors of the node. Even in a static network, it needs several send/receive cycles until the correct distance information is distributed all over the network. In a mobile network, the routing tables contain only an approximation of the correct shortest path information.

Let us now consider how we approximate the initial state of the routing table at time t. When running a simulation, the researcher is in the position of an omniscient external observer. Knowing the mobility models deployed in the simulation, one can obtain the correct location information of the nodes at any time point. Using this information, an "ideal" routing table can be obtained by simply running Dijkstra's shortest path algorithm for each node. Note that having a global view of the network, there is no point in running a distributed algorithm. The resulting routing table is the one that the DSDV algorithm would converge to *if the nodes would be immobile* for a sufficiently long time; this table will be used as the approximate initial state $\mathcal{I}_i$ in the time-parallel simulation. In practice, the actual routing tables will be somewhat out of date due to node mobility.

This approach can be readily adapted to routing protocols which use a distance vector based routing table; routing protocols which use tables constructed based on different principles (e.g. geographic routing algorithms, directed diffusion, and so on) need different approximation methods.

5.4 Simulation Study

We present the results of an investigation of the performance, accuracy, and benefits of our methodology for the time-parallel simulation. We first performed the simulation using the serial NS-2 simulator, obtaining a baseline result. Next, we repeated the simulation using the iteratively extended warmup model of time-parallel simulation as described in Section 5.3.1, with data concerning the packet loss ratio and the throughput collected after every iteration. We repeated the simulations for the widely used Ad-hoc On-demand Distance Vector (AODV) routing protocol and Destination Sequenced Distance Vector (DSDV) routing protocol; for the table-driven protocol DSDV, we run the simulation both with and without initial state approximation.

We are only concerned with the *relative error* of the simulation results; the absolute values of the measured metrics are not relevant for our study, since they are dependent on the scenario and the deployed protocols, rather than the parallelization model. However, the considerations in Section 5.2.3 show that certain parameters of the scenario, such as the mobility of the nodes and the network load, affect the number and nature of perturbations. To quantify this influence, we investigate the accuracy of the time-parallel simulation function of these scenario parameters.

In all our experiments, we found that the first several iterations lead to a major decrease in the relative errors of metrics, followed by a smaller improvement in subsequent iterations. Thus, we find it useful to use a logarithmic scale for the presentation of the results.

5.4.1 Simulation Setup

To run our simulations in a realistic setting, we chose a setting representative for practical scenarios. We consider a set of mobile nodes moving in a rectangular area, with a set of pre-determined communication patterns. The transmission range of the nodes is significantly smaller than the simulation area. The node-to-node communication is facilitated by an ad hoc routing protocol. One of the challenges of the scenario is that the mobility of the nodes changes the network topology and the routing of the packets.

Our scenarios use two well-known protocols, representative of the major classes of wireless ad hoc routing protocols. DSDV [PB94] is a pro-active routing protocol in which the nodes maintain routing tables and perform actions to keep them up-to-date. AODV [PR99] is a reactive, on-demand routing protocol where the routes are established only as a result of explicit demand. These two classes of protocols exhibit different behaviors in relation to the time-parallel simulation.

We use the "random waypoint" model [BMJ98] to simulate the node movement. Traffic patterns are generated by CBR sources sending 512-byte UDP packets at a rate of 1 packet per second. The simulation area is 500×500 m^2 square area and the default number of nodes is 80. All the nodes have a transmission range of 100 meters. The scenario extends over a time interval of 600 seconds. Table 5.1 shows the default settings and the range of the parameters for our experiments.

We investigate the relative error for the packet loss ratio and the throughput of the given algorithm. Notice that both of these are average measurements.

Table 5.1: The default values and the range of the parameters for our simulation studies

Field	**Value**	**Range**
simulation area	500×500 (m^2)	
number of nodes	80	
transmission range	100 (m)	
speed	1 (m/s)	1 - 21 (m/s)
pause time	15 (s)	
simulation time	600 (s)	
segment duration	30 (s)	10 - 60
number of CBR sources	20	4 - 40
CBR packet size	512 (bytes)	
CBR sending rate	4 (kbps)	

For each experiment, we randomize the source-destination pairs of CBR sources, and execute 10 times to obtain the average, as well as, 95% confidence interval for each quantity. The iterations will stop when the desired accuracy is reached. We assume that the desired accuracy is 95% and the simulation requires k_{95} iterations to reach this level of accuracy. The speedup of the time-parallel simulation will be $\kappa = m/k_{95}$. The value of k_{95} depends on many factors: the choice of m, the length of the simulation, the deployed protocols and the simulation scenario. The use of initial state approximation can reduce the required number of iterations.

As we discussed in Section 5.2.4, we are interested in investigating the techniques that could potentially improve the accuracy of the time-parallel simulation. We implemented the initial state approximation techniques for both DSDV and AODV routing protocols. In the follow context, the time-parallel simulation algorithm without ISA is referred as *plain* time-parallel simulation, while the one with ISA is called *ISA* time-parallel simulation.

5.4.2 Simulation Results

Segment Duration. This set of experiments (Figures 5.4 and 5.5) allows us to determine the number of iterations required and the level of accuracy that could be achieved by the time-parallel simulation, for different segment durations. Figure 5.4 and Figure 5.5 are the simulation results obtained by *plain* time-parallel simulation and *ISA* time-parallel simulation, respectively. We experiment with segment durations of 10, 20, 30, 40, 50, and 60 sec. As the simulation time is fixed at 600 sec., the number of segments are 60, 30, 20, 15, 12, and 10, respectively.

The curves labeled *PROTOCOL.ITERATION.i* in Figure 5.4 show the relative error after iteration i for the two protocols. Table 5.2 summarizes the number of iterations needed (k_{95}), the accuracy $(1 - \varepsilon)$, as well as the speedup (κ) compared to sequential execution, for *plain* time-parallel simulation with both DSDV and AODV. Table 5.3 reflects the same parameters for *ISA* time-parallel simulation with DSDV.

Table 5.2: The number of iterations needed (k_{95}), the accuracy $(1-\varepsilon)$ and the speedup (κ), function of segment duration, for *plain* time-parallel simulation with both DSDV and AODV

Segment Duration (s)	**DSDV**			**AODV**		
	k_{95}	$1-\varepsilon$	κ	k_{95}	$1-\varepsilon$	κ
10	14	97.3%	4.28	3	95.6%	20.0
20	8	96.9%	3.75	2	95.4%	15.0
30	5	96.7%	4	2	95.4%	10.0
40	4	96.5%	3.75	2	95.8%	7.5
50	4	97.7%	3	2	95.8%	6.0
60	3	97.3%	3.3	2	95.7%	5.0

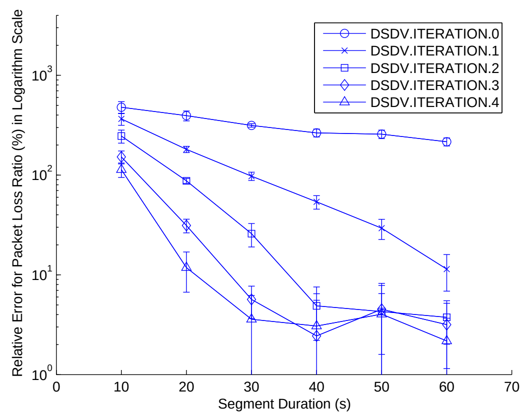

(a)

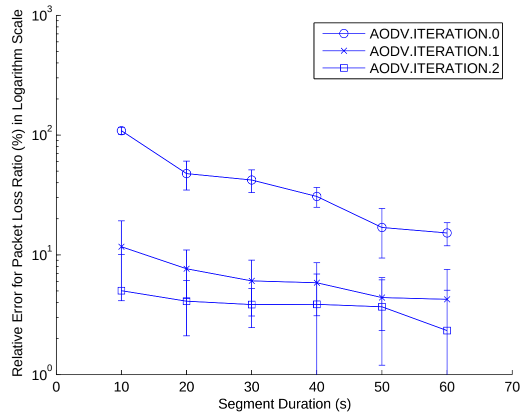

(b)

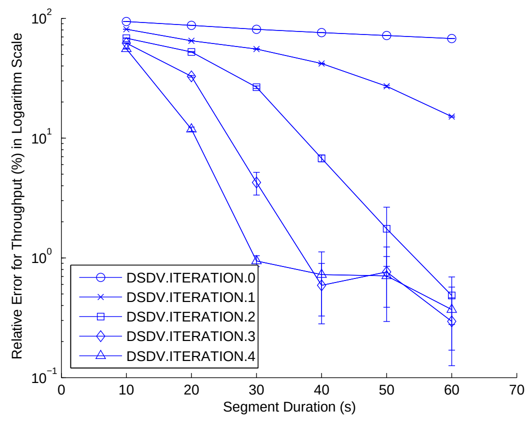

(c)

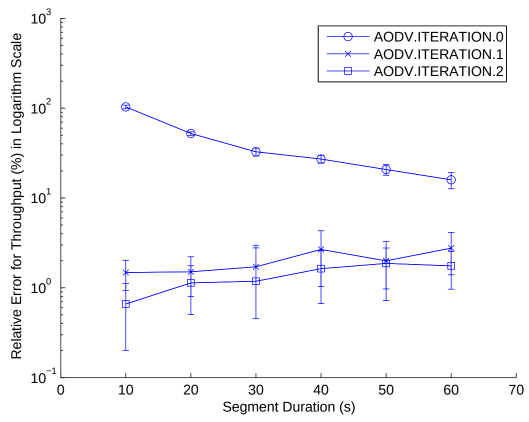

(d)

Figure 5.4: The relative error for the packet loss ratio and the throughput, function of the segment duration in a logarithmic scale; DSDV (left) and AODV (right). (a) and (b) show the relative error for the packet loss ratio; (c) and (d) show the relative error for the throughput. *Plain* time-parallel simulation is applied in this set of experiments.

For *plain* time-parallel simulation with DSDV (Table 5.2), the accumulated warmup intervals of the time-parallel simulation with segment duration of 10, 20, 30, 40, 50, and 60 sec. are 130, 140, 120, 120, 150, and 120 sec., respectively; the same figures for *ISA* time-parallel simulation with DSDV (Table 5.3) are 60, 60, 60, 80, 50, and 60 sec., respectively. We observed that with the

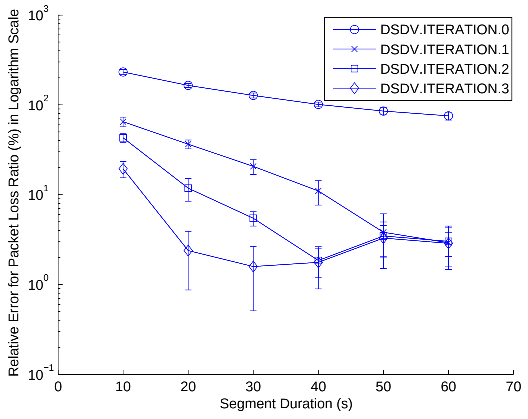

(a)

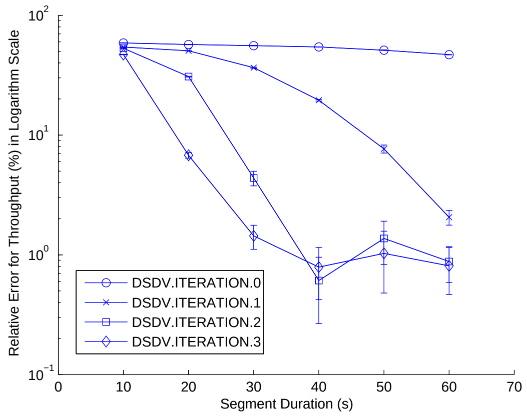

(b)

Figure 5.5: The relative error for the packet loss ratio and the throughput for DSDV, function of the segment duration in a logarithmic scale. (a) shows the relative error for the packet loss ratio; (b) shows the relative error for the throughput. *ISA* time-parallel simulation is applied in this set of experiments.

Table 5.3: The number of iterations needed (k_{95}), the accuracy ($1-\varepsilon$) and the speedup (κ), function of segment duration, for *ISA* time-parallel simulation with DSDV

Segment Duration (s)	**DSDV**		
	k_{95}	$1-\varepsilon$	κ
10	7	98.4%	8.6
20	4	97.6%	7.5
30	4	98.4%	5.0
40	3	98.1%	5.0
50	2	96.3%	6.0
60	2	97.2%	5.0

similar duration of warmup intervals, the accuracy achieved by the time-parallel simulation with different segment durations are approximately the same.

For AODV, the performance increases when the warmup interval increases from 0 to 20 sec., however, it does not further increase when the warmup interval exceeds 20 sec. AODV is a reactive routing protocol which does not require the maintenance of routing tables (largest victim of perturbations), so the perturbation effect is relatively small. This indicates that in our time-parallel simulation with AODV, the extinction time for events is less than 20 sec., which explains that no further performance can be enhanced when the warmup interval is greater than 20 sec.

We also notice that the speedup is significantly improved when the initial state approximation technique is applied in the time-parallel simulation. *ISA* time-parallel simulation greatly improves the speedup/accuracy compared to *plain* time-parallel simulation.

We note that the speedup for a single iteration is equal with the number of simulation segments (provided that there are a sufficient number of computational nodes); however, smaller segments require a larger number of iterations to achieve equivalent precision. Overall, however, the speedup tends to increase with the decrease of segment size. Thus, a proper segment duration need to be chosen according to the simulation time and the number of available computational nodes.

Network Load. This set of experiments (Figure 5.6, 5.7) investigate the effect of the network load upon the number of iterations and the accuracy. The number of CBR sources ranges from 4 to 40. The size of a CBR packet is 512-bytes, and the rate for each source is 1 packet per second.

The simulation results presented by Figure 5.6 and Figure 5.7 are obtained by *plain* time-parallel simulation and *ISA* time-parallel simulation, respectively. We notice that for both *plain* and *ISA* time-parallel simulation, the relative error fluctuates around a stable value regardless of workload after a certain number of iterations. For *plain* time-parallel simulation, the number of iterations, the approximate accuracy and speedup for DSDV are: 5, $95.3\% - 98.4\%$, and 4.0

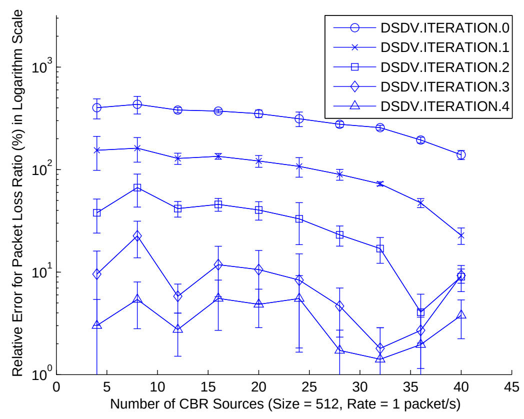

(a)

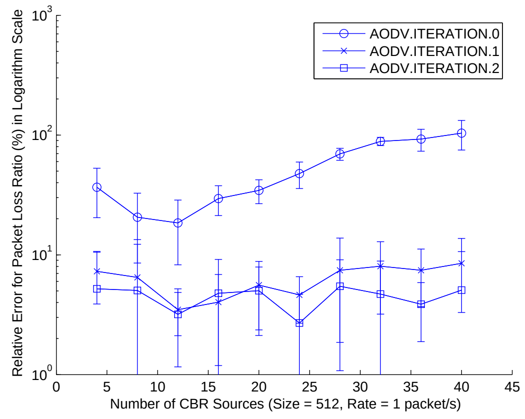

(b)

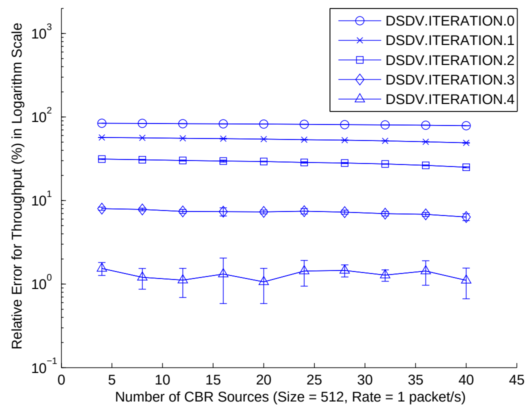

(c)

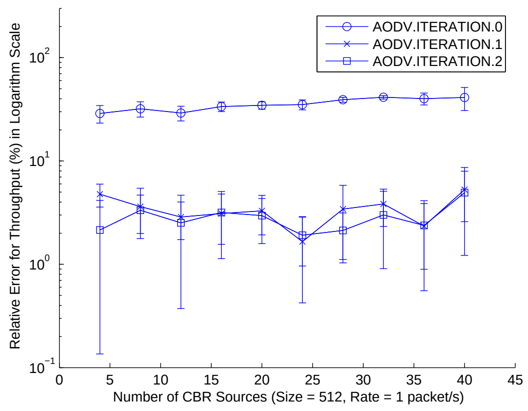

(d)

Figure 5.6: The relative error for the packet loss ratio and the throughput, function of the network load in a logarithmic scale; DSDV (left) and AODV (right). (a) and (b) show the relative error for the packet loss ratio; (c) and (d) show the relative error for the throughput. *Plain* time-parallel simulation is applied in this set of experiments.

respectively; the same figures for AODV are 2, $93.8\% - 96.6\%$, and 10.0 respectively. For *ISA* time-parallel simulation with DSDV, the number of iterations, the approximate accuracy and speedup are: 4, $97.5\% - 98.5\%$. and 5.0 respectively. The number of iterations required to obtain the simulation results is about the same regardless of the number of CBR sources.

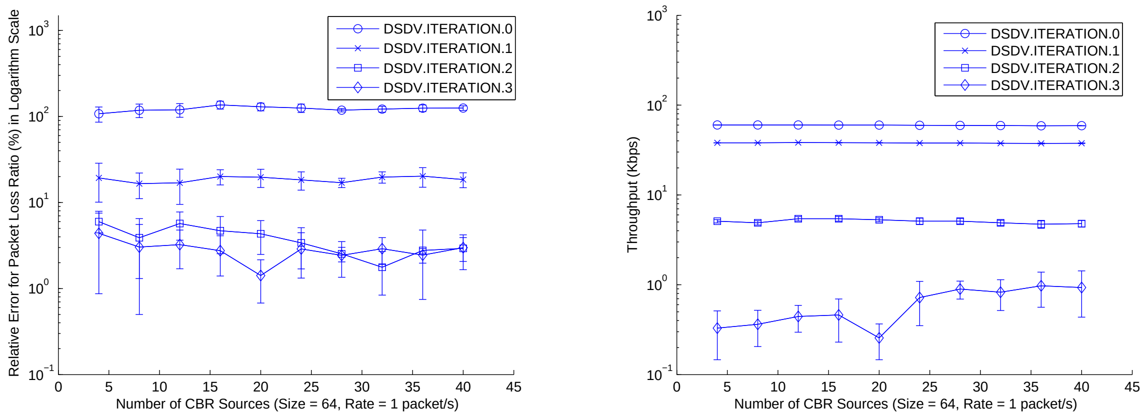

(a) (b)

Figure 5.7: The relative error for the packet loss ratio and the throughput for DSDV, function of the network load in a logarithmic scale. (a) shows the relative error for the packet loss ratio; (b) show the relative error for the throughput. *ISA* time-parallel simulation is applied in this set of experiments.

Node Mobility. We conducted this set of experiments (Figures 5.8 and 5.9) to reveal whether the node mobility will affect the number of iterations required to achieve a relative error threshold. The node mobility ranges from 1 to 21 m/sec.

The simulation results presented by Figure 5.8 and Figure 5.9 are obtained by *plain* time-parallel simulation and *ISA* time-parallel simulation, respectively. From Figure 5.8 and Figure 5.9, we can see that for both protocols the relative error for the metrics we investigate fluctuates around a relatively stable value regardless of the node mobility. The results are increasingly more accurate as the number of iterations increases. The number of iterations and the speedup for both protocols are identical with those presented earlier, when we allowed node mobility to vary.

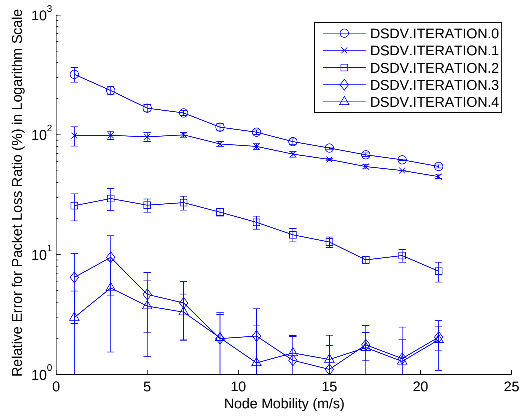

(a)

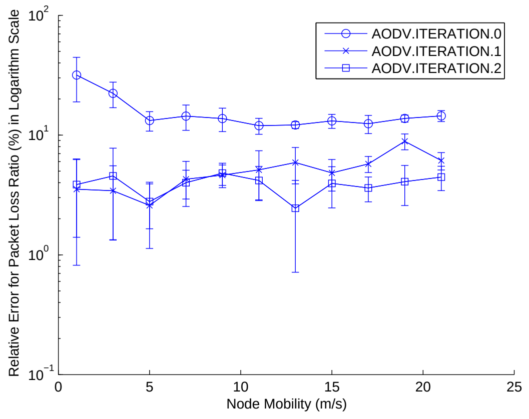

(b)

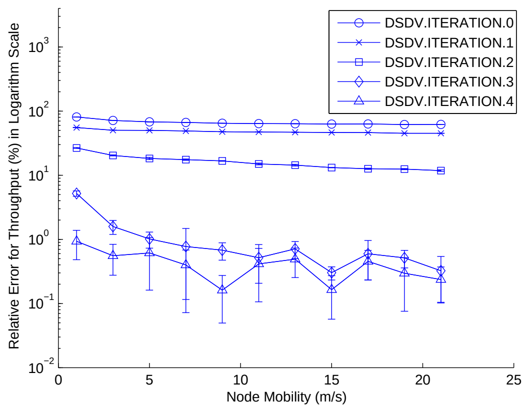

(c)

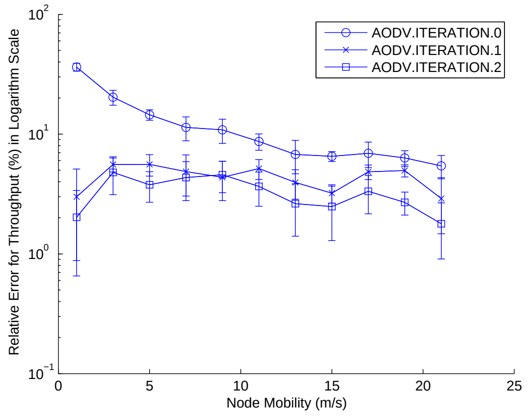

(d)

Figure 5.8: The relative error for the packet loss ratio and the throughput, function of the node mobility in a logarithmic scale; DSDV (left) and AODV (right). (a) and (b) show the relative error for the packet loss ratio; (c) and (d) show the relative error for the throughput. *Plain* time-parallel simulation is applied in this set of experiments.

We conclude that *the performance of the time-parallel simulation is not sensitive to the network load, or to the node mobility*.

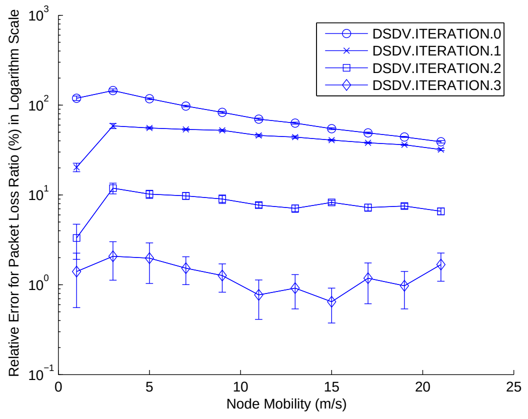

(a)

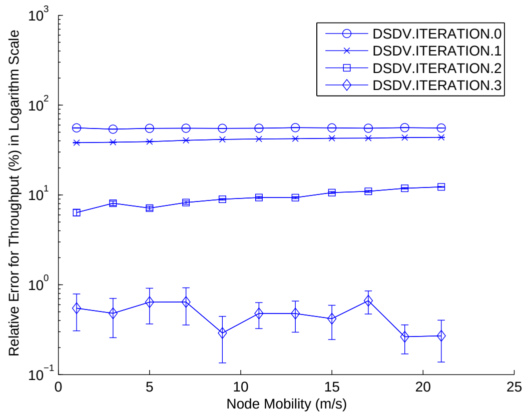

(b)

Figure 5.9: The relative error for the packet loss ratio and the throughput for DSDV, function of the node mobility in a logarithmic scale. (a) shows the relative error for the packet loss ratio; (b) show the relative error for the throughput. *ISA* time-parallel simulation is applied in this set of experiments.

Speedup and Maximum Network Size. In our experiments the number of nodes range from 100 to 1500. The density of the map is fixed at 4×10^{-4} nodes/m^2, and the other parameters are set as default (Table 5.1).

For DSDV the actual execution time for 1400 simulated nodes is approximately 110 minutes. The time-parallel simulation requires almost 24 minutes and has a speedup of almost 5. If we restrict the execution time to 10 minutes the maximum number of nodes is 180, for sequential simulation and 1000 for the time-parallel simulation. The execution time for AODV is: 90 minutes for sequential simulation and 15 minutes for the parallel one. When we restrict the execution time to 10 minutes the maximum number of nodes is 200 for the sequential and 1200 for the time-parallel simulation.

5.5 Summary

In this chapter, we described a methodology for time-parallel simulation of wireless ad hoc networks. We presented an analysis of perturbations, which gives us some understanding of the source of errors in one-shot time-parallel simulation results. Based on a layer-by-layer analysis of the propagation of perturbations in the wireless networking stack, we proposed several avenues for improving the accuracy of the simulation results. Building on these considerations, we described an implementation of time-parallel simulation based on the NS-2 simulator. The techniques deployed are the iterative extension of the warmup interval and initial state approximation for the table-driven routing protocols. A series of experiments showed that 5-20 times speedup can be obtained for an accuracy of 95%, depending on the choice of the routing protocol and whether initial state approximation was deployed or not. In general, the simulations of reactive routing protocols show a higher accuracy and/or speedup than the one for proactive protocols. We demonstrate, however, that the accuracy is relatively independent of other parameters of the scenario, such as network load or node mobility. We conclude that time-parallel simulation allows us to study relatively large wireless ad hoc networks consisting of a few thousand nodes over extended periods of time.

CHAPTER 6
THE TIME-PARALLEL SIMULATION OF WIRELESS AD HOC NETWORKS WITH COMPRESSED HISTORY

We have adapted the technique of *time-parallel simulation* (TPS) to the simulation of wireless ad hoc networks. In general, the time-parallel simulation yields accurate results only if the stochastic model of the system is regenerative, and the time partitioning happens at the regeneration points, which is a situation rarely encountered for wireless ad hoc networks. The accuracy of the time-parallel simulation depends on our ability to estimate the state of the system at the beginning of the simulation segment. With a perfect estimation of the initial state, the speedup is limited only by the available processors.

In our previous work, we were relying on the combination of *a priori* initial state approximation and a warmup simulation. A warmup simulation approximates the initial state because the perturbations caused by network events will eventually diminish or extinguish after a certain time. It is observed as an application of the general principle of temporal locality, with many applications in computer science.

In this chapter, we discuss a method to improve the speedup of time-parallel simulation, by replacing the warmup simulation interval completely or partially with a *compressed history* [WBT07b, WBT07a] of the simulation. Note that the warmup simulation represents the complete simulation of a time period (a history) before the measured part of the simulation. From this simulation, we only retain the final state, which will serve as the initial state for the measured simulation segment. The idea behind the compressed history is that we can replace the warmup interval with a simplified simulation scenario, which might not yield the same simulation trace, but will leave the network in the same (or very similar) final state. Thus, we replace the computation of a long complex warmup interval with a computationally much cheaper compressed history.

Though the technique of compressed history is quite general and can be applied for time-parallel simulation in any domain, the way in which the compressed history calculates a good approximation of the final state at a cheaper cost is dependent on the domain. We need to apply domain specific knowledge about what type of events have an impact on the final state of the simulation and which are the events which can be removed or substituted with simpler events. It is also critical to focus removing the events whose simulation is computationally the most expensive.

The domain on which we focus in this chapter is the simulation of wireless ad hoc networks with proactive routing protocols (such as DSDV). We have seen that these protocols require a comparatively long warmup interval to achieve the required accuracy, which limits the speedup to 4-5 times. We have identified the periodic routing table updates as the most expensive component of the warmup interval, and generate the compressed history by reducing the frequency of the routing table updates in the warmup interval. Naturally, this is just one of the possible techniques which can be deployed: other techniques would be the elimination of events whose effects are shadowed by later events, or replacing long trains of identical packet transmission with a smaller set of transmissions between the same sources.

This chapter is organized as follows. We provide a formal model of the compressed history technique in Section 6.1, while our implementation is detailed in Section 6.2. A simulation study analyzing the benefits of compressed history is described in Section 6.3. We conclude in Section 6.4.

6.1 Compressed History

A simulation S of an ad hoc network calculates the simulation trace $\mathcal{T}$ of an event set $\mathcal{E}$ which occurs in a geographic area $\mathcal{A}$, within a time interval τ, when the initial state is $\mathcal{I}$, and the final state is $\mathcal{F}$. Formally, we denote a simulation as a six-tuple $S = (\mathcal{A}, \tau, \mathcal{E}, \mathcal{I}, \mathcal{F}, \mathcal{T})$. We partition the temporal dimension of the simulation S into m time intervals $\{\tau_i | \tau_i = [(i-1)\frac{|\tau|}{m}, i\frac{|\tau|}{m}], 1 \leq i \leq m\}$, where $|\tau|$ is the duration of time interval τ.

A time-parallel simulation is a set of simulation segments

$$L = \{S_i | S_i = (\mathcal{A}, \tau_i, \mathcal{E}_i, \mathcal{I}_i, \mathcal{F}_i, \mathcal{T}_i), 1 \leq i \leq m\} \tag{6.1}$$

For any simulation S_i, the event set $\mathcal{E}_i \subset \mathcal{E}$ is the events from $\mathcal{E}$ which fall in the time interval of S_i. Thus the segments of the time-parallel simulation simulate the full spatial component $\mathcal{A}$, but only a subset of the temporal span τ_i. In order to have an exact simulation, the initial state of S_{i+1}

needs to match the final state of S_i, $1 \leq i \leq m-1$. This final state, however, cannot be obtained without actually running all the previous simulation segments.

A crude approximation can be obtained by assuming that every segment starts with initial network state, $\mathcal{I}_i = \mathcal{I}$, and combining the simulation traces $\mathcal{T} = \mathcal{T}_1 \cup \mathcal{T}_2 \cup \ldots \cup \mathcal{T}_m$ of the simulation segments. We call this raw time-parallel simulation method as the TPS algorithm.

A better approximation can be obtained through a *warmup interval*. For every simulation segment S_i, define a warmup simulation $S_{Wi} = (\mathcal{A}, [\tau_i^s - T_w, \tau_i^s], \mathcal{E}_{Wi}, \mathcal{I}, \mathcal{F}_{Wi}, \mathcal{T}_{Wi})$. We will use the final state of the warmup interval as the initial state of the measured part of the simulation $\mathcal{F}_{Wi} = \mathcal{I}_i$. We will call this simulation approach as the TPS-U algorithm (with the U denoting that the warmup interval is uncompressed). Naturally, the longer the warmup interval T_w, the better the approximation of the initial state. In the extreme case, $T_w = \tau_i^s$, and the warmup simulation S_{Wi} produces an exact initial state for the simulation segment S_i. However, this would not provide any speedup over a linear simulation of the entire interval.

Let us now introduce the notion of the compressed history. Note that from the warmup simulation we are only interested in the final state $\mathcal{F}_{Wi}$. The computational effort to perform this simulation is monotonically dependent on the set of events in the warmup simulation. Our goal is to find a simplified set of events $\hat{\mathcal{E}}_{Wi}$, which, when replaces in the warmup simulation, will provide a final state which is either equal to the one of the full warmup ($\hat{\mathcal{F}}_{Wi} = \mathcal{F}_{Wi}$) or a close approximation ($\hat{\mathcal{F}}_{Wi} \approx \mathcal{F}_{Wi}$). Naturally, we are interested only in the cases where the simulation of $\hat{\mathcal{E}}_{Wi}$ is significantly cheaper than that of $\mathcal{E}_{Wi}$.

Let us now discuss the ways in which the compressed history $\hat{\mathcal{E}}_{Wi}$ can be determined. Intuitively, we need to retain the events that produce significant perturbations of the final state. Some of these considerations can be expressed in a generic way. For instance, if some events have a limited effect in time and their effect extinguishes before the start of the measured part of the simulation, they can be removed from the warmup simulation when composing the compressed history. Another approach is to replace a set of events with an event which summarizes them. For example, when we wish to simulate the behavior of a lightly or moderately loaded system we can define recursively past windows and summarize the effect of each one on the next. We can calculate an average request arrival rate λ_{avg} and an average service time μ_{avg} for a window of duration δ, ignore all other events (e.g., events signaling completion of a request, preemptive actions, etc.), and replace all events in this interval with a single request with the service time $\lambda_{avg} \cdot \mu_{avg}$ arrived at a random time in the interval $(0, \delta)$.

In general, the knowledge of the application domain, the perturbations caused by the specific classes of events, their interrelationships, as well as their impact on the simulation interval can help us design compressed histories with high compression ratio and high accuracy.

Let $\underline{S_i}$ be the complete sequential simulation prior to S_i,

$$\underline{S_i} = (\mathcal{A}, [0, \tau_i^s], \underline{\mathcal{E}_i}, \mathcal{I}, \underline{\mathcal{F}_i}, \underline{\mathcal{T}_i}), \;\; 2 \leq i \leq m \tag{6.2}$$

The initial state of a simulation batch S_i can be approximated by the final state of the compressed history of its prior simulation $\underline{S_i}$,

$$\underline{\hat{S_i}} = (\mathcal{A}, [0, \tau_i^s], \underline{\hat{\mathcal{E}_i}}, \mathcal{I}, \underline{\hat{\mathcal{F}_i}}, \underline{\hat{\mathcal{T}_i}}), \;\; 2 \leq i \leq m \tag{6.3}$$

Thus, we obtain a new time-parallel simulation set

$$L' = \{S'_i | S'_i = (\mathcal{A}, \tau_i, \mathcal{E}', \mathcal{I}'_i, \mathcal{F}'_i, \mathcal{T}'_i), 1 \le i \le m\} \tag{6.4}$$

where

$$\mathcal{I}'_i = \begin{cases} \mathcal{I}, & \text{for } i = 1; \\ \underline{\hat{\mathcal{F}}_i}, & \text{for } 2 \le i \le m. \end{cases} \tag{6.5}$$

We call the time-parallel simulation algorithm with compressed history as the TPS-C algorithm. Figure 6.1 illustrates an example of the TPS-C algorithm.

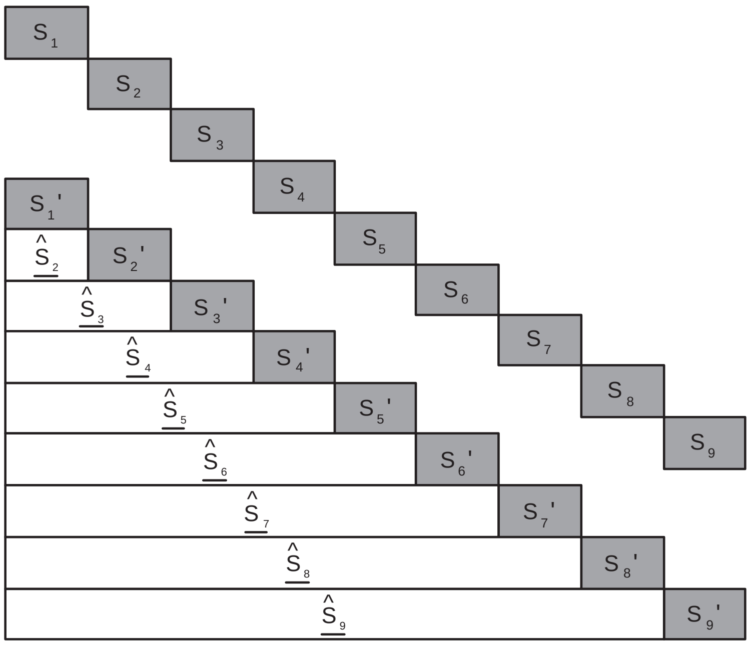

Figure 6.1: The TPS and TPS-C (TPS with compressed history) algorithms. The $|\tau| = 180$ sec. simulation interval is segmented into 9 simulation intervals of 20 sec. each. The shaded simulation segments are used to compose the final simulation trace. $\{S_i\}$ is the set of simulation without initial state approximation, while $\{S'_i\}$ is the set of simulation batches with their initial states approximated by the compressed history of their prior simulations.

We define the *compression ratio* of the compressed history $\hat{S}$ by

$$\eta(\hat{S}_i, S_i) = \frac{|\mathcal{E}|}{|\hat{\mathcal{E}}|} \tag{6.6}$$

Assume $S = (500 \times 500, [0, 180], \mathcal{E}, \mathcal{I}, \mathcal{F}, \mathcal{T})$ is segmented into 9 equal intervals, with $\tau_i = [20(i-1), 20i], 1 \leq i \leq 9$. The compressed history of the prior simulation for each simulation batch S_i is

$$\underline{\hat{S}_i} = (500 \times 500, [0, 20(i-1)], \underline{\hat{\mathcal{E}}_i}, \mathcal{I}, \underline{\hat{\mathcal{F}}_i}, \underline{\hat{\mathcal{T}}_i}),\ 2 \leq i \leq 9 \tag{6.7}$$

The set of simulation batches improved by the application of compressed history are

$$S_i' = (500 \times 500, [20(i-1), 20], \mathcal{E}_i', \mathcal{I}_i', \mathcal{F}_i', \mathcal{T}_i'),\ 1 \leq i \leq 9 \tag{6.8}$$

where

$$\mathcal{I}_i' = \begin{cases} \mathcal{I}, & \text{for } i = 1; \\ \underline{\hat{\mathcal{F}}_i}, & \text{for } 2 \leq i \leq 9. \end{cases} \tag{6.9}$$

Experimental results show that an aggressive compression of the warmup interval can produce high approximation errors. It turns out, however, that the events at the very end of the compressed interval (that is, immediately before the start of the measurement interval) are responsible for a large part of the approximation errors. One way to improve the accuracy is to introduce a short *uncompressed interval* between the compressed history and the beginning of the measurement interval. The introduction of uncompressed simulation interval reduces the influence of perturbations at the measured point.

In the improved algorithm (the TPS-CU algorithm), the simulation interval $[0, \tau_i^s]$ is split to two parts, the uncompressed interval $\tau_{Ui} = [\tau_i^s - T_u, \tau_i^s]$ with a fixed duration $|\tau_{Ui}| = T_u$,

$$S_{Ui} = (\mathcal{A}, \tau_{Ui}, \mathcal{E}_{Ui}, \mathcal{I}_{Ui}, \mathcal{F}_{Ui}, \mathcal{T}_{Ui}), \;\; 2 \leq i \leq m \tag{6.10}$$

and the compressed history of the simulation interval $\tau_{Ci} = [0, \tau_i^s - T_u]$,

$$\underline{\hat{S}_{Ui}} = (\mathcal{A}, \tau_{Ci}, \underline{\hat{\mathcal{E}}_{Ui}}, \mathcal{I}, \underline{\hat{\mathcal{F}}_{Ui}}, \underline{\hat{\mathcal{T}}_{Ui}}), \;\; 2 \leq i \leq m \tag{6.11}$$

Note that the previously introduced TPS-C and TPS-U algorithms are variations of TPS-CU algorithm; TPS-C is the special case when $|\tau_{Ui}| = 0$, while TPS-U corresponds to $|\tau_{Ci}| = 0$.

Figure 6.2 illustrates the improved TPS algorithm for the same example. We fixed the duration of the uncompressed interval as 10 seconds for each simulation segment; the compressed history for simulation segment S_{Ui} is

$$\underline{\hat{S}_{Ui}} = (500 \times 500, [0, 20i - 30], \underline{\hat{\mathcal{E}}_{Ui}}, \mathcal{I}, \underline{\hat{\mathcal{F}}_{Ui}}, \underline{\hat{\mathcal{T}}_{Ui}}), \;\; 2 \leq i \leq 9 \tag{6.12}$$

and the uncompressed simulation for simulation segment i is

$$S_{Ui} = (500 \times 500, [20i - 30, 20i - 20], \mathcal{E}_{Ui}, \underline{\hat{\mathcal{F}}_{Ui}}, \mathcal{F}_{Ui}, \mathcal{T}_{Ui}), \;\; 2 \leq i \leq 9 \tag{6.13}$$

Thus, we obtain a new time-parallel simulation set

$$L' = \{S'_i | S'_i = (500 \times 500, [20i - 20, 20i], \mathcal{E}'_i, \mathcal{I}'_i, \mathcal{F}'_i, \mathcal{T}'_i), 1 \leq i \leq m\} \tag{6.14}$$

where

$$\mathcal{I}'_i = \begin{cases} \mathcal{I}, & \text{for } \; i = 1; \\ \mathcal{F}_{Ui}, & \text{for } \; 2 \leq i \leq m. \end{cases} \tag{6.15}$$

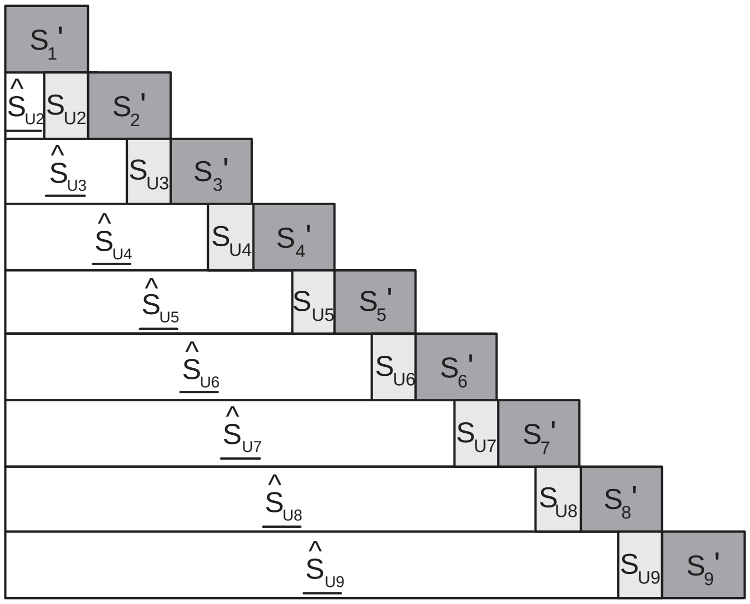

Figure 6.2: The TPS-CU (TPS with compressed history and uncompressed interval) algorithm. The $|\tau| = 180$ sec. simulation interval is segmented into 9 intervals of 20 sec. each. The uncompressed interval duration is 10 sec. for each simulation segment. The prior simulation of S_i is composed of an uncompressed interval S_{Ui} and the compressed history of its prior simulation $\underline{\hat{S}_{Ui}}$. The shaded simulation segments are used to compose the final simulation trace. $\{S_i'\}$ is the set of simulation batches with their initial states approximated by the compressed history of their prior simulations and uncompressed intervals.

6.2 Implementation of Compressed History

As we have seen in the previous theoretical analysis, there are several ways to implement the compressed history, and a careful domain specific analysis is necessary to find the best approach in a particular situation.

In this section, we concentrate on wireless ad hoc networks with pro-active, table driven routing protocols. In our previous work related to TPS [BTW06, WTB07c], we have achieved speedups of 16-20 times for scenarios involving reactive routing protocols, but only 4-5 times for pro-active routing protocols. The reason behind the lower speedup is that pro-active protocols maintain more state information (in the form of the routing tables), and thus require longer and more expensive warmup for equivalent accuracy. Our goal is to replace part of the warmup interval with compressed history, such that the overall speedup will be brought closer to the reactive protocols.

In order to find an efficient compression mechanism, we will use our domain specific knowledge. The specific protocol we will consider is Destination Sequenced Distance Vector (DSDV) [PB94], although the same considerations apply to most other pro-active routing protocols. In DSDV, the nodes periodically update their routing tables even in the absence of any data flow (hence the pro-active nature of the protocol). The justification for the frequent routing table updates is the mobility of the nodes. The routing table updates involve a significant number of packet exchanges, which are computationally expensive to simulate. However, note that for the measurement interval, we are interested only in the final configuration of the routing tables, and the history of the routing table entries does not affect the current state of the network.

Thus, one possible strategy to generate the compressed history is based on the selective removal of the routing table update packets. The event that updates a routing table entry which will be overwritten before the start of the measurement interval is called a *shadowed event*, and can be removed from the compressed history without a loss of accuracy. Similarly, we could remove the events concerning routing table entries which are not used during the measurement interval (*irrelevant events*). Unfortunately, the exact computation of which events are shadowed and/or irrelevant is a complex task, and it might cancel the benefits of the resulting compressed history.

The approach we propose is based on the observation that the earlier is a routing table update in the history of the simulation, the more likely is that it will be shadowed by a future event. Thus, we can perform a compression of the history by reducing the frequency of the routing table updates. Note that there is no guarantee that this method will yield a final state identical to the uncompressed history. It is possible, for instance, that a particularly long lived routing entry was created at a routing table update which was skipped, and never overwritten afterwards. On the other hand, there is a high likelihood that the missing entry will be, in fact, created at the next update, resulting in the same routing table at the beginning of the measurement interval.

Figure 6.3 illustrates three possible strategies for adjusting the routing table update frequency. In the figure, a sequential simulation is divided into a set of sub-intervals: in the *idle interval* no routing table update happens, in the *compressed history* the routing table updates are rarer than in the default setting of the protocol, while in the *measurement interval* the routing table updates are regular. The vertical lines indicate the routing table update events, thus the density of the lines indicate the local frequency of routing table updates. With strategy 6.3(a), the frequency increases gradually in the compressed history interval, and the regular frequency is met right before the measured point. With strategy 6.3(b), the routing table updates sent long time ago are all ignored in the compressed history. Strategy 6.3(c) assumes that routing table updates happen at a constant interval during the compressed history, but less frequently than during the measurement interval.

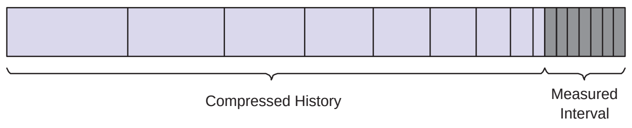

(a)

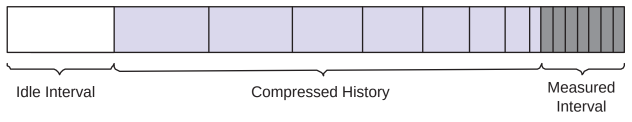

(b)

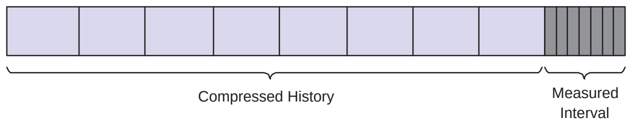

(c)

Figure 6.3: Strategies to adjust the routing table update frequency when composing the compressed history.

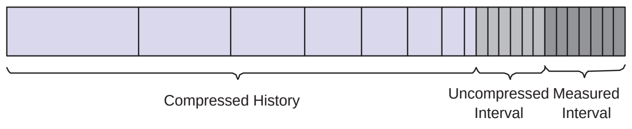

(a)

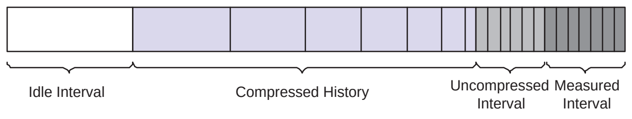

(b)

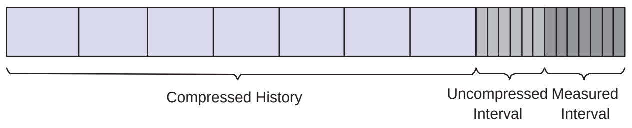

(c)

Figure 6.4: Strategies to adjust the routing table update frequency when composing the compressed history, with the application of uncompressed interval.

Figure 6.4 illustrates the corresponding strategies with an uncompressed warmup interval inserted between the compressed history and the measurement interval. The routing table updates are sent at a regular level within the uncompressed interval. In our simulation, we implemented and investigated strategies 6.3(c) and 6.4(c). As the experimental results will show, even a small uncompressed interval can provide a significant improvement in the accuracy of the simulation.

6.2.1 Load Balancing TPS with Compressed History

The overall execution time of a parallel simulation is determined by the simulation segment with the longest execution time. As the measurement interval of the individual time-parallel simulation threads starts at different time points, the length of the compressed history will be different. This leads to an imbalance in the execution time: with a constant compression ratio, the execution time of a simulation segment increases when its compressed history duration increases. Our goal is to balance the execution time of the compressed histories, by adjusting the compression ratio according to the compressed history duration.

Assume the routing table update frequency of a sequential simulation S_i is a constant λ_c, and the routing table update frequency of the compressed history $\underline{\hat{S}_{Ui}}$ is λ_i. The compression ratio $\eta \geq 1$ is the ratio of the original size of the history to the size of the compressed history. Thus a value of $\eta = 1$ represents no compression. The compression ratio of $\underline{\hat{S}_{Ui}}$ can be approximated by

$$\eta(\underline{\hat{S}_{Ui}}, \underline{S_{Ui}}) \approx \frac{\lambda_c}{\lambda_i} \tag{6.16}$$

Define the *normalized compressed history duration* as the compressed history duration divided by the compression ratio, which reflects the approximate duration of a compressed history if it was not compressed. The normalized compressed history duration of $\underline{\hat{S}_{Ui}}$ is $|\tau_{Ci}| \,/\, \eta(\underline{\hat{S}_{Ui}}, \underline{S_{Ui}})$.

The balancing of the execution time of different simulation segments can be achieved by equalizing the normalized compressed history duration. If all simulation segments have a constant normalized compressed history duration T_c, that is

$$T_c = \frac{|\tau_{Ci}|}{\eta(\underline{\hat{S}_{Ui}}, \underline{S_{Ui}})} \approx |\tau_{Ci}| \cdot \frac{\lambda_i}{\lambda_c} \tag{6.17}$$

Thus, the required routing table update frequency for each simulation segment can be obtained by

$$\lambda_i = \lambda_c \cdot \frac{T_c}{|\tau_{Ci}|} \tag{6.18}$$

6.2.2 Accuracy-speedup Tradeoffs

In the TPS-CU algorithm, the initial state of the measurement interval S'_i is obtained as the final state of the uncompressed interval S_{Ui}, whose initial state is approximated by the final state of the compressed history $\underline{\hat{S}_{Ui}}$.

Thus, we have two ways to increase the accuracy of the initial state in the TPS-CU algorithm: either we increase the normalized compressed history duration of $\underline{\hat{S}_{Ui}}$ (that is, decrease the compression ratio), or we increase the length of the uncompressed history duration. Unfortunately, this way we also reduce the speedup of the simulation.

Let us consider a simulation S over a duration τ, segmented into m equal measurement intervals. The duration of each measured simulation interval (S_i') is $T_i = |\tau|/m$, the normalized compressed history ($\underline{\hat{S}_{Ui}}$) duration is T_c, and the uncompressed interval (S_{Ui}) duration is T_u. Let $T(S)$ be the function that calculates the execution of a simulation S. The speedup of our algorithm is

$$\kappa = \frac{T(S)}{\max_i\{T(\underline{\hat{S}_{Ui}}) + T(S_{Ui}) + T(S_i')\}} \tag{6.19}$$

If we assume that the events are evenly distributed over the simulation interval and the execution of each event takes about the same time Δt,

$$T(S) \approx |\mathcal{E}| \cdot \Delta t \tag{6.20}$$

If we ignore the execution time for data packets, the speedup can be approximated by

$$\begin{aligned}
\kappa &= \frac{T(S)}{\max_i\{T(\underline{\hat{S}_{Ui}}) + T(S_{Ui}) + T(S_i')\}} \\
&\approx \frac{|\mathcal{E}| \cdot \Delta t}{\max_i\{(|\underline{\hat{\mathcal{E}}_{Ui}}| + |\mathcal{E}_{Ui}| + |\mathcal{E}_i'|) \cdot \Delta t\}} \\
&= \frac{\lambda_c \cdot |\tau|}{\max_i\{\lambda_i \cdot |\tau_{Ci}| + \lambda_c \cdot |\tau_{Ui}| + \lambda_c \cdot |\tau_i|\}} \\
&= \frac{\lambda_c \cdot |\tau|}{\lambda_c \cdot T_c + \lambda_c \cdot T_u + \lambda_c \cdot T_i} \\
&= \frac{|\tau|}{T_c + T_u + T_i}
\end{aligned} \tag{6.21}$$

According to this formula, there are three possible means to increase the speedup: (1) decrease the normalized compressed history duration T_c; (2) decrease the uncompressed interval duration T_u; or (3) decrease the duration of the individual measurement intervals T_i, which is equivalent to increasing the number of measurement intervals m. Each of these choices also affects the accuracy of the simulation. Our goal is to determine the optimal values of: (i) the normalized compressed history duration, (ii) the uncompressed interval duration, and (iii) the measurement interval duration such that we achieve the largest possible speedup while meeting accuracy constraints.

6.3 Simulation Study

In this section, we describe the results of a simulation study which studies the accuracy of time-parallel simulation with compressed history. We compare the approximate results produced by TPS-U, TPS-C and TPS-CU with those produced by exact sequential simulation over several frequently used metrics. Table 6.1 lists the abbreviations and notations used throughout this section.

Table 6.1: The abbreviation and notations used in our simulation studies

Notation	**Description**
TPS-C	the TPS algorithm with compressed history
TPS-U	the TPS algorithm with uncompressed interval
TPS-CU	the TPS algorithm with compressed history and uncompressed interval
T_c	the duration of the normalized compressed history
T_i	the duration of segment i
T_u	the duration of the uncompressed interval
ε_{PLR}	the relative error for the packet loss ratio
ε_{TPT}	the relative error for the throughput
ε_{max}	the relative error threshold
κ	the speedup of the algorithm

The simulation scenarios on which we test our implementations are representative for the scenarios used in the study of wireless ad hoc networks. A set of mobile nodes are moving in a rectangular area, while communicating using wireless connections. The transmission range of the nodes is smaller than the size of the area, and there are no fixed wireless access points available. Thus, in order to communicate, the nodes need to use hop-by-hop transmissions relying on ad hoc routing algorithms. Due to the mobility of the nodes, the routes need to be frequently updated, even during the course of the transmissions.

In our experimental study, 80 nodes move in a simulation area of size 500×500 m^2 square area; all nodes have a transmission range of 100 meters. The duration of the scenario is 600 seconds. The node movement is modeled by the random waypoint model [BMJ98, JM96]. The traffic patterns are generated by CBR sources sending 512-byte UDP packets at a rate of 1 packet/second. The nodes use the Destination-Sequenced Distance Vector (DSDV) routing algorithm. Table 6.2 shows the default settings of the parameters for our experiments.

Table 6.2: The default values of the parameters used in our simulation studies

Field	**Value**
simulation area	500×500 (m^2)
number of nodes	80
transmission range	100 (m)
speed	1 (m/s)
pause time	15 (s)
simulation time	600 (s)
number of CBR sources	20
CBR packet size	512 (bytes)
CBR sending rate	4 (kbps)

Let us now describe the specific approaches we compare.

- **TPS-U** is the time-parallel simulation with uncompressed warmup interval. This is the baseline algorithm described in [BTW06, WTB07c].

- **TPS-C** is the time-parallel simulation with the warmup interval being composed exclusively of the compressed history. The strategy used for this approach is the one described in Figure 6.3(c), that is, the warmup interval extends to the complete simulation scenario, and the routing table update frequency is equidistant. To balance the load of the simulation threads, we maintained a constant normalized compressed history duration.

- **TPS-CU** is the time-parallel simulation with a warmup interval composed of the compressed history followed by an uncompressed interval. The particular strategy used in this simulation study is the one described in Figure 6.4(c), that is, the compressed interval starts at the beginning of the simulation scenario and the routing table update frequency is constant for a given simulation. To balance the load of the simulation threads, we maintained an uncompressed component of constant duration and a compressed component of constant normalized compressed history duration.

Our approach for comparing the accuracy of different simulation runs is based on the calculation of the relative error of specific measurement types. The methodology is implemented as follows. First, we run a serial, accurate simulation and extract an exact measurement M_0 on its trace. Then, we perform a time-parallel simulation with one of the proposed algorithms (TPS-U, TPS-C and TPS-CU), assemble the simulation trace from the segments, and perform the same measurement, obtaining an approximate value M. The relative error of the specific algorithm for this scenario will be $\varepsilon_M = \frac{M-M_0}{M_0} \times 100\%$. As the relative error fluctuates from scenario to scenario, we repeat the experiment 20 times, each time with a different random configuration of the source destination pairs of the CBR sources. We calculate the mean, as well as the 95% confidence interval of the relative error. The two measurements considered in this study are the relative error for the packet loss ratio $\varepsilon_{\mathrm{PLR}}$ and the relative error for the throughput $\varepsilon_{\mathrm{TPT}}$.

As we described in the [BTW06], the relative error of simulation tends to be larger for metrics which measure rare phenomena (such as packet loss), compared to metrics which measure frequently occurring phenomena (such as throughput). As a result, $\varepsilon_{\mathrm{TPT}}$ is always smaller than $\varepsilon_{\mathrm{PLR}}$. The error threshold ε_{max} used in this study was 5%. In practice, this means that the measurement of the packet loss ratio will be roughly 95% accurate, while the accuracy of the measured throughput will be much higher, around 99.5% for most simulation runs. The speedup of the algorithm was determined by the method discussed in Section 6.2.2.

The time-parallel simulation was run on a cluster of 128 64-bit Opteron processors with Gigabit Ethernet interconnection. Each simulation segment was run on its own dedicated processor.

6.3.1 Tuning the Parameters of the Compressed History for Optimal Speedup

The TPS-C and TPS-CU algorithms have several parameters which can determine the speedup and accuracy of the algorithm. Before we perform a comparison between the accuracy and speedup of the TPS-U, TPS-C and TPS-CU algorithms, we need to determine the parameters under which the compressed history approach works best. These tuned parameters will be then used in the actual comparisons.

The most general case is the algorithm TPS-CU which has three parameters: the segment duration T_i (which is inversely proportional with the number of simulation threads), the duration of the normalized compressed history T_c and the duration of the uncompressed interval T_u.

We tune these parameters by varying them over a range of values: $10 \leq T_i \leq 40$, $0 \leq T_c \leq 40$ and $0 \leq T_u \leq 40$. We retain the values which yield the highest speedup for a target accuracy.

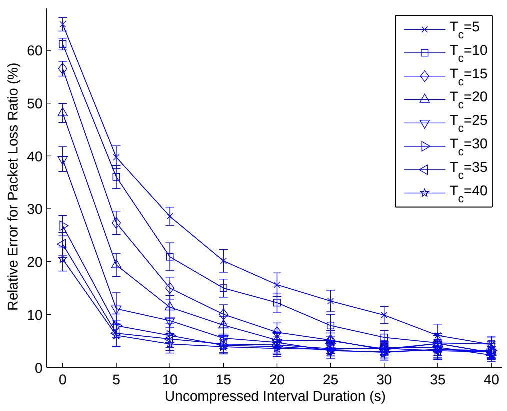

(a) Segment Duration T_i = 10 sec.

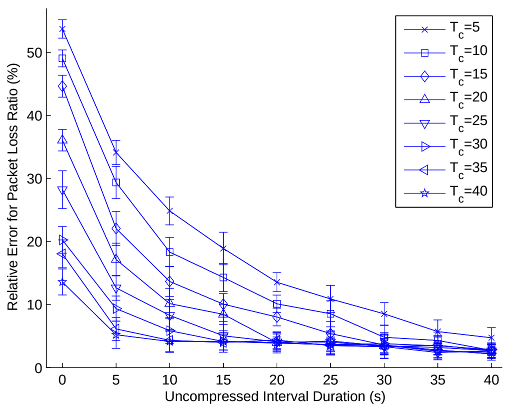

(b) Segment Duration T_i = 20 sec.

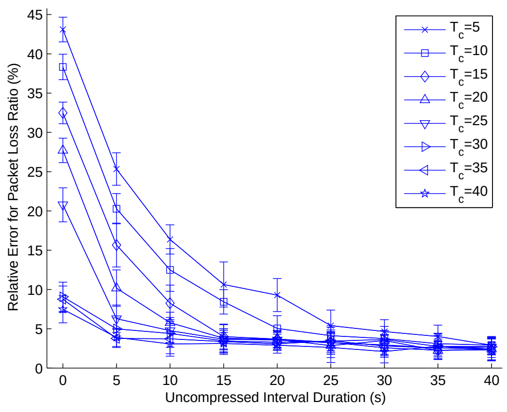

(c) Segment Duration T_i = 30 sec.

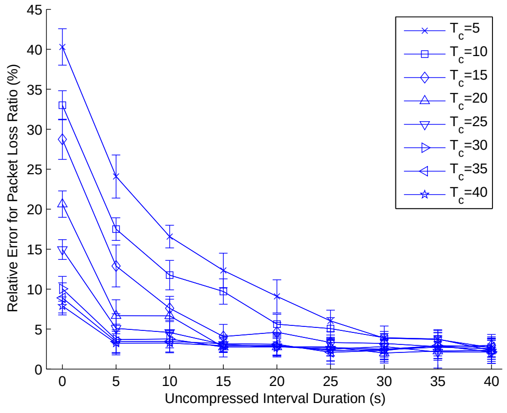

(d) Segment Duration T_i = 40 sec.

Figure 6.5: The TPS-CU algorithm: the relative error for the packet loss ratio function of uncompressed interval duration. The error decreases when we increase either the uncompressed interval duration, or the normalized history duration, or the segment duration.

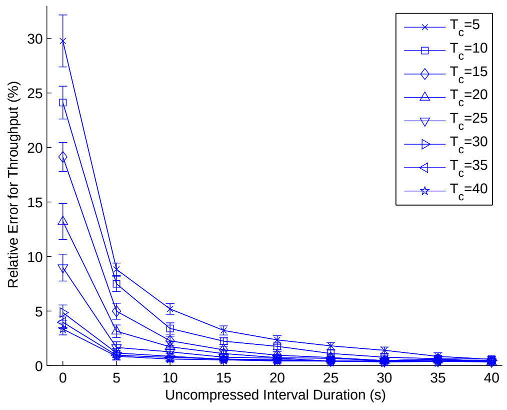

(a) Segment Duration T_i = 10 sec.

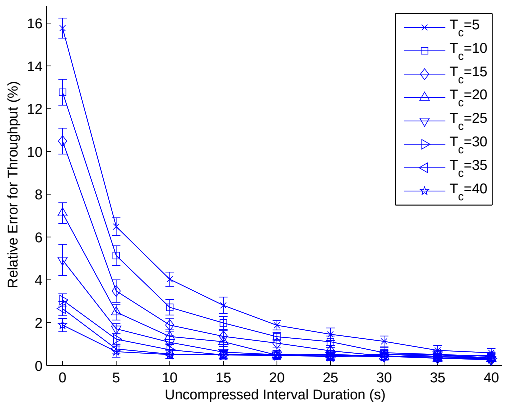

(b) Segment Duration T_i = 20 sec.

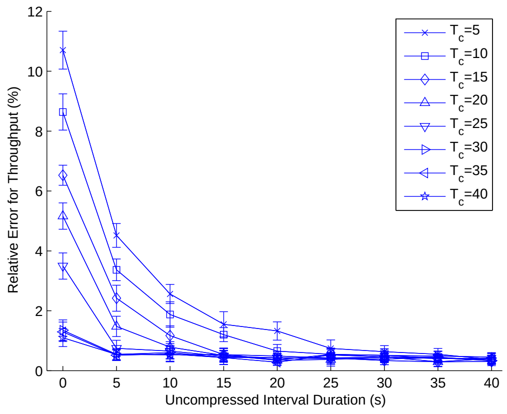

(c) Segment Duration T_i = 30 sec.

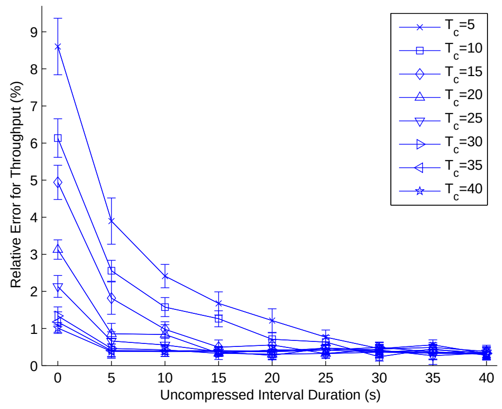

(d) Segment Duration T_i = 40 sec.

Figure 6.6: The TPS-CU algorithm: the relative error for the throughput function of the duration of the uncompressed interval. The error decreases when we increase either the uncompressed interval duration, the normalized history duration, or the segment duration.

Figures 6.5 and 6.6 show the relative error for the packet loss ratio and the throughput function of the duration of the uncompressed interval, for several segment lengths. Given a segment and a normalized compressed history of fixed length, the relative error for both metrics tend to decrease when the uncompressed interval duration increases. Also, the relative error for the two metrics tend to decrease when the normalized compressed history duration increases, given the duration of the segment and of the uncompressed interval. The relative errors for the two metrics decrease when the segment duration increases. For instance, with $(T_u, T_c) = (5, 5)$ sec., the relative error for the packet loss ratio is reduced from 39.76% when $T_i = 10$ sec., to 24.09% when $T_i = 40$ sec.; the relative error for the throughput is reduced from 8.82% when $T_i = 10$ sec., to 3.90% when $T_i = 40$ sec.

Table 6.3: Tuning the parameters of the TPS-CU algorithm based on the results of the experimental runs. The rows corresponding to the best choice of the uncompressed interval T_u for a given segment duration are shown in bold. The maximum achievable speedup for a given segment duration is bold and underlined.

T_u	$\min\{T_c\}$	ε_{PLR}	ε_{TPT}	κ
10	40	4.42%	0.59%	4.01
15	30	4.15%	0.57%	5.29
20	25	4.70%	0.67%	5.30
25	25	3.15%	0.41%	5.20
30	15	3.32%	0.45%	6.32
35	**10**	**4.63%**	**0.63%**	<u>**6.51**</u>
40	5	4.31%	0.58%	5.67

(a) Segment Duration T_i = 10 sec.

T_u	$\min\{T_c\}$	ε_{PLR}	ε_{TPT}	κ
10	35	4.32%	0.53%	6.62
15	30	4.13%	0.49%	6.33
20	**20**	**3.94%**	**0.48%**	<u>**7.34**</u>
25	20	4.21%	0.51%	6.43
30	10	4.80%	0.59%	7.30
35	10	4.29%	0.51%	6.39
40	5	4.73%	0.58%	6.39

(b) Segment Duration T_i = 20 sec.

T_u	$\min\{T_c\}$	ε_{PLR}	ε_{TPT}	κ
5	35	3.76%	0.51%	4.88
10	25	4.77%	0.65%	7.44
15	15	4.01%	0.54%	7.46
20	**15**	**3.70%**	**0.49%**	<u>**7.54**</u>
25	10	4.12%	0.55%	6.99
30	5	4.64%	0.63%	6.84

(c) Segment Duration T_i = 30 sec.

T_u	$\min\{T_c\}$	ε_{PLR}	ε_{TPT}	κ
5	30	3.70%	0.66%	5.51
10	25	4.59%	0.56%	6.17
15	**15**	**4.07%**	**0.50%**	<u>**6.79**</u>
20	15	4.61%	0.58%	6.04
25	15	3.33%	0.32%	6.43
30	5	3.86%	0.46%	6.14

(d) Segment Duration T_i = 40 sec.

To maximize the speedup for a given T_u, we choose the minimal T_c such that the relative errors for the corresponding metrics are below ε_{max}. We conducted a series of simulations with different segment durations. The simulation results are summarized in Tables 6.3. Each table, shows the minimal value of T_c, the normalized compressed history duration as well as ε_{PLR}, the relative error for the packet loss ratio, ε_{TPT}, the relative error for the throughput, and κ, the speedup, function of T_u, the uncompressed interval duration. The normalized compressed history duration required to achieve the accuracy threshold tends to decrease when the uncompressed interval duration increases. When $T_i = 10$ sec., the largest speedup is $\kappa = 6.51$ with $(T_u, T_c) = (35, 10)$ sec. and the relative errors are $(\varepsilon_{\text{PLR}}, \varepsilon_{\text{TPT}}) = (4.63\%, 0.63\%)$; when $T_i = 40$ sec., the largest speedup is 6.79 with $(T_u, T_c) = (15, 15)$ sec. and the relative errors are $(\varepsilon_{\text{PLR}}, \varepsilon_{\text{TPT}}) = (4.07\%, 0.50\%)$.

Table 6.4: The combination of uncompressed interval duration and normalized compressed history duration that achieve the maximum speedup for different segment durations

T_i	T_u	T_c	κ
10	35	10	6.51
20	20	20	7.34
30	**20**	**15**	**7.54**
40	15	15	6.79

Table 6.4 lists the combination of the uncompressed interval duration and the normalized compressed history duration that led to the largest speedup, under all segment durations simulated. The largest speedup increases when T_i increases from 10 to 30 sec., and starts to decrease when T_i increases beyond 30 sec. The largest speedup, $\kappa = 7.54$, is achieved when $(T_i, T_u, T_c) = (30, 20, 15)$ sec. These values will be chosen for the simulation results presented later.

6.3.2 *The Performance Improvement Provided by Compressed History: Comparing TPS-CU with TPS-U*

We investigate the effect of the compressed history, for a range of durations of the uncompressed interval when the segment duration is 30 sec., the normalized compressed history duration for the TPS-CU algorithm is 15 sec., and the uncompressed interval duration is $10 \leq T_u \leq 40$ sec.

Figure 6.7 shows the relative errors produced by the TPS-U and TPS-CU algorithms. For both algorithms the relative error for the packet loss ratio and the throughput tend to decrease when the uncompressed interval duration increases. For the same duration of the uncompressed interval the relative errors produced by the TPS-CU are smaller than the ones produced by the TPS-C algorithm; the TPS-U algorithm produces errors below ε_{max} for considerably smaller values of the uncompressed interval.

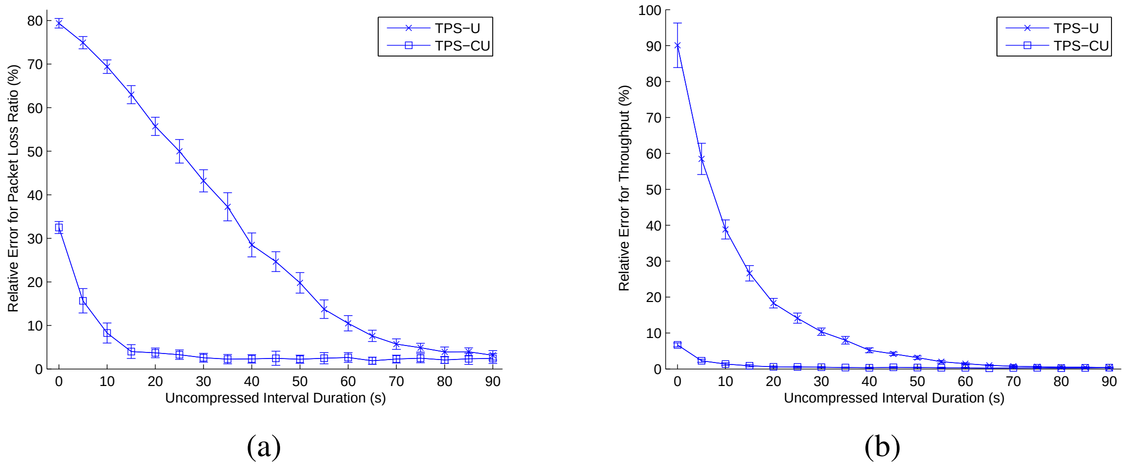

Figure 6.7: The TPS-U and TPS-CU algorithms: the relative error function of the duration of the uncompressed interval for (a) the packet loss ratio and (b) the throughput, when the segment duration is 30 sec., and the normalized compressed history duration for TPS-CU is 15 sec.

Table 6.5: The effect of the compressed history upon the relative error for the packet loss ratio and the throughput

T_u	ε_{PLR}		ε_{TPT}	
	$T_c = 0$	$T_c = 15$	$T_c = 0$	$T_c = 15$
0	79.38%	**32.48%**	90.10%	**6.70%**
10	69.42%	**8.26%**	38.84%	**1.39%**
20	55.71%	**3.70%**	18.32%	**0.59%**
30	43.20%	**2.58%**	10.38%	**0.50%**
40	28.49%	**2.31%**	5.21%	**0.34%**
50	19.77 %	**2.24%**	3.15%	**0.40%**
60	10.49%	**2.64%**	1.47%	**0.34%**
70	5.72%	**2.28%**	0.75%	**0.31%**
80	3.93%	**2.09%**	0.50%	**0.25%**

Table 6.5 summarizes the effect of the compressed interval upon the relative errors. A 15-sec. normalized compressed history, leads to the reduction of the relative error for the packet loss ratio from 69.42% to 8.26% when $T_u = 10$ sec. and from 43.20% to 2.58% when $T_u = 30$ sec. the relative error for the throughput is reduced from 38.84% to 1.39% when $T_u = 10$ sec., and from 10.38% to 0.50% when $T_u = 30$ sec.

We conclude that the compressed history allows us to obtain a better approximation for both the packet loss ratio and the throughput.

6.3.3 The Performance Improvement Provided by the Uncompressed Interval: Comparing TPS-CU with TPS-C

The next question we investigate is whether we can dispense the uncompressed interval entirely and just rely on the compressed history to provide the warmup simulation, which is the case of the

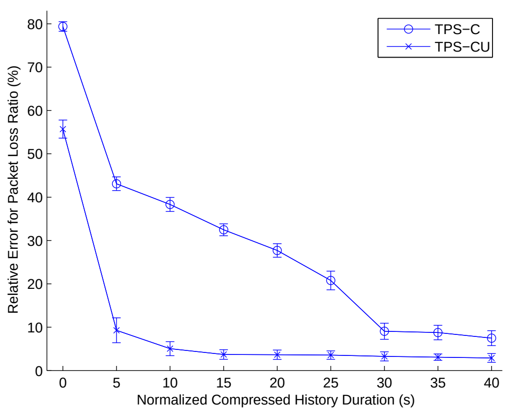

(a)

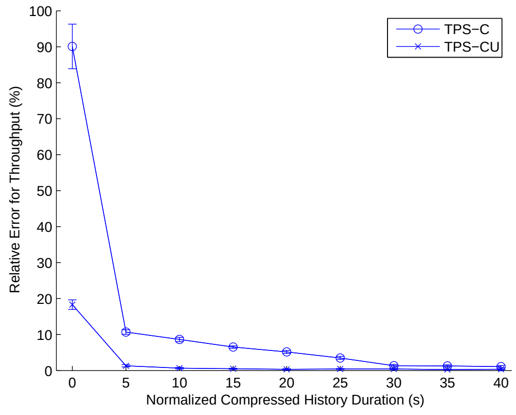

(b)

Figure 6.8: The TPS-C and TPS-CU algorithms: the relative error function of the duration of the uncompressed interval for (a) the packet loss ratio and (b) the throughput, when the segment duration is 30 sec., and the uncompressed interval duration for TPS-CU is 20 sec.

TPS-C algorithm. We compared the TPS-CU and TPS-C algorithms over a variety of values of normalized compressed history duration. In the experiments, the segment duration is set to 30 sec. and the uncompressed interval duration for the TPS-CU algorithm is set to 20 sec., based on the parameter tuning experiments performed previously. We vary the normalized compressed history duration T_c from 0 to 40 sec. The TPS-U algorithm is represented by the scenario when $T_u = 0$.

Figure 6.8 compares the performance of the two algorithms, as function of the normalized compressed history duration. The relative errors for the packet loss ratio and the throughput tend to decrease when the normalized compressed history duration increases, for both algorithms. The relative error for the TPS-CU algorithm is consistently lower than for TPS-U, for a given the normalized compressed history duration. We find that the TPS-C algorithm requires significantly larger segment durations than TPS-CU to maintain the relative error below ε_{max}.

Table 6.6: The effect of the uncompressed interval upon the relative error for the packet loss ratio and the throughput

T_c	ε_{PLR}		ε_{TPT}	
	$T_u = 0$	$T_u = 20$	$T_u = 0$	$T_c = 20$
0	79.37%	**55.71%**	90.10%	**18.32%**
5	43.09%	**9.29%**	10.70%	**1.32%**
10	38.33%	**5.05%**	8.64%	**0.65%**
15	32.48%	**3.70%**	6.53%	**0.49%**
20	27.71%	**3.64%**	5.16%	**0.35%**
25	20.79%	**3.57%**	3.49%	**0.43%**
30	9.07%	**3.28%**	1.35%	**0.43%**
35	8.77%	**3.09%**	1.29%	**0.28%**
40	7.48%	**2.91%**	1.10%	**0.36%**

Table 6.6 summarizes the effect of the uncompressed interval. A 20-seconds uncompressed interval leads to a reduction of the relative error for the packet loss ratio from 43.09% to 9.29% for $T_c = 5$ sec., and from 32.48% to 3.70% for $T_c = 15$ sec.; the relative error for the throughput is reduced from 10.70% to 1.32% for $T_c = 5$ sec., and from 6.53% to 0.49% for $T_c = 15$ sec.

We conclude that the uncompressed interval in the TPS-CU algorithm provides a significant improvement over the TPS-C algorithm which relies exclusively on compressed history warmup.

6.4 Summary

In this chapter, we introduce the time-parallel simulation of wireless ad hoc networks with the application of compressed history. The compressed history defines the critical events that perturb the measurements the most and ignores events that either do not affect at all the initial state of the measurement stage, or affect it only marginally. Though the technique we propose is application-specific, it is based upon the temporal locality of perturbations rooted on the assumption that causality has a limited scope, the effect of perturbations caused by distant events in the past will eventually diminish or extinguish after a certain time. Time-parallel simulation with compressed history allows us to speed up the simulation and produces good approximations to the exact simulation results; there is a tradeoff between the accuracy of the results and the speedup.

We propose several strategies for generating the compressed history for wireless ah hoc networks; we also introduce an uncompressed interval method that further improves the quality of the solution. Finally, we present a simulation study and discuss the accuracy of the algorithms as well as the speedup. We study the accuracy of simulated results for the packet loss ratio and the throughput for a table-driven routing protocol – DSDV. The results of the simulations are better in terms of speedup and accuracy than the results without the application of compressed history, reported in [BTW06, TWB06, WTB06b, WTB07c]. We compare the performance of TPS-CU, TPS-U, and TPS-C algorithms and conclude that the introduction of compressed history and uncompressed interval improves the accuracy of the solution; the new algorithms allow us to study wireless ad hoc networks with several thousand nodes for extended periods of time.

We plan to further investigate the strategies illustrated in Figure 6.4 and determine the best way to generate the compressed history, and then to implement compressed history for simulation of on-demand routing protocols, such as AODV [PR99].

CHAPTER 7
CONCLUSIONS

In this dissertation, we developed *MAC layer and routing protocols* suitable for heterogeneous MANETs with *asymmetric links*, and evaluated their performance. We also designed a time-parallel simulation (TPS) of ad hoc networks and evaluated its performance using the NS-2 simulation tool.

We first introduced m-limited forwarding, a technique to optimize the performance of ad hoc routing algorithms by reducing the power consumption as well as the fraction of the network bandwidth used to disseminate routing information. We introduced two alternative functions: a distance-based function $\mathcal{F}^d$ and an area-based function $\mathcal{F}^a$. We evaluate the performance of m-limited forwarding through a series of simulation studies. Our first objective is to determine the optimal value of m, the cardinality of the set of nodes which retransmit a packet containing routing information. We have found that $m = 3$ yields reasonable output. We implemented a version of AODV with m-limited forwarding (m-AODV), and simulation results show that for most simulation scenarios, m-AODV has a lower power consumption and packet loss ratio than both plain AODV and LAR.

We applied the m-limited forwarding concept in our location-aware and power-aware routing protocol (A^{4}LP) for heterogeneous ad hoc networks with asymmetric links. A^{4}LP has three types of neighbors: In-, Out- and In/Out-bound. We introduced the concept of an m-party proxy set as a subset of nodes that can reach each other either directly or through a subset of members. Simulation results show that both packet loss ratio and latency are reduced as a result of the A^{4}LP routing protocol.

Although we have proposed a routing protocol to utilize the asymmetric links in heterogeneous MANETs, when we survey the literature of MAC layer protocols, we found that most MAC layer protocols simply assume symmetric links and ignore all asymmetric links. We proposed a MAC layer protocol (AsyMAC) which serves as the underlying MAC layer protocol for A^{4}LP in heterogeneous MANETs. Most current MAC protocols are unable to exploit the asymmetric links present in a network, thus leading to an inefficient overall bandwidth utilization, or, in the worst case, to loss of connectivity. The AsyMAC protocol is able to exploit the asymmetric links in such networks, and solves the problem of delivering the acknowledgements back to the sender against the direction of the asymmetric link. Some of the current solutions proposed in the literature reduce the probability of a collision, however, they silence more nodes than required. This is because hidden nodes appear more often and in more complex forms in heterogeneous MANETs, thus the traditional definition becomes invalid. We redefine the meaning of hidden nodes in our context as *nodes out of the range of the sender and whose ranges cover the receiver.* Simulation results demonstrate that the AsyMAC protocol utilizes asymmetric links efficiently and the benefits of our protocol outweighs its cost.

Once we have developed the logic of MAC layer and routing protocols that exploit asymmetric links we had to provide convincing arguments that these new protocols are functional, and, even though more complex than the ones that ignore the asymmetry, can lead to an acceptable level of performance. We turned to analytical modeling and realized shortly that it would be rather difficult, if possible at all, to develop analytical models. We also realized the limitations of existing simulation tools such as NS-2. Thus, we turned our attention to time-parallel simulation that could allow us to use existing tools, but study networks with a larger number of nodes and for extended periods of time. In Chapter 5, we explored the challenges and the benefits of time-parallel simulation of wireless ad hoc networks. We introduced the notion of perturbation of measurements and present a layer-by-layer analysis of the impact of perturbations on the functioning of the wireless network. We have found ways to predict the accuracy of a time-parallel simulation and proposed the following methods: time interval shift, warmup interval, warmup with compressed history, and warmup with initial state approximation (ISA). We have presented an iterative approach for the time-parallel simulation with equal intervals and variable lengths of warmup intervals. We study the speedup and the accuracy of simulation results for packet loss ratio and throughput for two popular ad hoc routing algorithms: AODV and DSDV. The simulation results are in good concordance with the predictions made through the model.

The compressed history methodology is based upon the conjectured principle of temporal locality of perturbations. One could consider a more general approach to define significant events, or an application-specific approach as in the case of wireless ad hoc networks discussed in this dissertation. There are many ways to implement compressed history, e.g. reducing the route discovery events that do not contribute to routing during the measured simulation interval. In this dissertation, we notice the fact that table-driven routing protocols require a considerable amount of computations on the frequent routing table updates, thus, the compressed history of such simulation can be implemented by reducing the frequency of insignificant routing table updates. We use DSDV routing protocol to investigate the performance of the time-parallel simulation with the application of the compressed history strategy. We propose several strategies for generating the compressed history of a simulation. We study the accuracy of simulated results for packet loss ratio and throughput. The results of the simulations are better than our previous results without the application of *compressed history*, in both aspects of speedup and accuracy. We compared the performance of the TPS-CU, TPS-U, and TPS-C algorithms, and conclude that the introduction of uncompressed interval and compressed history can greatly improve the accuracy of time-parallel simulation. We conclude that time-parallel simulation with *compressed history* allows us to study relatively large wireless ad hoc networks consisting of a few thousand nodes over extended periods of time.

APPENDIX
PUBLICATIONS

Book Chapters

- **G. Wang**, Y. Ji, D. C. Marinescu, D. Turgut, and L. Bölöni. "Location- and power-aware protocols for wireless networks with asymmetric links." In *E. Gelenbe, editors, Computer System Performance Modeling in Perspective: A Tribute to the Work of Prof. Kenneth C. Sevcik (Advances in Computer Science and Engineering: Texts)*, pp. 101-136, Imperial College Press, 2006.

- X. Bai, H. Yu, **G. Wang**, Y. Ji, G. M. Marinescu, D. C. Marinescu and L. Bölöni. "Intelligent grids." *Grid Computing: Software Environments and Tools*, pp. 45-74, Springer, 2005.

- L. Bölöni, M. A. Khan, X. Bai, **G. Wang**, Y. Ji, and D. C. Marinescu. "Software engineering challenges for mutable agent systems." *Software Engineering for Multi-Agent Systems II, Lecture Notes in Computer Science Vol 2940*, pp. 149-167, Springer, 2004.

Journals

- **G. Wang**, L. Bölöni, D. Turgut, and D. C. Marinescu. "Time-Parallel simulation of wireless ad hoc networks with compressed history." Submitted to *Transactions on Parallel and Distributed Systems*, 2007.

- **G. Wang**, D. Turgut, L. Bölöni, Y. Ji, and D. C. Marinescu. "Improving routing performance through *m*-limited forwarding in power-constrained wireless ad hoc networks." Accepted for publication in *Journal of Parallel and Distributed Computing (JPDC)*, 2007.

- **G. Wang**, D. Turgut, L. Bölöni, Y. Ji, and D. C. Marinescu. "A MAC layer protocol for wireless networks with asymmetric links." *Ad hoc Networks Journal* (in print), 2007.

- **G. Wang**, D. Turgut, L. Bölöni, and D. C. Marinescu. "Time-parallel simulation of wireless ad hoc networks." Accepted for publication in *ACM/Springer Journal of Wireless Networks (WINET)*, 2006.

- X. Bai, H. Yu, **G. Wang**, Y. Ji, G. M. Marinescu, D. C. Marinescu, and L. Bölöni. "Coordination in intelligent grid environments." *Proceedings of the IEEE*, 93(3), pp. 613-630, 2005.

Conferences

- **G. Wang**, L. Bölöni, D. Turgut, and D. C. Marinescu. "Time-parallel simulation with compressed history." In *The 3rd International Conference on Wireless and Mobile Communications (ICWMC)*, pp. 48-56, 2007.
- **G. Wang**, D. Turgut, L. Bölöni, and D. C. Marinescu. "Accuracy-speedup tradeoffs for a time-parallel simulation of wireless ad hoc networks." In *2nd IEEE International Workshop on Performance and Management of Wireless and Mobile Networks (IEEE P2M-Net 2006)*, pp. 730-737, 2006.
- **G. Wang**, Y. Ji, D. Turgut, L. Bölöni, and D. C. Marinescu. "A simulation study of a MAC layer protocol for wireless networks with asymmetric links." In *International Wireless Communications and Mobile Computing Conference (IWCMC)*, pp. 929-936, 2006.
- **G. Wang**, Y. Ji, D. C. Marinescu, and D. Turgut. "A routing protocol for power constrained networks with asymmetric links." In *Proceedings of ACM Workshop on Performance Evaluation of Wireless Ad Hoc, Sensor, and Ubiquitous Networks (PE-WASUN 2004)*, pp. 69-76, IEEE Press, 2004.
- D. Turgut, **G. Wang**, L. Bölöni, and D. C. Marinescu. "Speedup-precision tradeoffs in time-parallel simulation of wireless ad hoc networks." In *10th IEEE International Symposium on Distributed Simulation and Real Time Applications (DS-RT)*, pp. 265-268, 2006.
- L. Bölöni, D. Turgut, **G. Wang**, and D. C. Marinescu. "Challenges and benefits of time-parallel simulation of wireless ad hoc networks." In *1st International Conference on Performance Evaluation Methodologies and Tools (Valuetools-2006)*, 2006.
- H. Yu, X. Bai, **G. Wang**, Y. Ji, and D. C. Marinescu. "Metainformation and workflow management for solving complex problems in grid environments." In *Proceedings of 18th International Parallel and Distributed Processing Symposium*, pp. 107-120, 2004.
- L. Bölöni, M. A. Khan, X. Bai, **G. Wang**, Y. Ji, and D. C. Marinescu. "Software engineering challenges for mutable agent systems." In *2nd International Workshop on Software Engineering for Multi-Agent Systems II, Research Issues and Practical Applications (SELMAS 2003)*, 2003.

LIST OF REFERENCES

[ABJ03] C. Adjih, E. Bacelli, and P. Jacquet. “Link state routing in wireless ad-hoc networks.” Technical Report 4874, INRIA, 2003.

[Aga00] S. Agarwal. “Handling unidirectional links in ad-hoc wireless networks.” Technical report, University of California, Berkeley, 2000.

[ALF03] Arun Avudainayagam, Wenjing Lou, and Yuguang Fang. “DEAR: A Device and Energy Aware Routing protocol for heterogeneous ad hoc networks.” *Journal of Parallel and Distributed Computing*, 63(2):228–236, 2003.

[AO95] S. Andradóttir and T. J. Ott. “Time segmentation parallel simulation of networks of queues with loss or communication blocking.” *ACM Transactions on Modeling and Computer Simulations*, 5(4):269–305, 1995.

[AT96] H. Avril and C. Tropper. “The dynamic load balancing of clustered time warp for logic simulation.” In *PADS ’96: Proceedings of the 10th Workshop on Parallel and Distributed Simulation*, pp. 20–27, 1996.

[BBM03] F. Baccelli, B. Blaszczyszyn, and P. Mühlethaler. “A spatial reuse aloha MAC protocol for multihop wireless mobile networks.” Technical Report 4955, INRIA, 2003.

[BCS98] S. Basagni, I. Chlamtac, V. R. Syrotiuk, and B. A. Woodward. “A Distance Routing Effect Algorithm for Mobility (DREAM).” In *Proceedings of 4th Annual ACM/IEEE International Conference on Mobile Computing and Networking (MOBICOM ’98)*, pp. 76–84, 1998.

[BD97] A. Boukerche and S. K. Das. “Dynamic load balancing strategies for conservative parallel simulations.” In *PADS ’97: Proceedings of the 11th Workshop on Parallel and Distributed Simulation*, pp. 20–28, 1997.

[BDF99] A. Boukerche, S. K. Das, A. Fabbri, and O. Yildiz. “Exploiting model independence for PCS parallel simulation.” In *Proceedings of the 13th ACM/IEEE workshop on Parallel and Distributed Simulation*, pp. 166–173, 1999.

[BDF01a] Azzedine Boukerche, Sajal K. Das, and Alessandro Fabbri. “Analysis of a randomized congestion control scheme with DSDV routing in ad hoc wireless networks.” *Journal of Parallel and Distributed Computing*, 61(7):967–995, 2001.

[BDF01b] Azzedine Boukerche, Sajal K. Das, and Alessandro Fabbri. "SWiMNet: A scalable parallel simulation testbed for wireless and mobile networks." *ACM/Kluwer Wireless Networks*, 7(5):467–486, 2001.

[BDS94] V. Bharghavan, A. Demers, S. Shenker, and L. Zhang. "MACAW: A media access protocol for wireless LAN's." In *ACM Special Interest Group on Data Communications (ACM SIGCOMM)*, pp. 221–225, 1994.

[BEF00] L. Breslau, D. Estrin, K. Fall, S. Floyd, J. Heidemann, A. Helmy, P. Huang, S. McCanne, K. Varadhan, Y. Xu, and H. Yu. "Advances in network simulation." *IEEE Computer*, 33(5):59–67, 2000.

[BF00] A. Boukerche and A. Fabbri. "Partitioning parallel simulation of wireless networks." In *Proceedings of the 2000 Winter Simulation Conference*, pp. 1449–1457, 2000.

[BG01] L. Bao and J.J. Garcia-Luna-Aceves. "Channel access scheduling in ad hoc networks with unidirectional links." In *Proceedings of Workshop on Discrete Algorithms and Methods for Mobile Computing and Communications (DIALM)*, pp. 9–18, 2001.

[Bha97] V. Bharghavan. "A new protocol for medium access in wireless packet networks." Technical report, Urbana, IL: Timely Group, 1997.

[Bia00] G. Bianchi. "Performance analysis of the IEEE 802.11 Distributed Coordination Function." *IEEE Journal on Selected Areas in Communications*, 18(3):535–547, 2000.

[BMJ98] J. Broch, D. A. Maltz, D. B. Johnson, Y.-C. Hu, and J. Jetcheva. "A performance comparison of multi-hop wireless ad hoc network routing protocols." In *Proceedings of 4th Annual ACM/IEEE International Conference on Mobile Computing and Networking (MOBICOM '98)*, pp. 85–97, 1998.

[Bri91] J. Briner. "Fast parallel simulation of digital systems." In *Proceedings of Multiconference on Advances in Parallel and Distributed Simulation*, pp. 71–77, 1991.

[BT94] A. Boukerche and C. Tropper. "A static partitioning and mapping algorithm for conservative parallel simulations." *ACM SIGSIM Simulation Digest*, 24(1):164–172, 1994.

[BTW06] L. Bölöni, D. Turgut, G. Wang, and D. C. Marinescu. "Challenges and benefits of time-parallel simulation of wireless ad hoc networks." In *Proceedings of 1st International Conference on Performance Evaluation Methodologies and Tools (Valuetools)*, 2006.

[CFE94] C. D. Carothers, R. M. Fujimoto, P. England, and Y. B. Lin. "Distributed simulation of large-scale PCS networks." In *Proceedings of the 2nd IEEE International Workshop* *on Modeling, Analysis, and Simulation of Computer and Telecommunication Systems*, pp. 2–6. IEEE Computer Society, 1994.

[CFL95] C. D. Carothers, R. M. Fujimoto, and Y. B. Lin. "A case study in simulating PCS networks using time warp." In *Proc. of the 9th Workshop on Parallel and Distributed Simulation*, pp. 87–94. ACM/SCS, 1995.

[CJL01] T. Clausen, P. Jacquet, A. Laouiti, P. Muhlethaler, A. Qayyum, and L. Viennot. "Optimized link state routing protocol for ad hoc networks." In *Proceedings of the 5th IEEE Multi Topic Conference (INMIC 2001)*, pp. 62–68, 2001.

[CJV02] T. Clausen, P. Jacquet, and L. Viennot. "Optimizing route length in reactive protocols for ad hoc networks." In *The 1st Annual Mediterranean Ad Hoc Networking Workshop (Med-hoc-Net)*, 2002.

[CJV04] T. Clausen, P. Jacquet, and L. Viennot. "Analyzing control traffic overhead versus mobility and data traffic activity in mobile ad-hoc network protocols." *ACM Wireless Networks Journal (WINET)*, 10(4):447–455, 2004.

[CL03] F. Chung and L. Lu. "The average distance in a random graph with given expected degrees." *Internet Mathematics*, 1(1):91–114, 2003.

[CMU] "CMU Monarch Extensions to ns." URL *http://www.monarch.cs.cmu.edu/*.

[CR89] Y.-C. Cheng and T. G. Robertazzi. "Critical connectivity phenomena in multi-hop radio models." *IEEE Transactions on Communications*, 37(7):770–777, 1989.

[CT99] M. Choe and C. Tropper. "On learning algorithms and balancing loads in time warp." In *PADS '99: Proceedings of the 13th Workshop on Parallel and Distributed Simulation*, pp. 101–108, 1999.

[CWL97] C. Chiang, H. Wu, W. Liu, and M. Gerla. "Routing in clustered multihop, mobile wireless networks." In *Proceedings of IEEE Singapore International Conference on Networks (SICON '97)*, pp. 197–211, 1997.

[DBT03] O. Dousse, F. Baccelli, and P. Thiran. "Impact of interferences on the connectivity of ad hoc networks." In *The 22nd Conference of the IEEE Computer and Communications Societies (INFOCOM)*, volume 3, pp. 1724–1733, 2003.

[DBT05] O. Dousse, F. Baccelli, and P. Thiran. "Impact of interferences on the connectivity of ad hoc networks." *IEEE Transactions on Networking*, 13(2):425–436, 2005.

[DHB00] K. Devine, B. Hendrickson, E. Boman, M. St. John, and C. Vaughan. "Design of dynamic load-balancing tools for parallel applications." In *ICS '00: Proceedings of the 14th international conference on Supercomputing*, pp. 110–118, 2000.

[DJ96] G. Dommety and R. Jain. "Potential networking applications of Global Positioning Systems (GPS)." Technical Report TR-24, Ohio State University, 1996.

[DPR01] S. R. Das, C. E. Perkins, and E. E. Royer. "Performance comparison of two on-demand routing protocols for ad hoc networks." In *IEEE Personal Communications Magazine speccial issue on Ad hoc Networking*, pp. 16–28, 2001.

[DS98] E. Deelman and B. K. Szymanski. "Dynamic load balancing in parallel discrete event simulation for spatially explicit problems." In *PADS '98: Proceedings of the 12th Workshop on Parallel and Distributed Simulation*, pp. 46–53, 1998.

[Erl09] A. K. Erlang. "The theory of probabilities and telephone conversations." *Nyt Tidsskrift for Matematik*, B(20), 1909.

[Erl17] A. K. Erlang. "Solution of some problems in the theory of probabilities of significance in automatic telephone exchanges." *Elektroteknikeren*, 13:5–13, 1917.

[FCS] "DARPA Advanced Technology Office - FCS Communications program." URL *http://www.darpa.mil/ato/programs/fcs_comm.htm*.

[FG95] C. Fullmer and J. J. Garcia-Luna-Aceves. "Floor Acquisition Multiple Access (FAMA) for packet-radio networks." In *Proceedings of ACM SIGCOMM '95*, pp. 262–273, 1995.

[FTB02] T. Fujii, M. Takahashi, M. Bandai, T. Udagawa, and I. Sasase. "An efficient MAC protocol in wireless ad-hoc networks with heterogeneous power nodes." In *The 5th International Symposium on Wireless Personal Multimedia Communications (WPMC '2002)*, pp. 776–780, 2002.

[Fuj89] R. M. Fujimoto. "Time warp on a shared memory multiprocessor." *Transactions of the Society for Computer Simulation*, 6(3):211–239, 1989.

[Fuj90] R. M. Fujimoto. "Parallel discrete event simulation." *Communications of ACM*, 33(10):30–53, 1990.

[GHH06] R. Gowaikar, B. Hochwald, and B. Hassibi. "Communication over a wireless network with random connections." *IEEE Transactions on Information Theory*, 52(7):2857–2871, 2006.

[GK98] P. Gupta and P. Kumar. "Critical power for asymptotic connectivity in wireless networks." In *Stochastic Analysis, Control, Optimization and Applications*, pp. 547–566, 1998.

[GK00] P. Gupta and P. R. Kumar. "The capacity of wireless networks." *IEEE Transactions on Information Theory*, 46(2):388–404, 2000.

[GT93] D. W. Glazer and C. Tropper. "On process migration and load balancing in time warp." *IEEE Transactions on Parallel and Distributed Systems*, 4(3):318–327, 1993.

[GT02] M. Grossglauser and D. Tse. "Mobility increases the capacity of ad hoc networks." *IEEE Transactions on Networking*, 10(4):477–486, 2002.

[GTS04] P. C. Gurumohan, T. J. Taylor, and V. R. Syrotiuk. "Topology control for MANETs." In *Proceedings of the IEEE Wireless Communications and Networking Conference (WCNC'04)*, pp. 600–604, 2004.

[HA96] M. Hoseyni-Nasab and S. Andradóttir. "Parallel simulation by time segmentation: Methodology and applications." In *Proceeding of the 1996 Winter Simulation Conference*, pp. 376–381, 1996.

[HA98] M. Hoseyni-Nasab and Sigrún Andradóttir. "Time segmentation parallel simulation of tandem queues with manufacturing blocking." In *Proceeding of the 1998 Winter Simulation Conference*, 1998.

[HN93] P. Heidelberger and D.M. Nicol. "Conservative parallel simulation of continuous time Markov chains using uniformization." *IEEE Transactions on Parallel and Distributed Systems*, 4(8):906–921, 1993.

[HP98] Z. J. Haas and M. R. Pearlman. "The Zone Routing Protocol (ZRP) for ad hoc networks." In *Internet Draft*, 1998.

[HZ01] Hossam Hassanein and Audrey Zhou. "Routing with load balancing in wireless ad hoc networks." In *MSWIM '01: Proceedings of the 4th ACM international workshop on Modeling, analysis and simulation of wireless and mobile systems*, pp. 89–96, 2001.

[Jac98] P. Jacquet. "Elements of analytical information theory, models and performance evaluation." Technical Report 3505, INRIA, 1998.

[Jac03] P. Jacquet. "Geometry of information propagation in massively dense ad hoc networks." Technical Report 4992, INRIA, 2003.

[Jef85] D. R. Jefferson. "Virtual time." *ACM Transactions on Programming Languages and System*, 7(3):404–325, 1985.

[JM96] D. B. Johnson and D. A. Maltz. "Dynamic source routing in ad hoc wireless networks." In Imielinski and Korth, editors, *Mobile Computing*, volume 353. Kluwer Academic Publishers, 1996.

[JSA01] C. E. Jones, K.M. Sivalingam, P. Agrawal, and J. C. Chen. "A survey of energy efficient network protocols for wireless networks." *Wireless Networks*, 7(4):343–358, 2001.

[JTR] "Joint Tactical Radio System (JTRS)." URL *http://jtrs.army.mil/*.

[JV00] P. Jacquet and L. Viennot. "Overhead in mobile ad-hoc network protocols." Technical Report 3965, INRIA, 2000.

[Kar90] P. Karn. "MACA - a new channel access method for packet radio." In *Proceedings of the 9th ARRL Computer Networking Conference*, pp. 134–140, 1990.

[Kie04] T. Kiesling. "Approximate time-parallel cache simulation." In *Procedings of 2004 Winter Simulation Conference*, pp. 345–354, 2004.

[Kie05] T. Kiesling. "Using approximation with time-parallel simulation." *Simulation*, 81(4):255–266, 2005.

[KRD06] Sunil Kumar, Vineet S. Raghavan, and Jing Deng. "Medium access control protocols for ad hoc wireless networks: A survey." *Ad Hoc Networks Journal, Elsevier*, 4:326–358, 2006.

[KT75] L. Kleinrock and F.A. Tobagi. "Packet switching in radio channels: Part I - carrier sense multiple-access modes and their throughput-delay characeteristics." *IEEE Transactions on Communications*, COM-23(12):1400–1416, 1975.

[KV98] Y. Ko and N.H. Vaidya. "Location-Aided Routing (LAR) in mobile ad hoc networks." In *Proceedings of the 4th Annual ACM International Conference on Mobile Computing and Networking (MobiCom 1998)*, pp. 66–75, 1998.

[Leb05] D. Lebedev. "A framework for the comparison of AODV and OLSR protocols." In *1st Asian Internet Engineering Conference (AINTEC)*, 2005.

[Leb06] D. Lebedev. *Ad hoc networks: Study of protocol behavior*. PhD thesis, Ecole Polytechnique, 2006.

[LL90] Y. B. Lin and E. D. Lazowska. "Exploiting lookahead in parallel simulation." *IEEE Transactions on Parallel and Distributed Systems*, 1(4):457–469, 1990.

[LL91] Y. Lin and E. D. Lazowska. "A time-division algorithm for parallel simulation." *ACM Transactions on Modeling and Computer Simulations*, 1(1):73–83, 1991.

[MAC99] IEEE Std 802.11b 1999. Part 11. "Wireless LAN medium access control (MAC) and physical layer (PHY) specifications." IEEE Standard 802.11, August 1999.

[MDP02] M. Maleki, K. Dantu, and M. Pedram. "Power-aware source routing protocol for mobile ad hoc networks." In *Proceedings of the 2002 International Symposium on Low Power Electronics and Design*, pp. 72–75, 2002.

[MG96] S. Murthy and J. J. Garcia-Luna-Aceves. “An efficient routing protocol for wireless networks.” *MONET*, 1(2):183–197, 1996.

[MMJ03] D. C. Marinescu, G. M. Marinescu, Y. Ji, L. Bölöni, and H. J. Siegel. “Ad hoc grids: Communication and computing in a power constrained environment.” In *Proceedings of the Workshop on Energy-Efficient Wireless Communications and Networks (EWCN)*, pp. 113–122, 2003.

[MWM91] V. K. Madisetti, J. C. Walrand, and D. G. Messerschmitt. “Asynchronous algorithms for the parallel simulation of event-driven dynamical systems.” *ACM Transactions on Modeling and Computer Simulations*, 1(3):244–274, 1991.

[NFC93] I. Nikolaidis, R. Fujimoto, and C. A. Cooper. “Parallel simulation of high-speed network multiplexers.” *IEEE Conference on Decision and Control*, 3(1):2224–2229, 1993.

[NFC94] I. Nikolaidis, R. Fujimoto, and C. A. Cooper. “Time-parallel simulation of cascaded statistical multiplexers.” In *Proceedings of the 1994 ACM SIGMETRICS conference on Measurement and modeling of computer systems*, pp. 231–240, 1994.

[Nic92] D. Nicol. “Conservative parallel simulation of priority class queuing networks.” *IEEE Transactions on Parallel and Distributed Systems*, 3(3):294–303, 1992.

[OPN] “OPNET Network Simulator.” URL *http://www.opnet.com/*.

[PB94] C. E. Perkins and P. Bhagwat. “Highly dynamic Destination-Sequenced Distance-Vector routing (DSDV) for mobile computers.” In *ACM Special Interest Group on Data Communications (ACM SIGCOMM)*, pp. 234–244, 1994.

[PC97] V. D. Park and M. S. Corson. “A highly adaptive distributed routing algorithm for mobile wireless networks.” In *The 16th Conference of the IEEE Computer and Communications Societies (INFOCOM)*, pp. 1405–1413, 1997.

[PDN] “PDNS – Parallel/Distributed NS.” URL *http://www.cc.gatech.edu/computing/compass/pdns/*.

[Pen97] M. D. Penrose. “The longest edge of the random minimal spanning tree.” *Annals of Applied Probability*, 7(2):340–361, 1997.

[PGH00] G. Pei, M. Gerla, and X. Hong. “LANMAR: Landmark routing for large scale wireless ad hoc networks with group mobility.” In *Proceedings of the 1st ACM Interational Symposium on Mobile Ad Hoc Networking and Computing (MobiHoc)*, pp. 11–18, 2000.

[PKD01] N. Poojary, S. V. Krishnamurthy, and S. Dao. "Medium access control in a network of ad hoc mobile nodes with heterogeneous power capabilities." In *Proceedings of IEEE ICC 2001*, volume 3, pp. 872–877, 2001.

[PKL98] Jignesh Panchal, Owen Kelly, Jie Lai, Narayan Mandayam, Andrew T. Ogielski, and Roy Yates. "WiPPET, a virtual testbed for parallel simulations of wireless networks." In *PADS '98: Proceedings of the 12th Workshop on Parallel and Distributed Simulation*, pp. 162–169. IEEE Computer Society, 1998.

[PR99] C. E. Perkins and E. M. Royer. "Ad hoc On-demand Distance Vector routing." In *Proceedings of the 2nd IEEE Workshop on Mobile Computing Systems and Applications*, pp. 99–100, 1999.

[Pra99] R. Prakash. "Unidirectional links prove costly in wireless ad-hoc networks." In *Proceedings of DIMACS Workshop on Mobile Networks and Computers*, pp. 15–22, 1999.

[Pre05] Francesco Lo Presti. "Joint congestion control: Routing and media access control optimization via dual decomposition for ad hoc wireless networks." In *MSWiM '05: Proceedings of the 8th ACM international symposium on Modeling, analysis and simulation of wireless and mobile systems*, pp. 298–306, 2005.

[QN] "QualNet Network Simulator." URL *http://www.scalable-networks.com/*.

[QS03a] F. Quaglia and A. Santoro. "Modeling and optimization of non-blocking checkpointing for optimistic simulation on myrinet clusters." In *ICS '03: Proceedings of the 17th annual international conference on Supercomputing*, pp. 130–139. ACM Press, 2003.

[QS03b] F. Quaglia and A. Santoro. "Nonblocking checkpointing for optimistic parallel simulation: description and an implementation." *IEEE Transactions on Parallel and Distributed Systems*, 14(6):593–610, 2003.

[Qua01] F. Quaglia. "A cost model for selecting checkpoint positions in time warp parallel simulation." *IEEE Transactions on Parallel and Distributed Systems*, 12(4):346–362, 2001.

[RCM02] V. Ramasubramanian, R. Chandra, and D. Mosse. "Providing a bidirectional abstraction for unidirectional ad-hoc networks." In *Proceedings of INFOCOM 2002*, pp. 1258–1267, 2002.

[RH00] Ram Ramanathan and Regina Hain. "Topology control of multihop wireless networks using transmit power adjustment." In *Proceedings of INFOCOM*, pp. 404–413, 2000.

[RJ90] P. L. Reiher and D. Jefferson. "Dynamic load management in the time warp operating system." *Transactions of the Society for Computer Simulation*, 7(2):91–120, 1990.

[RM02] V. Ramasubramanian and D. Mossé. "Statistical analysis of connectivity in unidirectional ad hoc networks." In *Proceedings of the International Workshop on Ad Hoc Networking 2002, Vancouver*, pp. 109–115, 2002.

[SE98] H. M. Soliman and A. S. Elmaghraby. "An analytical model for hybrid checkpointing in time warp distributed simulation." *IEEE Transactions on Parallel and Distributed Systems*, 9(10):947–951, 1998.

[Sha48] C. E. Shannon. "A mathematical theory of communication." *The Bell System technical journal*, 27:379–423, 1948.

[Sha49] C. E. Shannon. "Communications in the presence of noise." *Proceedings of the Institute of Radio Engineers (IRE)*, 37:10–21, 1949.

[SHM02] Ahmed Safwat, Hossam Hassanein, and Hussein Mouftah. "Energy-aware routing in MANETs: analysis and enhancements." In *MSWiM '02: Proceedings of the 5th ACM international workshop on Modeling analysis and simulation of wireless and mobile systems*, pp. 46–53, 2002.

[SKM95] D. Stoyan, W. S. Kendall, and J. Mecke. *Stochastic geometry and its applications*. John Wiley and Sons, 2 edition, 1995.

[SKM03] N.-O. Song, B.-J. Kwak, and L. El Miller. "On the stability of exponential backoff." *Journal of Research of the National Institute of Standards and Technology*, 108(4):289–297, 2003.

[SS00] T. K. Som and R. G. Sargent. "Model structure and load balancing in optimistic parallel discrete event simulation." In *PADS '00: Proceedings of the 14th Workshop on Parallel and Distributed Simulation*, pp. 147–154, 2000.

[SWR98] S. Singh, M. Woo, and C.S. Raghavendra. "Power-aware routing in mobile ad hoc networks." In *Proceedings of 4th Annual ACM/IEEE International Conference on Mobile Computing and Networking (MOBICOM '98)*, pp. 181–190, 1998.

[TCC06] H.-W. Tsai, T.-S. Chen, and C.-P. Chu. "An on-demand routing protocol with backtracking for mobile ad hoc networks." *Wireless Personal Communications*, 38(3):279–300, 2006.

[Toh97] C.-K. Toh. "Associativity-based routing for ad-hoc mobile networks." In *Wireless Personal Communications Journal, Special Issue on Mobile Networking and Computing Systems.*, volume 4, pp. 103–139. Kluwer Academic Publishers, 1997.

[TWB06] D. Turgut, G. Wang, L. Bölöni, and D. C. Marinescu. "Speedup-precision tradeoffs in time-parallel simulation of wireless ad hoc networks." In *Proceedings of 10th IEEE*

International Symposium on Distributed Simulation and Real Time Applications (DS-RT), pp. 265–268, 2006.

[VIN] "The UCB/LBNL/VINT Network Simulator - NS (Version 2)." URL *http://www.isi.edu/nsnam/ns.*

[WA92] J. J. Wang and M. Abrams. "Approximate time-parallel simulation of queueing systems with losses." In *Proceedings of the 24th conference on Winter simulation (WSC '92)*, pp. 700–708. ACM Press, 1992.

[WA93] J. J. Wang and M. Abrams. "Determining initial states for time-parallel simulations." In *Proceedings of the 7th Workshop on Parallel and Distributed Simulation (PADS '93)*, pp. 19–26. ACM Press, 1993.

[WAH06] Michele C. Weigle, Prashanth Adurthi, Felix Hernandez-Campos, Kevin Jeffay, and F. Donelson Smith. "Tmix: a tool for generating realistic TCP application workloads in ns-2." *SIGCOMM Computer Communication Review*, 36(3):65–76, 2006.

[WBT07a] G. Wang, L. Bölöni, D. Turgut, and D. C. Marinescu. "Time-parallel simulation of wireless ad hoc networks with compressed history." *Submitted to Transactions on Parallel and Distributed Systems (TPDS)*, 2007.

[WBT07b] G. Wang, L. Bölöni, D. Turgut, and D. C. Marinescu. "Time-parallel simulation with compressed history." In *Proceedings of the 3rd International Conference on Wireless and Mobile Communications (ICWMC)*, pp. 48–56, 2007.

[Wie01] F. Wieland. "Practical parallel simulation applied to aviation control." In *Proceedings of the 15th Workshop on Parallel and Distributed Simulation*, pp. 109–116. ACM/IEEE Computer Society, 2001.

[WJM04] G. Wang, Y. Ji, D. C. Marinescu, and D. Turgut. "A routing protocol for power constrained networks with asymmetric links." In *Proceedings of the ACM Workshop on Performance Evaluation of Wireless Ad Hoc, Sensor, and Ubiquitous Networks (PE-WASUN)*, pp. 69–76, 2004.

[WJM06] G. Wang, Y. Ji, D. C. Marinescu, D. Turgut, and L. Bölöni. "Location- and power-aware protocols for wireless networks with asymmetric links." In E. Gelenbe, editor, *Computer System Performance Modeling in Perspective: A Tribute to the Work of Prof. Kenneth C. Sevcik (Advances in Computer Science and Engineering: Texts - Vol. 1)*, pp. 101–136. Imperial College Press, 2006.

[WLB01] Roger Wattenhofer, Li Li, Paramvir Bahl, and Yi-Min Wang. "Distributed topology control for wireless multihop ad-hoc networks." In *Proceedings of INFOCOM*, pp. 1388–1397, 2001.

[WN96] L. F. Wilson and D. M. Nicol. "Experiments in automated load balancing." In *PADS '96: Proceedings of the 10th Workshop on Parallel and Distributed Simulation*, pp. 4–11, 1996.

[WTB06a] G. Wang, D. Turgut, L. Bölöni, Y. Ji, and D. C. Marinescu. "A simulation study of a MAC layer protocol for wireless networks with asymmetric links." In *International Wireless Communications and Mobile Computing Conference (IWCMC)*, pp. 929–936, 2006.

[WTB06b] G. Wang, D. Turgut, L. Bölöni, and D. C. Marinescu. "Accuracy-speedup tradeoffs for a time-parallel simulation of wireless ad hoc networks." In *2nd IEEE International Workshop on Performance and Management of Wireless and Mobile Networks (P2M-Net)*, pp. 730–737, 2006.

[WTB07a] G. Wang, D. Turgut, L. Bölöni, Y. Ji, and D. C. Marinescu. "Improving routing performance through m-limited forwarding in power-constrained wireless ad hoc networks." *Accepted for publication in Journal of Parallel and Distributed Computing (JPDC)*, 2007.

[WTB07b] G. Wang, D. Turgut, L. Bölöni, Y. Ji, and D. C. Marinescu. "A MAC layer protocol for wireless networks with asymmetric links." *Ad hoc Networks Journal (in print)*, 2007.

[WTB07c] G. Wang, D. Turgut, L. Bölöni, and D. C. Marinescu. "Time-parallel simulation of wireless ad hoc networks." *Accepted for publication in ACM/Springer Journal of Wireless Networks (WINET)*, 2007.

[XHE01] Y. Xu, J. S. Heidemann, and D. Estrin. "Geography-informed energy conservation for Ad Hoc routing." In *Proceedings of 7th Annual International conference on Mobile Computing and Networking (MOBICOM '01)*, pp. 70–84, 2001.

[XHG03] K. Xu, X. Hong, and M. Gerla. "Landmark routing in ad hoc networks with mobile backbones." *Journal of Parallel and Distributed Computing*, 63(2):110–122, 2003.

[XK04] F. Xue and P. R. Kumar. "The number of neighbors needed for connectivity of wireless networks." *Wireless Networks*, 10(2):169–181, 2004.

[ZBG98] X. Zeng, R. Bagrodia, and Mario Gerla. "Simulation of large-scale wireless network." In *Proceedings of the 12th Workshop on Parallel and Distributed Simulation*, pp. 154–161, 1998.